Nils Rüther

Computational fluid dynamics in fluvial sedimentation engineering

Thesis for the degree of doctor philosophiae

Trondheim, November 2006

Norwegian University of
Science and Technology
Fakultet for ingeniørvitenskap og teknologi
Institutt for vann- og miljøteknikk

NTNU
Innovation and Creativity

NTNU
Norwegian University of Science and Technology

Thesis for the degree of doctor philosophiae

Fakultet for ingeniørvitenskap og teknologi
Institutt for vann- og miljøteknikk

ISBN 82-471-8188-6 (printed ver.)
ISBN 82-471-8187-8 (electronic ver.)
ISSN 1503-8181

Doctoral Theses at NTNU, 2006:205

Printed by Tapir Uttrykk

Computational fluid dynamics in fluvial sedimentation engineering

A dissertation
submitted to the Faculty of Civil Engineering
at the Norwegian University of Science and Technology
in partial fullfillment of the requirements for the degree of

Doctor of Philosophy (PhD)

by

Nils Rüther

1. Referee:	Prof. Peter Rutschmann University of Insbruck, Austria
2. Referee:	Dr. Einar Tesaker Tesaker Vann AS, Heimdal, Norway
Administration:	Dr. Knut Alfredsen NTNU, Trondheim, Norway

Trondheim, November 2006

NTNU
Norwegian University of Science and Technology
Faculty of Engineering Science and Technology
Department of Hydraulic and Environmental Engineering

ISBN 82-471-8187-8 (electronic version)

ISBN 82-471-8188-6 (printed version)

NTNU, 2006:205

Printed by Tapir Uttrykk

La science est faite d'erreurs,
mais d'erreurs qu'il est bon de commettre,
car elles mènent peu à peu à la vérité

Jules Verne (1864)

Foreword

The present thesis is based on the results of five scientific papers which are included in Appendix A. The five scientific papers are about three-dimensional numerical modelling of sediment transport in channel bends. The author has generated the necessary input data files for the numerical model, done the computations and processed the output data. Furthermore the author wrote the text to all the scientific papers except the one with Dr. Fischer-Antze. The author has additionally made new algorithms for several of the modelled sediment processes and coded these into the model using dynamic link libraries. The paper on the intake modelling is co-authored by Mr. J. M. Singh and Mr. E Atkinson. Mr. Singh worked on the case for his MSc thesis, supervised by Mr. Rüther. Mr. Atkinson provided the measurement data and did the computations using the PHOENICS model. The paper together with Dr. Tim Fischer-Antze is composed of two parts. The work for the generation of the input data and grids, the computation and the analysis of the results were divided equally. Dr. Fischer-Antze did most of the writing for the scientific paper. Prof. Gutknecht was involved in the proof-reading process. Prof. Olsen was involved in all the five papers. He was responsable for the daily supervision including his literally never-ending source of productive ideas and for the support of the numerical model used in this study.

Acknowledgements

First of all I would like to express my gratitude to Professor Nils Reidar B. Olsen of the Department of Hydraulic and Environmental Engineering at the Norwegian University of Science and Technology (NTNU), Norway, for his outstanding supervision and inspiring attitude during the time I have been working on my dissertation. I would like to thank him for his support and giving me the freedom to realize my own ideas and to achive my goals. At the same time I strongly appreciate his effort in pushing me to my limits every single day.
When I first met Dr. Sebastian Palt, I was impressed by his dedication to research. He symbolized an archetype when he was working as a PhD-student and I admired his enthusiasm. He taught me how to remain focused. I would like to thank him for introducing me to the fascination of sediment transport and for encouraging me to take a Ph.D.
Then I would like to thank Dr. Thorsten Stoesser, Technical University of Karlsruhe, Germany, for sharing his profound knowledge of Computational Fluid Dynamics with me. He continuously supported me no matter how busy he was.
A huge thanks is addressed to all my colleagues I met and worked with since I graduated from Karlsruhe University in 2001. Tim, Burkhard, Ingo, Stefan, Jörn, Jagadishwar Man, Catherine, Durga, Meg, Kiflom, Morten, Péter, Knut and Tone, thanks for just being there when questions or doubts arouse. Your advice and support have meant a lot to me and helped me finish the disstertation.
Thanks to Stewart Clark, Student and Acadamic Division at NTNU, Norway, for editing the dissertation.
Finally I want to express my gratitude to Petra and my parents. All the time they gave me the feeling of doing something special. Actually, it is priceless knowing that somebody is proud of what you are doing. I admire Petra for accepting me as I am.

Abstract

The present dissertation describes the improvement of a numerical model when predicting sedimentation and erosion processes in fluvial geomorphology. Various algorithms and parameters were implemented in a computational fluid dynamic model for simulation of three-dimensional water flow and coupled sediment transport to gain an insight into the capabilities of the numerical model. Within the scope of the test cases the model simulated suspended load concentrations at a water intake, transient bed deformation in a 90° channel bend, grain sorting processes as well as an unsteady flow regime in a 180° channel bend, transient bed deformation in a sine-shaped meandering channel with occurring bed forms and the free-forming meander evolution of an initially straight channel. All results matched well with the measurements. The results also showed that using computational fluid dynamics for modeling water flow and sediment transport is one step closer of having a universal predictor for processes in fluvial geomorphology. However, there are limitations and some uncertainties in computing the water surface location and alluvial roughness as well as in turbulence modeling. These should be clarified in future investigations.

Table of Contents

List of Figures

Chapter 1

Introduction

1.1 General

The simulation of water flow and sediment transport in rivers is a matter of considerable interest in the field of river engineering and sedimentation research. Modeling the physical process of time-dependent sediment transport, the corresponding bed changes and lateral migration of rivers is still a research topic. During the last century the physical processes of interaction of water and sediment transport were investigated by the means of field studies and laboratory experiments. However, in the last two decades, computational power has increased tremendously, and computational fluid dynamic[1] models have progressively become more of a competitior to laboratory experiments. While there is a well-defined state-of-the-art for computing the hydraulics of flows in channels and natural rivers, highly sophisticated computations of sediment transport and associated morphodynamics are still being researched. Due to the need for excessive computational resources, especially for multidimensional modeling, the application and development of numerical-morphodynamic models is mainly limited to research institutions. Therefore it is of considerable importance to push progress and ensure that CFD will be a useful tool in practical sedimentation engineering in future.

[1] In the following abbreviated by CFD

1.2 Structure of the thesis

Chapter 1 presents a general introduction to the topic and defines the motivation and the objectives. Chapter 2 reviews fluvial geomorphology with special interest to hydraulics and sediment transport in channel bends. Chapter 3 presents the theory of three-dimensional numerical modeling of flow and sediment transport. Chapter 4 summarizes the five scientific papers in the dissertation. Chapter 5 gives the conclusion and recommendations for further research. Finally, the Appendix A includes the five scientific papers.

1.3 Modeling sediment transport in channel bends

1.3.1 Overview

Numerical models for coupled flow and sediment transport simulation can be distinguished by the calculated flow dimensions and the application range. There exists a number of one-, two- and three-dimensional[2] approaches for the computation of the dynamics of flow and sediment movement. Some models are applied to rivers with non-erodable banks and others that include bank erosion algorithms, are used to predict lateral migration.
Considering the calculated flow dimension the following statements can be made. 1D approaches are well documented but they are inherently limited to 1D flow and sediment transport problems, such as section integrated erosion or deposition processes in a straight and homogeneous river reach. Overall evolution of bed changes and the calculation of transported material are found to match with measurements (Neary et al., 2001; Guo and Jin, 1999). When calculating local bed changes using a 1D method, the results have to be treated with care since they might contain errors. A widely used alternative to 1D approaches are 2D numerical models. 2D numerical models can predict morphological changes accurately, when the 3D nature of the processes is of minor importance, such as in many straight open channel flows, when the width-to-depth ratio is large,

[2]In the following abbreviated by 1D, 2D, and 3D

so that the vertical velocity component is much smaller than the horizontal components and the pressure distribution is virtually hydrostatic. Using a 2D numerical model, large scale investigations of sediment transport can be accomplished. The advantage of 3D approaches is the possibility of modeling many processes in a complex river geometry, such as meandering or curved channels. The correct modeling of the helical flow is of major importance here. The helical flow exists due to the difference between the centrifugal forces acting on the upper and lower layers of flow. The helical flow plays an important role in the evolution of channel topography, inducing deposition along the inner bank and erosion along the outer bank of a bend. The application of a fully 3D model should give superior results compared to a parameterized 2D model when calculating flow and sediment transport in channel bends.
In the following a short literature review is given of 2D and 3D numerical models simulating water flow coupled with sediment transport in river bends and meandering channel systems. It is distingueshed between numerical models with moving and non-moving lateral boundaries.

1.3.2 CFD codes for hydraulic and sedimentation engineering

In recent years, several 2D and 3D numerical morphodynamic models have been developed, that have the capability to predict bed deformation in channels with non-moving boundaries. Minh Duc et al. (2004) proposed a 2D depth-averaged model using a finite volume method with boundary-fitted grids and fixed channel sides. The sediment transport module comprised of semi-empirical models of suspended and non-equilibrium bed load. The secondary flow transport effects were taken into account by adjusting the dimensionless diffusivity coefficient in the depth-averaged k-ϵ turbulence model. For the calculation of the bed shear driven resultant bed load, the empirical formulas by van Rijn (1984a) have been used. Among others, the model has been validated by computing the bed changes of the experiments by Odgaard and Bergs (1988) and Yen and Lee (1995). For the numerical modeling, the experiments by Yen and Lee (1995) were simplified by assuming the sediment to be uniform. As a

consequence, the observed sorting processes were not considered by the 2D model. In some cases sorting processes for graded sediment mixtures were included in the sediment transport calculation routine. Wu and Wang (2004) proposed a 2D depth-averaged model for computing flow and sediment transport in curved channels, simulating sediment transport in a channel bend with fixed sides. Owing to the fact that helical flow significantly affects the flow, sediment transport and morphological evolution in curved channels, a semi-empirical formula was presented to determine the cross-stream distribution of the helical flow intensity in the developed regions of a channel bend. The formula was used to evaluate the dispersion terms in the depth-averaged 2D momentum equations and suspended load transport equation as well as the bed load transport angle. The experiments by Yen and Lee (1995) were also used for validation. Here, eight sediment size fractions were used to represent the nonuniform sediment mixture, so that the sediment sorting processes were considered in the model. A 3D model for the calculation of flow and sediment transport was proposed by Wu et al. (2000). Suspended load transport was simulated through the general convection-diffusion equation with an empirical settling velocity term. Bed load transport was simulated with a non-equilibrium method and the bed deformation was obtained from an overall mass-balance equation. The empirical formulas by van Rijn (1984a,b) were implemented for the computation of bed and suspended load. The model was not able to account for the effect of transverse bed slope on the bed load transport. The model was tested by calculating the flow and sediment transport of the experiments by Odgaard and Bergs (1988), a 180° channel bend with fixed sides. Zeng et al. (2005) presented a fully 3D model to solve the flow, bed load sediment transport and bed morphology changes in open channel flows in non-movable channel banks. The non-hydrostatic model solved the 3D Reynolds averaged Navier-Stokes equations with integrations up to the wall such that the use of wall functions was avoided. The $k-\Omega$ model was used together with a non-equilibrium bed load sediment transport model with additional introduction of down-slope gravitational force effects. The empirical formulas proposed by van Rijn (1984a) for the equilibrium bed load transport rate were used in the study. Among others, the experiments by Odgaard and Bergs (1988) were employed to validate the model. The results showed fairly

small improvements over simulations using models with wall functions.

1.3.3 CFD codes for predicting alluvial channel migration

During recent decades, considerable progress has been made in the understanding of meandering rivers. The pioneering work of Ikeda et al. (1981), Parker et al. (1982) and others explained why rivers meander and provided the research community with a foundation for later studies. In the linear theory of Ikeda et al. (1981) the channel migration rate is assumed to be proportional to the near-bank water flow velocities. Johannesson and Parker (1989) extended the model of Ikeda et al. (1981) by relaxing the constraint that the bed is unerodable, thus explicitly taking into account the coupling between the flow field, the bed load transport and the bed topography. This added a new process to the model in which the bank stability is the sole mechanism for river meandering. The model of Johannesson and Parker (1989) was then extended by Sun et al. (2001a,b). They incorporated an algorithm which takes the multiple grain sizes and sediment sorting into account. These kind of models are called process-based and they are very effective when predicting long-term behavior and a large scale meandering river system. Shortcomings were reported when predicting detail migration rates over a shorter time period.
In addition to this type of models, some researchers suggest using a physical based model. Here, sediment transport and bank erosion rates are calculated to assess the advance or retreat of a channel bank line (Osman and Thorne, 1988). These models can be specifically used to determine the rate of bank erosion at individual locations in the channel by knowing the flow field, bank geometry and bank material.
The previously mentioned process- and physical-based model for meander migration and bank erosion are based on the mean values of the occurring flow, i.e. the mean velocity and shear stress of a river cross-section are split into the longitudinal and lateral flow direction. These approaches for splitting the mean flow values differ from model to model with the level of sophistication.
With increasing computer power, 2D hydrodynamic-based models were coupled with sediment transport models to predict lateral and vertical erosion rates of

alluvial channels. Mosselman (1998), Duan et al. (2001) and Darby et al. (2002) presented a 2D hydrodynamic model in a structured grid, including algorithms for basal bank erosion to predict migration of meander evolution. To incorporate the effects of the 3D flow in a channel bend, the 2D hydrodynamic approach was enhanced by empirical formulas. Mosselman (1998) came to the conclusion that these formulas were the main reasons for the shortcomings in his simulations. In the study by Olsen (2003) a fully 3D model was presented and verified with the same data set Duan et al. (2001) used. The results from the simulation showed good agreement when predicting the meander migration from an initially straight channel with an upstream perturbation in terms of a single bend.

1.4 Motivation and objectives

There is a wide range of application when using numerical models in sedimentation engineering for predicting flow and sediment transport. The complexity of geometry and sediment properties increases the number and complexity of the numerical algorithms and consequently the computational time. Due to the increasing computer power in recent years, numerical models are more frequently used in sedimentation engineering. Today, 1D and 2D models are standard tools in engineering praxis. Although the prediction of flow and sediment transport is reliable, for some complex flow situations there are some considerable drawbacks. As a result of the increasing demand for prediction of 3D flow and corresponding sediment transport, Olsen (2004) presented a numerical model solving the three-dimensional Reynolds-averaged Navier-Stokes equation, with the turbulence modeled by the standard two equation k-ϵ model. Space can be discretized on structured as well as on unstructured grids. When starting the investigations for the present study, Olsen's investigations were mainly focused on the computation of flow and sediment concentration in water reservoirs and sand traps (Olsen, 1999; Olsen and Kjellesvig, 1999; Olsen and Skoglund, 1994). Initial results were published on the simulation of sediment transport in complex geometries (Olsen, 2003; Olsen and Kjellesvig, 2000). Based on these results the goal of the present study was to enhance the numerical model further by improving and adding algorithms as well as eliminating the drawbacks. The goal was accomplished first by testing how far the model was able to compute sediment transport and its asso-

ciated transient bed deformation in channel bends and second by implementing numerical formulation for the physical processes of sediment transport in channel bends. The simulated test cases were laboratory studies carried out by various researchers. It was sought to keep the computational time as short as possible on order to study a wide range of sensitivity tests.

Chapter 2

Fluvial geomorphology of bended and meandering rivers

2.1 Flow in river bends

Figure 2.1 shows a definition sketch of a meandering channel of the width B and the wavelength Λ_M. The wavelength is the shortest distance between points of inflection 0_i and 0_{i+2}. The point of inflection is the center point of a so-called cross-over cross section. Meander length L is the distance between these two

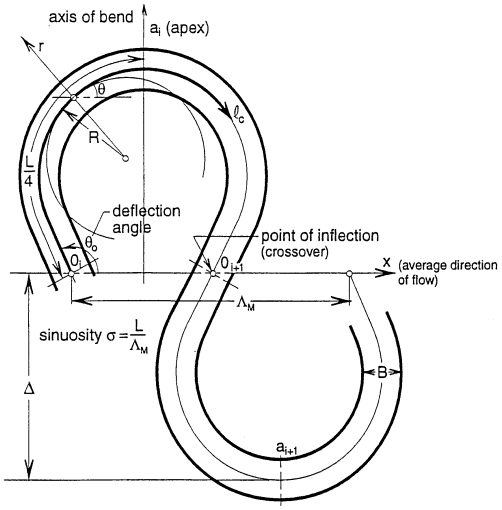

Figure 2.1: Definition sketch of a meander bend. (Yalin and da Silva, 2001)

points along the centerline of the channel. L divided by Λ_M gives the sinuosity σ of the meander bend. The opposite of the cross-over cross section is the apex a_i. The apex is located at the peak of the meander bend, $L/4$ after the point of inflection. The shortest distance between the point of inflection and the apex is called the meander width or amplitude Δ_M. The outside river bank is called concave and the inside one convex. The deflection angle of a meander bend Θ_0 describes the degree of meandering. Theoretically Θ_0 varies from 0° to 135°.

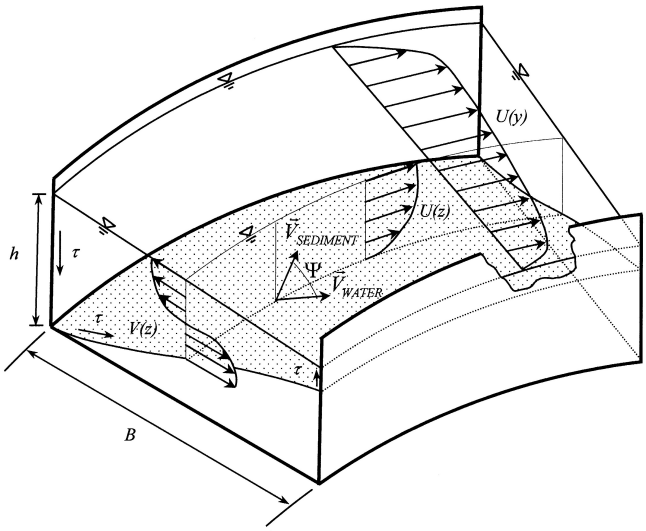

Figure 2.2: Sketch of flow- and sediment transport direction in a channel bend

The water flow and the sediment movement in a channel bend are mainly influenced by the spiral motion of the water body, also called *helical flow*. This process is initialized by the centrifugal forces accelerating water particles on the water surface being then transported toward the outer part of the bend. This causes a pressure difference between the inner and the outer streamline of the bend flow, being balanced by a near bed current pointing toward the inner part of the bend. Consider the velocity profiles in Figure 2.2. The transversal velocities on the surface are pointing at the concave river bank, whereas the bottom flow is directed at the convex bank. The superposition of this transversal velocity profile with the main flow direction produces the well known spiral motion occurring in river bends. Being influenced by this spiral motion the

transported sediment particles are moving slightly more toward the inner part of the bend where they deposit due to smaller flow velocities, forming a point bar. Additionally, a grain size sorting is associated with the formation of a point bar. The point bar consists mainly of smaller size material being eroded at the concave river bank and transport with the spiral motion to the convex one. This leads to a lateral gradient of the sediment size, decreasing from the concave to the convex river bank. This process destabilizes the balance of the sediment distribution in a cross section, causing erosion at the outer part of the bend. The transversal slope increases with greater scour depth and point bar height. Within meander bends, the cross-section profile becomes strongly asymmetric. At a certain angle of the point bar the gravity force gains importance and deflects the sediment particle. The particle is then no longer following the direction of the bed shear stress $\bar{V}_{WATER}$. It deviates with a certain angle Ψ from the bed shear stress direction and is termed $\bar{V}_{SEDIMENT}$. If then the sediment transport is in equilibrium, the sediment particle is balanced between the secondary current pointing upwards and the gravity force pointing downwards in the slope.

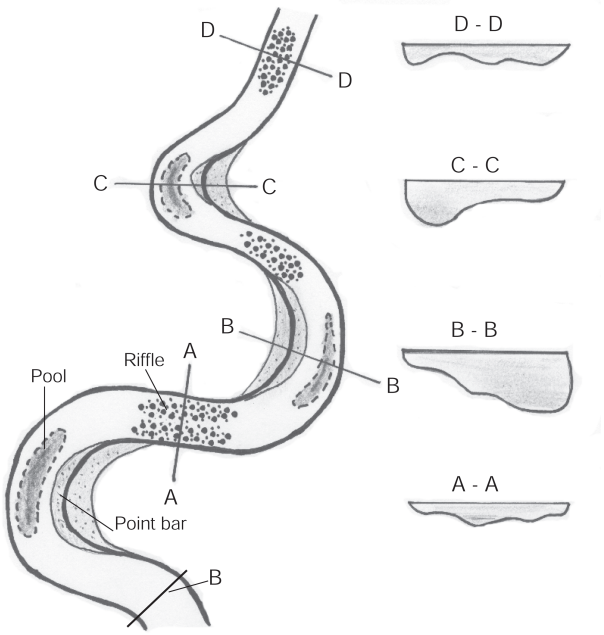

Figure 2.3: Pool riffle sequences in a developing meander system (Mount, 1970), modified

Figure 2.3 illustrates the mechanism of meander bend formation. While the concave bank is continously eroding laterally and vertically due to the increased shear stress produced by the spiral motion, a point bar is formed at the convex river bank. Here the local velocites decrease and the sediment particles tend to settle down. Looking at cross section $C - C$ in Figure 2.3, for example, one can see the deeply eroded part at the concave river bank and the shallow water with the point bar on the convex river bank. Such formation is characteristic for transversal bed topography in a meander bend. The cross sections $B - B$ and $D - D$ in Figure 2.3 illustrate the bed topography in a cross-over section. Here, the water depth is very low and the river bed is characterized by a riffle sequence.

2.2 Planform of alluvial river systems

Rivers are in motion all the time. Several channel classifications broadly characterize the general differences in channel patterns and processes. In general, one can say that river or stream channel patterns can be grouped into two general classes, single channels and multichannel channels. Based on that statement, different researchers having classified various river channel patterns. Leopold and Wolman (1994) quantitatively differentiated straight, meandering and braided channel patterns based on relationships between the slope and discharge. Schumm (1977) classified alluvial channels based on the dominant modes of sediment transport and recognized three geomorphic zones within a watershed. Mollard (1973), and later Church (1992) and Hütte et al. (1994) classified floodplain rivers into a continuum of channel patterns related to differences in discharge, valley slope, sediment supply and channel stability.
Figure 2.4 shows different possible planforms of alluvial channels according to Hütte et al. (1994). The valley slope and the sediment transport capacity are considered to have the main influence on the planform development. In the upper reaches of a river system where the highest valley slopes occur, the channel tends to stay straight. Depending on the bed material, the channel morphology will be characterized by step pool or multi-bar sequences. With decreasing valley slope, the channel starts to develop alternate bars and consequently meander

bends. However, if the transport capacity is too low for the incoming sediment load, braided structures develop.

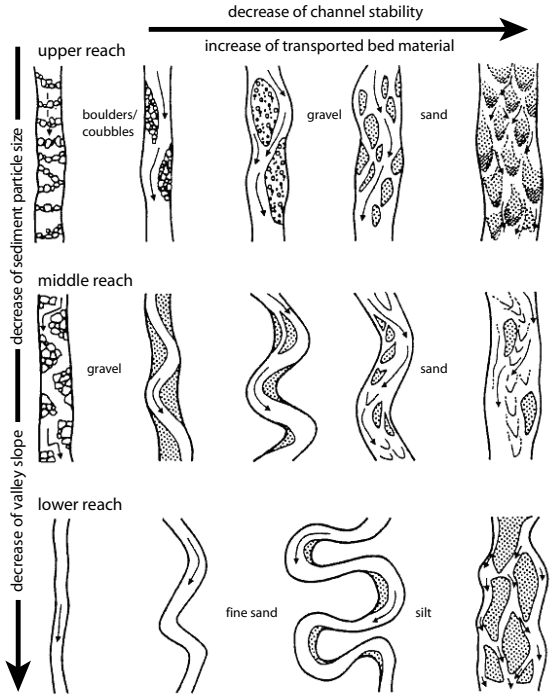

Figure 2.4: Planform evolution of alluvial channels (Hütte et al., 1994)

2.3 Initiation and migration of meander bends

The formation and migration of river meanders is a very interesting and challenging problem. In hydraulic engineering it is of fundamental importance to understand the mechanisms controlling the water flow and the sediment transport causing the meander phenomenon in an alluvial channel. Why rivers tend to meander is still a subject of debate. It is known that if a single channel is not forced to stay straight like a regulated rivercourse, the river tends to meander. The arguments revolve around the view that meandering is a response

to either external force mechanisms, such as discharge, sediment supply and watershed characteristics, or internal mechanisms, such as flow separation and the development of vortices. The wavelength and amplitude of meanders within

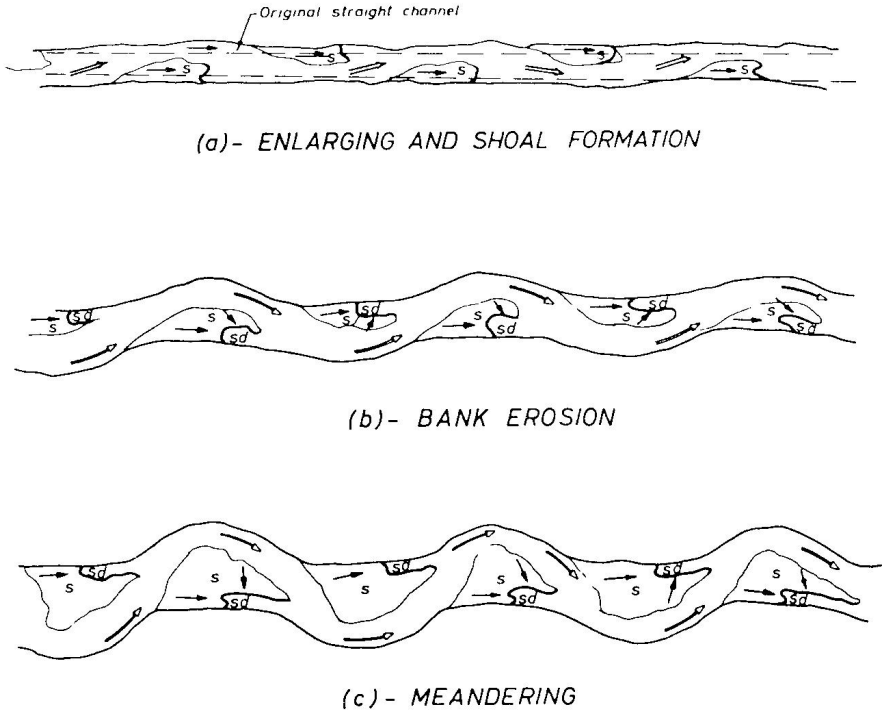

Figure 2.5: Initiation of meandering, *shoals s and stagnant water areas sd* (Ackers and Charlton, 1970)

rivers are clearly non-random. They can be correlated to the overall load, discharge and gradient of the valley. Thus meandering must be associated with the attempt of the river to handle its load and balance its energy expenditure. However, all of these adjustments in energy expenditure and load transport are initiated by the natural tendency of flow to be deflected or diverted by even the smallest inhomogeneities. These disturbances might be induced by turbulent secondary currents. According to (Yalin and da Silva, 2001) the secondary currents are composed of eddies which arise due to the friction of the water body to its boundaries. Flowing downstream, they increase up to the size of the external dimensions of the channel. At this stage the secondary currents are bursting. The released energy initializes erosion and starts forming the

river bed. At a particular flow condition the flow pattern tends to change from the flat river bed to the formation of alternate bars. These bars cause local scour in the riverbed at the outer region of the channel bend. The bar depth can be equivalent to several percentage of the channel width (Jäggi, 1984). In

Figure 2.6: Meandering river system with cut-offs. ©GoogleEarth

channels with fixed banks, the bar formation and the scour development tend towards a stable riverbed condition. Whereas in channels with movable river banks, pushed or hindered by local inhomogeneities in either the river bed or bank, the scour develops horizontally and erodes the banks (Ikeda, 1984). Once these phenomena occur, the flow becomes accelerated and hits the opposite bank further downstream to continue eroding the river banks. The interplay of erosion and deposition serves to exaggerate the curves in the stream channel to form long and looping bends, termed meanders. This process is illustrated in Figure 2.5. In conclusion, the driving force behind the initiantion of meandering is a mixture of external and internal processes.

Once the meander bends are fully developed, one can observe two typical phenomena of channel migration. First there is the meander cut-off. A meander cut-off occurs with a continuously ongoing erosion of the concave river bank. Once the river banks touch each other, the main channel will break through and form a new rivercourse. This leaves the cut-off meander bend beside the bank of the new rivercourse. The cut-off anabranch usually forms a still water area

and enhances the biodiversity of the river reach. In Figure 2.6 one can see a section of a river reach in eastern Russia. The river is flowing from right to left and the darker parts illustrate water with considerable depth. Above the main channel one can see three major meander bends that have recently been cut off the main channel (dark loops). In addition one can see the former paths of the main channel.

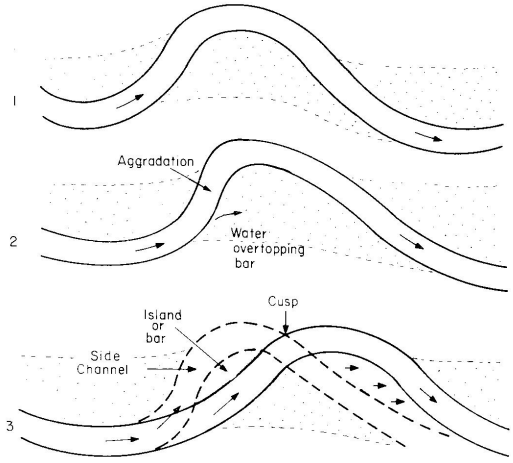

Figure 2.7: Schematic view of a meander shift. (Schumm et al., 1987)

The second phenomenum in meandering river systems is the so-called meander shift (Figure 2.7). Normally there are two types of movement in a meander pattern on a floodplain. The first is a meander sweep, which is a progressive downstream shift of the whole pattern. The second is the meander swing. This is the lateral movement of the channel back and forth across the valley. Both types of river behavior are well known and have been described by Davis (1902). In the investigation by Edgar (1973) and Zimpfer (1975) the meandering thalweg pattern also tended to develop and migrate in a uniform manner. However, certain bends deviated from this uniform manner. A scalloped form of the concave bank in plan was caused by an abrupt downstream shift in the thalweg through the bend. This in turn caused a downstream shift of the thalweg bend apex in the next bend downstream and formed bars and cusps at the edge of the floodplain.

The previously mentioned physical based phenomena have to be described numerically in order to predict sediment transport in fluvial hydraulics by the means of a 3D numerical model. The equations and algorithms are based on analytical, empirical or semi-empirical approaches. The following chapter summarizes the approaches which are used in the scope of this dissertation.

Chapter 3

3D modeling of fluid flow and sediment transport

3.1 Flow modeling

3.1.1 Governing equations

The law of conservation of mass states that mass can neither be destroyed nor created, but it can only be transformed by physical, chemical or biological processes. All mass flow rates into a control volume through a control surface are equal to all mass flow rates out of the control volume plus the time change in mass inside the control volume. The law of conservation of momentum describes the motion of a flow particle at any time at a given position in the flow field. Together they are the governing equations for the calculation of the three-dimensional flow field. The so-called Reynolds averaged Navier-Stokes equations for incompressible, fully turbulent flow, including the continuity (3.1) and momentum (3.2) equations are written as follows.

$$\frac{dU_i}{dx_i} = 0 \tag{3.1}$$

$$\frac{\partial U_i}{\partial t} + U_i \frac{\partial U_i}{\partial x_i} = \frac{1}{\rho}\frac{1}{\partial x_i}(-P\delta_{ij} - \rho\overline{u_i' u_j'}) + \frac{f_i}{\rho} \tag{3.2}$$

U is the velocity averaged over time t, x is the spatial geometrical scale, ρ is the water density, P is the pressure, δ_{ij} is the Kronecker delta and u is the velocity

fluctuation over time during one time step δt. The last term of Eq. (3.2) includes the turbulent stresses being modeled with the Boussinesq approximation (3.3)

$$\overline{u_i' u_j'} = \nu_t \left(\frac{\partial U_i}{\partial x_j} + \frac{\partial U_j}{\partial x_i} \right) - \frac{2}{3} k \delta_{ij} \tag{3.3}$$

Here, k is the turbulent kinetic energy and ϵ its dissipation rate. k is calculated with Eq. (3.4).

$$k = \frac{1}{2} \overline{u_i' u_i'} \tag{3.4}$$

In Eq. (3.3) the turbulent eddy viscosity ν_t is unknown and has to be modeled by a turbulence model described in Subsection 3.1.3.

3.1.2 Discretization

The transient term in Eq. (3.2) was modeled by an implicit method. When the difference in space is computed the question arises about whether the values of time step j or $j+1$ should be used. If the values of time step j are used then it is called an explicit method and otherwise one speaks of an implicit method. The implicit one is more stable so that longer time steps can be used, whereas the explicit method is easier to code.
The variable in the convective term in Eq. (3.2) is found by the help of the finite volume method. The main idea of the finite control volume method is to transform the partial differential equation into a new equation where the variable in one cell is the function of the variables in the surrounding cells.

$$c_P = \frac{a_W c_W + a_E c_E + a_N c_N + a_S c_S}{\sum a_{nb}} \tag{3.5}$$

$$\text{with} \qquad \sum a_{nb} = a_W + a_E + a_N + a_S \tag{3.6}$$

where a_{nb} are weighting factors and c the variable in the center cell P and in each of the surrounding cells. The indices W, E, N, S for west, east, north and south, show the location of the neighboring cell. In a three-dimensional case the indices B and T for bottom and top are added. Other equations for the coefficients a_{nb} must be found to solve Eq. (3.5). This is done by applying the continuity of water flow to the control volume. If one considers the surface area as A, velocity

normal to its surface, as U, the concentration as c and the turbulent diffusion coefficient as Γ, one can find the convective and the diffusive fluxes through surface A (Figure 3.1). The flux through A from the west side, for example, is then the sum of both and is written like the following

$$F_W = U_W A_W c_W + \Gamma_W \frac{A_W(c_W - c_P)}{\partial x} \tag{3.7}$$

Considering all the fluxes through the sides of a given volume, their sum has to be zero. With this term one can derive the equations for the coefficients a_{nb} and solve Eq. (3.5). It is possible either to use the first order or second order difference

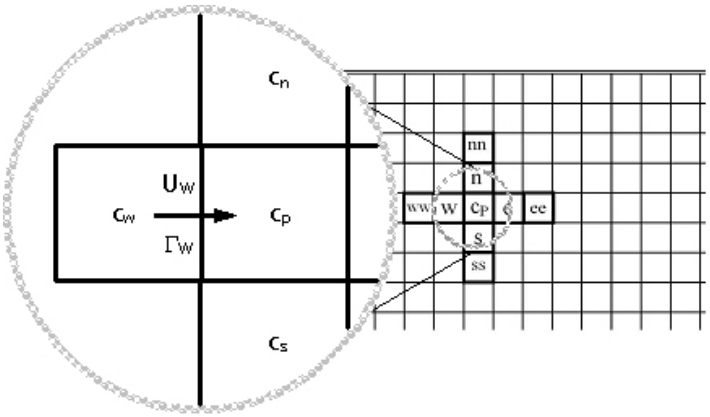

Figure 3.1: Plan view of the computational domain

schemes. The first order upwind method, the power-law scheme (POW) uses the information of the six surrounding cells to find the new value. The method of second order accuracy, second order upwind scheme (SOU), uses the twelve surrounding cells. The POW is known to be more inaccurate when calculating the convective fluxes. However it is easier to code, needs less computer power and is known to give stable performance.

3.1.3 Turbulence

Most flows which occur in practical river-, environmental- and sediment engineering are of a turbulent nature. This means that irregular fluctuations are superimposed on the main motion. Turbulence has disorder, performs efficient

mixing and transport and has vortices irregularly distributed in all three spatial dimensions. The large eddies are the main carriers of kinetic energy in the fluctuations. They obtain their energy from the mean motion. In a cascade process they decay and pass on their energy to several small eddies. At these smaller scales of motion, energy is dissipated by the action of viscosity, i.e. a transfer from mechanical energy to molecular energy. This observation is of great importance for numerical modeling of turbulence. To resolve these effects, a very fine grid is required increasing the computational time dramatically. Consequently the small-scale motion is modeled with a certain turbulence closure scheme. The stress term $\overline{u_i' u_j'}$ on the right-hand side of Eq. (3.2) represents the fluctuation part of the velocities. They cause an enhanced turbulent momentum transport and are called the Reynolds stresses. To solve these unknowns in order to calculate the turbulence, the equations must be supplemented by additional equations. This lack of equations is called a closure problem and therefore the Reynolds stresses must be connected with the mean flow quantities. This is done by using the Boussinesq approximation (3.3). This concept suggests that in analogy to Newton's second law, the turbulent stresses are proportional to the mean velocity gradients. For general flow situations, the turbulent stresses may be expressed as Eq. (3.3).

Here, $\nu_t(x, y, z, t)$ is not a physical property and not a constant value, but rather a function of position and time, i.e. it depends on the flow under consideration. Consequently, the distribution of ν_t across the flow field must be estimated. From a dimensional analysis (Rodi, 1980), the eddy viscosity is proportional to the following parameters

$$\nu_t \propto \rho \hat{U} L \tag{3.8}$$

where $\hat{U}$ is a velocity scale and L characterizes the large-scale turbulent motion. The distribution of these scales can be approximated reasonably well in many flows. The calculation of ν_t from the given parameters is then realized by the k-ϵ turbulence closure. The k-ϵ model is a two equation model. With the expression

$$\nu_t = c_\mu \frac{k^2}{\epsilon} \tag{3.9}$$

the two unknowns in Eq. (3.8) are replaced by transport equations for k and ϵ and consequently the equation system is closed (Rodi, 1980). The values for k

and ϵ are calculated by the following two equations.

$$\frac{\partial k}{\partial t} + U_i \frac{\partial k}{\partial x_i} = \frac{\partial}{\partial x_i}\left[\left(\nu + \frac{\nu_t}{\sigma_k}\right)\frac{\partial k}{\partial x_j}\right] + P_k - \epsilon \tag{3.10}$$

$$\frac{\partial \epsilon}{\partial t} + U_i \frac{\partial \epsilon}{\partial x_i} = \frac{\partial}{\partial x_i}\left[\left(\nu + \frac{nu_t}{\sigma_\epsilon}\right)\frac{\partial \epsilon}{\partial x_j}\right] + C_{\epsilon 1}\frac{\epsilon}{k}P_k - C_{\epsilon 2}\frac{\epsilon^2}{k} \tag{3.11}$$

The production of turbulent kinetic energy P_k is defined as:

$$P_k = \nu_t \frac{\partial U_i}{\partial x_j}\left(\frac{\partial U_j}{\partial x_i} + \frac{\partial U_i}{\partial x_j}\right) \tag{3.12}$$

Since ν_t is equal in all directions, the turbulence is isotropic. Even though the k - ϵ turbulence model is known for its universal area of application, its isotropy can be a drawback for some complex geometries.

3.1.4 Pressure and water surface elevation

Due to the fact that the pressure in the Navier-Stokes equation is unknown, it has to be calculated by an additional algorithm. This algorithm is summarized in the *SIMPLE*-Method (Patankar, 1980). *SIMPLE* stands for Semi-Implicit Method for Pressure Linked Equations. As there is no explicit equation for the distribution of the pressure, the convergence and stability of a numerical solution of flowing incompressible fluids depends largely on how pressure gradients and velocities are evaluated in the equation of mass and momentum. The main idea is to guess a value for the pressure and use the continuity defect to obtain an equation for the pressure correction used in the next time step. When the pressure correction is then added to the pressure, water continuity is satisfied.
The pressure distribution is non-hydrostatic so that the water surface shows an authentic gradient when flowing through channel bends. In the numerical solution, the difference in vertical elevation of the surface cell was based on the pressure gradient. The free surface was computed by first solving the differential equation.

$$\frac{\partial z}{\partial x} = \frac{1}{\rho g}\frac{\partial P}{\partial x} \tag{3.13}$$

The pressure P in (3.13) is determined by an equation similar to Eq. (3.5). The variable P in one cell is a function of the pressure in the neighboring cells. The equations are solved iteratively.

3.1.5 Boundary conditions

As shown in Subsection 3.1.1, unknown variables in the cell center are determined as a function of the variables in the surrounding cells. However, there are cells in the computational domain having no neighbor, i.e. they are defined as boundary cells. Instead of getting information from a neighboring cell, boundary conditions have to be defined at the following locations in the computational domain:

- inflow
- outflow
- water surface
- wall

The following variables have to be identified with boundary conditions:

- velocities U_x, U_y, U_z
- turbulence variables k and ϵ
- pressure P

The outflow boundary as variables have a zero-gradient boundary condition i.e. they were set equal to the values of the cell next to the cells at the outflow. Variables at the inflowing boundary were defined by a Dirichlet boundary condition, i.e. the variables are set to a certain value. At the water surface, U_x, U_y, P and ϵ have zero gradient boundary conditions. U_z is set to a certain value and k is equal to zero, respectively. For all variables at the wall boundary, the wall law functions for rough boundary, introduced by Schlichting (1979) were used

$$\frac{U}{u^*} = \frac{1}{\kappa}\left(\frac{30y}{k_s}\right) \tag{3.14}$$

where u^* is the shear velocity, k_s the bed or wall roughness. In the default configuration the model computes the bed roughness as a function of the grain size distribution on the river bed. This worked well in cases where the roughness is dominated by influence of the grain form. In cases where fine bed material prevailed and bed roughness is affected by bed forms such as dunes and ripples

better results were obtained by using the following approach. First the bed form height Δ was calculated with Eq.(3.15) developed by van Rijn (1984c). The value mainly depended on the water depth y, the characteristic sediment grain d_{50} and the prevailing shear stress τ.

$$\frac{\Delta}{y} = 0.11 \left(\frac{d_{50}}{y}\right)^{0.3} \left(1 - e^{-0.5\left(\frac{\tau-\tau_{c,s}}{\tau_{c,s}}\right)}\right) \left(25 - \left(\frac{\tau - \tau_{c,s}}{\tau_{c,s}}\right)\right) \tag{3.15}$$

where $\tau_{c,s}$ is the critical shear stress for each fraction. Then the bed form height is converted into bed roughness k_s with the following equation.

$$k_s = 3.0 d_{90} + 1.1\Delta \left(1.0 - e^{\left(\frac{-25\Delta}{7.3y}\right)}\right) \tag{3.16}$$

The bed forms calculated by Eq.(3.15) were not assumed to be equally distributed over the cross section. This resulted in a varying roughness in the plan form.

3.2 Sediment transport modeling

3.2.1 General

There are basically two transport modes. Particles can be transported in suspension and as bed load, respectively. According to van Rijn (1984a) there is a third transport mode, but this is neglected here. Each particle size has a certain critical shear stress. Once it is exceeded, the particle moves. The Hunter-Rouse number defined in Eq. (3.17) determines whether the particle moves along the bed as bed load, or floats in the water body being transported as a suspended load.

$$z = \frac{w}{\kappa u_*} \tag{3.17}$$

where w is the particle fall velocity, κ a constant equal to 0.4 and u_* the shear velocity of the main flow. If z is larger than unity, the particle is mainly transported as bed load. The fall velocity is larger than the force of the turbulence preventing the particle from sinking. Accordingly, if z is smaller than unity, the particles are in suspension. Considering the computational domain illustrated in Figure 3.2 one can define where the two sediment transport modes are calculated. The

figure shows a longitudinal cut through a computational domain on a structured grid. Space is discretized in n-number of cells in the vertical direction. The white area including the hatched cells is named real computational domain. Water and sediment transport are calculated here. The light grey and dark gray shaded areas are named the virtual computational domain and are divided into an active and inactive sediment layer. The role of these two layers will be discussed in the following paragraphs. First the focus is on the real computational domain. The hatched area are the cells closest to the bed where bed load transport is calculated. The method is explained in subsection 3.2.2.1. The cells above are defined for suspended load transport calculation, described in subsection 3.2.2.2.

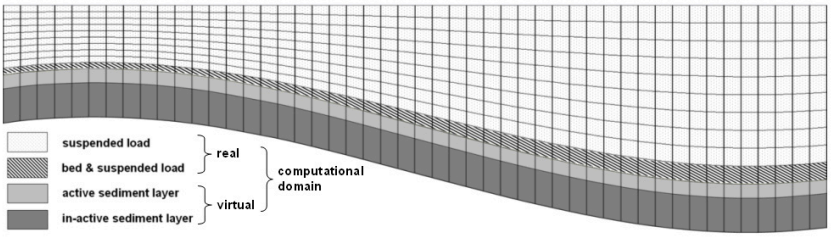

Figure 3.2: Longitudinal cut through the computational domain

3.2.2 Mass of sediment transport

3.2.2.1 Bed load calculation

As mentioned in the previous chapter, bed load transport is calculated in the hatched area of Figure 3.2. In this area the cells are close to the bed. The amount of bed load was calculated by an equation of van Rijn (1984a).

$$\frac{q_{bed,i}}{{d_i}^{1.5}\sqrt{\frac{g(\rho_s-\rho_w)}{\rho_s}}} = \eta \frac{T_i^{1.50}}{D_{*,i}^{0.3}} \tag{3.18}$$

where η is by default set to 0.053, T_i is the transport stage parameter for each particle size i defined in the following equation,

$$T_i = \left(\frac{\tau - \tau_{crit,i}}{\tau_{crit,i}}\right)^{1.50} \tag{3.19}$$

and $D_{*,i}$ the particle parameter for each particle size i defined as

$$D_{*,i} = d_i \left(\frac{(\rho_s/\rho_w - 1)g}{\nu^2} \right)^{1/3} \tag{3.20}$$

Eq. (3.18) is applied to each sediment size i and the calculated masses $q_{bed,i}$ are transferred to concentrations via Eq.(3.21).

$$c_{bed,bedload,i} = \frac{q_{bed,i}}{aU_{bed}} \tag{3.21}$$

Where a is a reference hight equal to half the height of the first cell and U_{bed} is the velocity in the first cell close to the bed.
The boundary conditions for the sediment transport computations were a user-specified value at the upstream boundary and zero gradients for the outlet and the sides.

3.2.2.2 Suspended load calculation

The suspended load is computed with the convection-diffusion equation. For non-transient transport processes the equation reads as follows

$$U_i \frac{\partial c}{\partial x_j} + U_i \frac{\partial c}{\partial x_j} = \frac{\partial}{\partial x_j} \left(\Gamma \frac{\partial c}{\partial x_j} \right) \tag{3.22}$$

where U_i is the velocity, c the concentration, w the fall velocity and Γ the diffusion coefficient. On the left-hand side of Eq.(3.22) are the convective terms and on the right-hand side the diffusive one. Eq.(3.22) is solved with the control volume approach (Eq.(3.5)) in a similar way to how Eq.(3.2) is solved. Due to its partial differential origin, boundary conditions are needed. The concentration at the inlet is set to a certain user defined value, for the outlet and the sides the boundary conditions are symmetric and at the water surface the concentration is set to zero. The boundary condition for the bed is given by Eq.(3.23). This is an empirical formula (van Rijn, 1984b), determining the reference concentration of suspended sediment load close to the bed, i.e. in the cells closest to the bed.

$$c_{bed,suspendedload,i} = 0.015 \frac{d_i}{a} \frac{T_i^{1.50}}{D_{*,i}^{0.3}} \tag{3.23}$$

where T_i and $D_{*,i}$ are defined by Eqs.(3.19) and (3.20), respectively. The coefficient a is a reference height equal to half the height of a cell.

3.2.2.3 Calculation of the bed changes

The bed changes were computed from sediment continuity for the bed cell, as the difference between the inflowing and outflowing sediment fluxes. The defect was converted into a vertical bed elevation by dividing it by the submerged density of the sediments (1320 kg/m^3) to find the volume of the deposits for each time step. This was then transformed into bed level changes for the grid. Both the sedimentation and the erosion processes were modeled using the same approach.

3.2.3 Direction of sediment transport

As mentioned in Section 2.1, under certain circumstances, the moving direction of a sediment particle can deviate from the direction of the bed shear stress. The derivation angle Ψ was the topic of several studies throughout the last five decades. Since the pioneering work of van Bendegom (1947) a number of relations are available in the literature to compute the transversal bed load transport. Detailed summaries of the models and the parameters used are given by Odgaard (1981) and Olesen (1987). In the scope of this study, the equation derived by Engelund (1981) was implemented and tested. In this model the drag force was considered to be a function of the relative flow velocity, i.e. the longitudinal drag on a sediment particle was balanced by both the friction and the lift force. The deviation angle Ψ between the sediment transport direction and the near bed flow direction reads

$$\tan \Psi = \frac{0.6}{\sqrt{\Theta'}} \frac{\partial z}{\partial n} \tag{3.24}$$

where $\partial z/\partial n$ is equal to the transversal slope of the channel bed with z equal to the bed elevation and n equal to the radial coordinate. The parameter Θ' is a potential function of the ratio of the prevailing shear stress to the critical one.

$$\Theta' = 0.4\Theta^2 + 0.06 \tag{3.25}$$

3.2.4 Critical shear stress and sloping bed

The critical shear stress is responsible for mobilizing the sediment. This criterion for incipient motion of a sediment particle was calculated according to the Shields (1936) curve. In cases where the sediment particle is exposed to a significant lateral slope, the criterion of incipient motion differs from that for particles on a flat bed. This physical process may have less influence on the bed evolution in a channel bend than the deviation angle of the sediments. However, both processes are related. In the present study a relation by Brookes (1963) was used which reduces the critical shear stress for particles on side slopes. The reduction is expressed with a factor R defined as

$$R = -\frac{(\sin\alpha \sin\beta)}{\tan\Phi} + \sqrt{\left(\frac{(\sin\alpha \sin\beta)}{\tan\Phi}\right)^2 - \cos^2\alpha \left[1 - \left(\frac{\tan\alpha}{\tan\Phi}\right)^2\right]} \tag{3.26}$$

The factor R is a function of β, the angle between the streamline and the direction of the bed shear stress and of α, the transversal slope of the channel bed and a slope parameter Φ, set to the angle of repose of submerged sediments. The critical shear stress coefficient for a particle on a side slope of the size i is then written like Eq. (3.27)

$$\tau^*_{c,i} = R\tau^*_{c,i,0} \tag{3.27}$$

3.2.5 Grain size sorting of sediment transport

The grain size distribution in the bed sediments was developed as a consequence of the particular flow situation in a channel bend. Longitudinal, lateral and vertical sorting processes in river beds can be observed by the presence of graded sediments. It is often observed in natural rivers that the upper layers of a river bed are composed of coarser sediments that protect the finer sediment layers below, a process denoted as armoring. If armoring develops, the top layer of sediments protects the particles below. Consequently there is less movement of the smaller sized fraction for a certain shear stress. In order to take this effect into account, a hiding and exposure coefficient is defined (Buffington and Montgomery, 1997; Egiazaroff, 1965). The hiding and exposure factor in Eq.(3.29) is multiplied by the critical shear stress for each sediment size

resulting in a corrected shear stress for each particle size (Eq.(3.28)).

$$\tau^*_{c,i} = \xi_i \tau^*_{c,i,0} \tag{3.28}$$

$$\text{with} \qquad \xi_i = \left(\frac{d_i}{d_{50}}\right)^P \tag{3.29}$$

According to Buffington and Montgomery (1997), there is no universal exponent P. The value has to be determined for the certain flow characteristic. Kleinhans and van Rijn (2002) proposed using different values of P for each individual grain size. In this study the best results were obtained with the exponent P set to the constant value of P=-0.3.

When fractional transport was computed, sorting mechanisms were considered by the definition of an exchange layer, denoted as the active layer (Figure 3.2), where the sediment continuity equation was solved separately for each fraction. Default configuration keeps the height of the active layer constantly equal to the size of the largest grain in the sediment mixture. The size of the inactive layer is set to a large value in order to supply the active layer with the sufficient amount of sediments. The grain distributions in the two bed layers were obtained by considering the sediment continuity for each fraction. If deposition occurred, each fraction f_a in the active layer was computed as:

$$f_a = \frac{f_{a,0} z_a + f_d z_d}{z_a + z_d} \tag{3.30}$$

where z_a is the height of the active layer, z_d is the height of the deposition, f_a and f_d denote the fractions in the active layer and of the deposited material, respectively. Because the vertical magnitude of the active layer remained constant, material had to be transferred to the inactive layer.

$$f_i = \frac{f_{i,0} z_i + f_d z_d}{z_i + z_d} \tag{3.31}$$

where the index i denotes the inactive layer. Erosion processes were treated in an analogous manner.

3.3 Grids and wetting and drying

The choice of the spatial discretization method is strongly dependent on the application case. In this study both structured and unstructured grids with tetra- and hexahedral cells were used. Fluvial geometries with fixed sides were computed on structured grids. These grids are adaptive in the vertical direction but not in the horizontal one. The left-hand side of Figure 3.3 shows an example of a structured grid. A structured grid is characterized by the fact that each cell center has a fixed index number, described by the indices i, j, k.

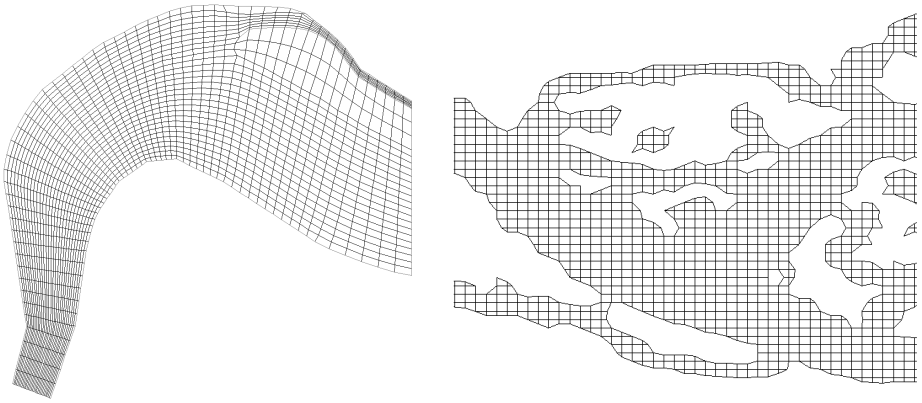

Figure 3.3: Examples of a structured (left) and unstructured grid (right)

Unstructured grids are mainly used in case of computing lateral movement of a fluvial domain (see Section 4.5). Each cell has a number which varies over compuational time, depending on the change of the grid. To allow changes in the bed morphology mainly in the lateral direction, the CFD program included an algorithm for wetting and drying (Olsen, 2003). This algorithm generated new cells in areas where erosion took place and let cells disappear where sediment was deposited. Consequently the grid changed its shape and size over time as the geometry was formed. Initially, the computational domain was allocated to a two-dimensional grid which determined the area where lateral changes could happen. Once a two-dimensional cell was activated, i.e. wetted, it was discretized with a certain amount of cells in the vertical direction. This number depended on the depth in the computational domain. The criterion for the formation or disappearance of a cell was correlated to a certain minimum water depth ζ_1 at

the four corners of each cell. A second value, ζ_2 was the responsible criterion for the formation of just one cell over the depth. Meaning, in areas with $\zeta_1 \leq y \leq \zeta_2$ only one cell was used and if $y \leq \zeta_1$ or $\zeta_1 \geq y$ cells will dry up or be wetted, respectively.

Chapter 4

Summary of the scientific papers

The results of the application of the numerical model to different test cases are published in peer-reviewed articles for scientific conferences and journals. The following chapter gives a short summary of each of the articles. Further details can be found in the article itself, in the appendix of the dissertation. All articles are dealing with modeling of sediment transport in channel bends. They differ in terms of their complexity in geometry, physical processes or both.

4.1 Paper I

3D computation of sediment transport at water intakes

For the present investigation suspended sediment concentrations in a water reservoir were calculated. The purpose of the study was to investigate how the CFD model would perform on a geometry with a non-moving bed and evaluate the model capabilities when solving the convection /diffusion equation for sediment concentrations in flow in channel bends.

Appropriate sediment control at water intakes is one of the primary goals of their design. The storage volume of any sedimentation chamber downstream has to last as long as possible and also the turbines must be protected from the incoming

sediments. The design of an intake has traditionally been refined by carrying out physical model studies. It has recently become more popular to improve the design process using the results from a three-dimensional numerical model study (Demny et al., 1998; Khan et al., 2004). The use of a three-dimensional model instead of a two-dimensional depth average one is strongly recommended since the change in sediment concentration in the vertical direction is the key aspect when designing a water intake and an appropriate sediment excluder.
In the present study, a general computational fluid dynamics (CFD) program was used to predict the flow field and the sediment transport at the Kapunga water intake in Tanzania. The results from the numerical model were verified using observed performance ratios at the water intake. A performance ratio was calculated from the sediment concentration in the river upstream of the intake and the sediment concentration at the water intake. The results from the numerical model and the field measurements were also compared to the results of an earlier numerical model study in which the commercial CFD program *PHOENICS* had been used.

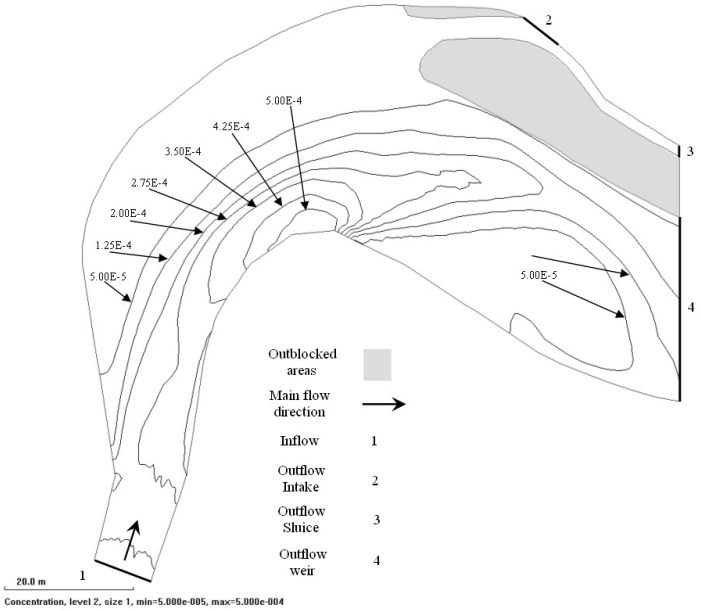

Figure 4.1: Distribution of the sediment concentration at Kapunga water intake

The investigations showed that the three-dimensional model presented in this study was able to calculate the distribution of sediment concentration in a river

reach at an intake. The calculated performance ratios at the Kapunga water intake showed an accuracy of 15 - 20 % when compared with the measurements. Sensitivity tests showed that using a higher discretization scheme improved the results significantly more than using a finer grid. In fact the use of the second order upstream scheme instead of the first order method, reduced the average deviation by about 8 %, whereas the doubling of the number of grid cells improved the result by only about 3%. When using the combination of these two measures, the best results were obtained. The study also showed that the results are not very sensitive to the variation of the bed roughness. E.g. Figure 4.1 shows the distribution of the calculated sediment concentration at the grid level close to the reservoir bed.

4.2 Paper II

Three-dimensional modeling of sediment transport in a narrow 90° channel bend

The purpose of this study was to test the capability of the model when calculating transient bed deformation in a channel bend. The geometry was chosen to be considerably small in order to avoid long computational time. Due to the fact that the radius of curvature was small the model had to be enhanced with algorithms taking into account the effect of steep side slopes on sediment transport.

A three-dimensional numerical model was used for calculating the velocity and the bed level changes over time in a 90° bended channel. The model was enhanced with relations for the movement of sediment particles on steep side slopes in river bends. Located on a transversally sloping bed, a sediment particle has a lower critical shear stress than on a flat bed. Also, the direction of its movement deviates from the direction of the shear stress near the bed. These phenomena are considered to play an important role in the morphodynamic process in sharp channel bends. Calculated velocities as well as bed changes over time were compared to data from a physical model study.
The comparison showed that in cases where the transversal slope is relatively

steep, it is not sufficient to use a sediment transport algorithm where the direction of transported sediment particles is identical with that of the bed shear stress. An appropriate formula describing the deviation angle of the direction of sediment movement as a function of the side slope was implemented in the model and tested against physical model data. Figure 4.2 showed that the calculated bed changes showed good agreement with the measurements.

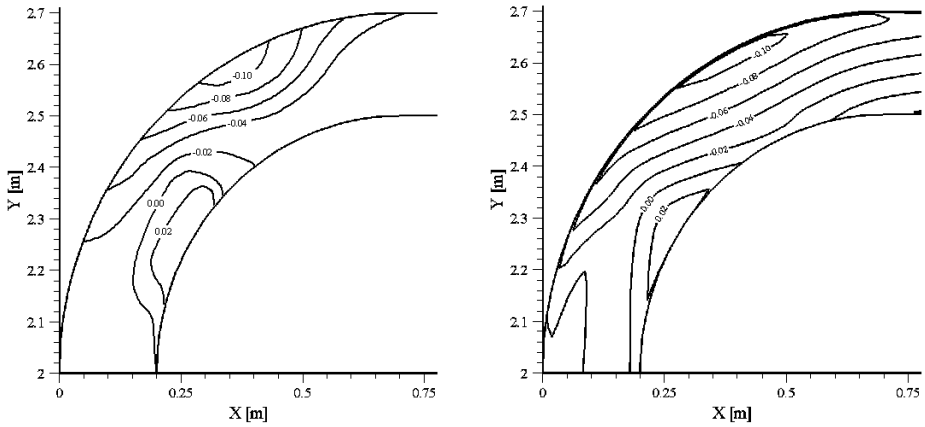

Figure 4.2: Measured (left) and calculated (right) bed changes in [m]

4.3 Paper III

Three-dimensional modeling of bed deformation and sorting processes in a channel bend with unsteady flow

Paper II showed that calculation of sediment transport in channel bends is possible in principle. Another channel bend was chosen as a test case to verify and prove this capability. In addition, fractional sediment transport and an unsteady flow regime were tested to enlarge the application range of the model.

A fully three-dimensional non-hydrostatic model was applied to compute the flow and morphodynamic processes in a laboratory flume. The laboratory experiments provided data for bed deformation and grain sorting processes in a 180° channel

bend. The data were used for validating the numerical model applying three different sediment transport approaches. A formula for uniform sediments was compared with two advanced non-uniform sediment transport formulas that considered the interaction between individual grain sizes by defining hiding-exposure approaches. Figure 4.3 shows an example of a three-dimensional view of the calculated bed deformation in the 180° channel bend.

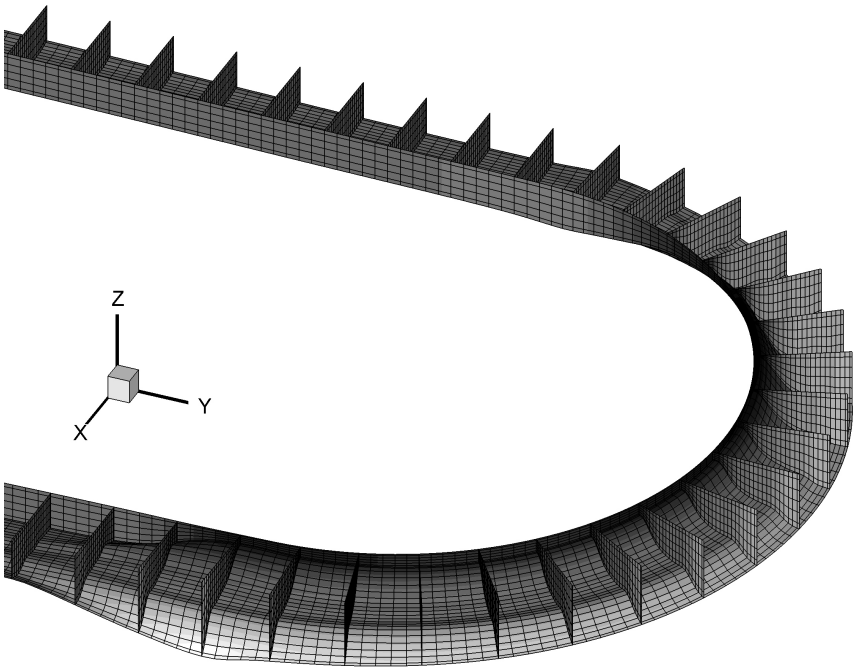

Figure 4.3: 3D view of the simulated bed deformation

Results showed that the three-dimensional model is able to predict bed deformations and sorting processes in the laboratory bend with the correct magnitude and trend when using the default configuration. However, the computed results considerably overestimated the bar evolution. Computed results improved significantly when applying any of the two non-uniform sediment transport approaches. The best results were obtained when the absolute values of the hiding-exposure exponents were reduced for both approaches. The results of the non-uniform approaches showed less sorting intensity and smaller bar heights, both giving a better fit to the measured data. The computed results of the non-uniform approaches in comparison with the default configuration represent the physical

mechanisms of the hiding-exposure effect well. The superior agreement with compared to the default approach shows that these mechanisms ocour in nature and that they significantly influence the bed deformation and sorting processes. Both non-uniform approaches predicted the total sediment transport with satisfactory agreement.

4.4 Paper IV

3D modeling of transient bed deformation in a sine-generated laboratory channel with two different width to depth ratios

In the following the model capabilities were tested when calculating sediment transport in channels with subsequent bends and width-to-depth ratios occurring in large natural rivers.

A three-dimensional numerical model is presented to calculate the sediment transport rate and the corresponding transient bed changes in sine-shaped meandering laboratory channels. The transient flow pattern as well as bed movements in simple bended laboratory channels have been successfully modeled with 2D and 3D numerical models before. However, when it comes to the successive formation of meander bends, the spatial propagation of the helical flow and its effect on the bed deformation is still under research. It is strongly dependent on the deflection angle Θ of the meander bend and the width-to-depth ratio of the channel. In addition to this geometric characteristic, bed forms were prevailing in the experiments. The numerical model was enhanced with a roughness approach taking into account the presence of bed forms.
The present study showed that the transient bed changes of a meandering laboratory channel with two different width-to-depth ratios have been successfully modeled. The calculated bed changes were in good agreement with the measurements in both cases. Figure 4.4 shows the comparison of the measured and the calculated bed changes for the width-to-depth ratio B/h=10.67. However, the results were sensitive to the formulas for bed form height and bed roughness. The roughness approach seemed to be strongly connected to the development stage of

a bed form and therefore to the sediment transport capacity. In the opinion of the authors more research is needed for the universal implementation of a roughness approach taking bed form roughness into account. Furthermore, a wider range of the width-to-depth ratio should be tested in order to validate the present results. It seems that the width-to-depth ratio has a greater influence on the bed pattern in meandering channels than it is suggested in literature today. In addition, the model should be tested on data from experiments with different deflection angles Θ before any reliable conclusion can be drawn.

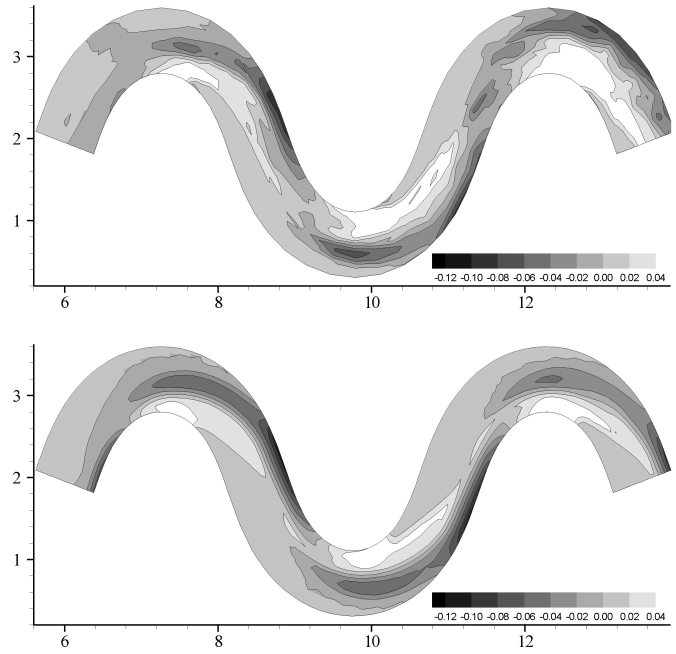

Figure 4.4: Plan view of the measured (top) and calculated (bottom) bed changes in [m]

4.5 Paper V

Modeling free-forming meander evolution in a laboratory channel using three-dimensional computational fluid dynamics

The previously mentioned tested and verified capability of the model were applied to see how the numerical code performed when predicting free-forming meander evolution from an initially straight channel without upstream perturbation and sediment feed.

The present paper investigated the use of CFD in predicting the formation, development and migration of free-forming meander bends. The three-dimensional CFD model computed water flow and sediment transport in alluvial channels and predicted vertical and horizontal bed changes. Different algorithms and parameters were tested to provide an insight into the application range of CFD when modeling free-forming meander formation. The simulation was started from an initially straight grid, with neither sediment feed nor any perturbation at the inflow boundary. The model computed the river bed evolution over a real time period of three days. The results were compared with laboratory experiments.

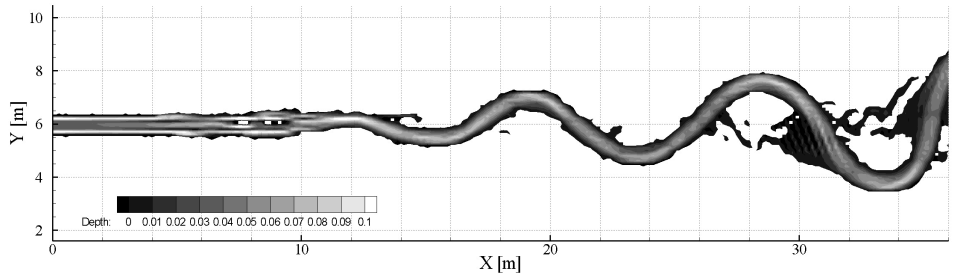

Figure 4.5: Calculated meander evolution, depth in [m].

The results matched the measurements of a physical model study concerning the meander amplitude and downstream growth of the meander bends. The maximum meander wavelength was underestimated by around 15 %. In addition, the helical flow and the characteristic river bed development in a meander bend

could be identified in the numerical simulation. Consindering the present case the results showed that using CFD functions well for modeling of free-forming meander formation. The simulated meander evolution is illustrated in Figure 4.5. Figure 4.6 shows the comparison of the measured and calculated centerlines, respectively. However, the investigations showed that the model has to be tested in other cases, too, in order to obtain a universal predictor for meander formation in alluvial channels. More complex bank erosion algorithms may need to be developed especially when applying the model to natural cases where the bank material is influenced by cohesion and vegetation.

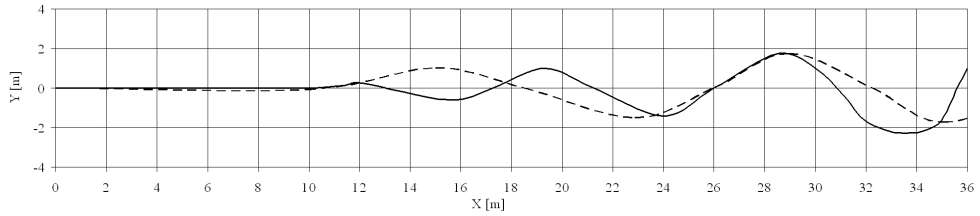

Figure 4.6: Measured (dashed) and calculated (solid) centerlines of the channel, all measurements in [m].

Chapter 5

Conclusions and recommendations

5.1 Conclusions

The present research was designed to test and improve the capability of a numerical model when predicting erosion and deposition processes in fluvial geomorphology. By the means of a computational fluid dynamics model for simulation of three-dimensional water flow and coupled sediment transport, various algorithms and parameters were implemented and investigated to provide an insight into the capabilities of the numerical model. Five test cases were documented with different topics in the field of sedimentation engineering and fluvial geomorphology. The conclusions drawn from this study are summarized in the following points.

- **3D flow computation**
  Sediment transport in channel bends is strongly influenced by secondary currents. Therefore it is of major importance to predict the so-called helical flow precisely. The presented model is fully 3D and is able to predict the helical flow in channel bends without using empirical approximations.

- **Free surface calculation**
  The presented model has a non-hydrostatic pressure distribution. The simulations were sucessfully carried out with the computation of the free water surface.

- **Simulation of transient bed changes in channel bend during steady and unsteady flow**
  The transient bed changes in a narrow sharp 90° and a 180° channel bend were succesfully modelled. The model could simulate the typical point bar and local scour evolution in both channels. The bed changes in the 180° channel bend were computed for an unsteady flow regime.

- **Simulation of physical proccesses in fluvial geomorphology**
  The presented model was able to simulate the transport of multiple sediment sizes and the corresponding sorting mechanisms. The calculation of the sediment transport direction was achieved with full success. The resulting point bar and local scour development matched the measured values very well. In addition, the model was able to simulate alternate bar development, initiation of meandering, meander bend migration, meander cut-offs and meander-shifts.

5.2 Recommendations for further research

Modeling sediment transport by the means of a CFD model is a highly complex topic. The following issues require further work:

- **Computation of alluvial roughness**
  Modeling alluvial roughness is extremely complex and dynamic. More research has to be done in the field of measuring the initiation growth, movement and the influence of bed forms on the flow field. Today, such numerical implementation is limited and still under development.

- **Computation in shallow areas**
  The accuracy of the simulated results is strongly dependend on the stability performance of the numerical model. The presented model showed some limitations and drawbacks especially when dealing with unstructured grids in combination with the modeling of wetting and drying processes. It is a matter of great interest to solve these problems in future investigations.

- **Turbulence modeling**
  As discribed in Subsection 3.1.3, in the presented model the turbulence

is modeled with the standard k-ϵ model. This standard model is well known for its universal application range and its performance. However, the standard k-ϵ model has two major drawbacks. On the one hand there is a slight over-estimation of the kinetic energy in some cases. This leads to an over-estimation of the shear stress and consequently the sediment transport capacity is over-estimated.
On the other hand, the turbulence modeled by the standard k-ϵ model is isotropic. That means the eddy viscosity ν_t is equal in all three directions. This might lead to retarded development of the helical flow especially in channels with more than two subsequent channel bends.

In conclusion, one can say that the presented model can be considered to be a research tool for sediment transport phenomena in channel bends. Although the widespread application range proves its universal character, the code has to be applied to other similar cases. Future investigations could show how far it is possible to use this model as a prediction tool in sedimentation engineering practice.

References

Ackers, P. and Charlton, F. G. (1970). *Experiments on small streams in alluvium, Rept. 77*. HR Wallingford, Oxfordshire, UK.

Bendegom, L. (1947). Some flow considerations on river morphology and river improvements. *De Ingenieur, (in Dutch; English translation available as translation 1054, National Research Council of Canada, 1963)*, 59(4):B1–B11.

Brookes, H. N. (1963). Discussion of Boundary shear stress in curved trapezoidal channels' by A. T. Ippen and P. A. Drinker. *Journal of Hydraulic Engineering*, 89(3):327–333.

Buffington, J. M. and Montgomery, D. R. (1997). A systematic analysis of eight decades of incipient motion studies, with special reference to gravel-bedded rivers. *Water Resources Research*, 33(8):1993–2029.

Church, M. (1992). Channel morphology and typology. In *The River Handbook by P. Carlow and G.E Petts*, pages 126–143, Blackwell, Oxford, UK.

Darby, S. E., Alabyan, A. M., and de Viel, M. J. V. (2002). Numerical simulation of bank erosion and channel migration in meandering rivers. *Water Resources Research*, 38(9):1136–1175.

Davis, W. M. (1902). River terraces in New England. *Museum of comparative Zoology*, 38:281–346.

Demny, G., Rettemeier, G., Forkel, C., and Köngeter, J. (1998). 3d-numerical investigation for the intake of a river run of power plant. In *Proceedings of the 3rd International Conference on Hydroinformatics*, pages 1331–1338, Copenhagen, Denmark.

Duan, J., Wang, S. S. Y., and Jia, Y. (2001). The applications of the enhanced cche2d model to study the alluvial channel migration process. *Journal of Hydraulic Research*, 39(5):1–12.

Edgar, D. P. (1973). *Geomorphic and hydraulic properties of laboratory rivers, Unpublished M.S. thesis*. Colorado State University, Fort Collins, Col.

Egiazaroff, I. V. (1965). Calculation of non-uniform sediment concentrations. *Journal of Hydraulic Division*, 91(HY4):225–247.

Engelund, F. (1981). The motion of sediment particles on an inclined bed. *Prog. report 53, Inst. for Hydrodynamic and Hydraulic Engineering, Tech. University of Denmark, Copenhagen, Denmark*.

Guo, Q. C. and Jin, Y. C. (1999). Modeling sediment transport using depth-averaged and moment equations. *Journal of Hydraulic Engineering*, 125(12):1262–1269.

Hütte, M., Bundi, U., and Peter, A. (1994). *Konzept für die Bewertung und Entwicklung von Bächen and Bachsystemen im Bereich Kanton Zürich*. EAWAG, Zürich, Switzerland.

Ikeda, S. (1984). Prediction of alternate bar wavelength and height. *Journal of Hydraulic Engineering*, 110(4):371–386.

Ikeda, S., Parker, G., and Sawai, K. (1981). Bend theory of river meanders, 1. linear development. *Journal of Fluid Mechanics*, 112:363–377.

Jäggi, M. N. R. (1984). Formation and effects of alternate bars. *Journal of Hydraulic Engineering*, 110(2):142–156.

Johannesson, H. and Parker, G. (1989). Linear theory of river meanders. In *River Meandering, Water Resources Monograph, Vol.12*, pages 181–213, AGU, Washington D.C. edited by S. Ikeda and G. Parker.

Khan, L. A., Wicklein, E. A., Rashid, M., Ebner, L. L., and Richards, N. A. (2004). Computational fluid dynamics modelling of turbine intake hydraulics at a hydropower plant. *Journal of Hydraulic Research*, 42(1):61–69.

Kleinhans, M. G. and van Rijn, L. (2002). Stochastic prediction of sediment transport in gravel sand-gravel bed rivers. *Journal of Hydraulic Engineering*, 128(4):412–425.

Leopold, L. B. and Wolman, M. G. (1994). *River channel patterns: braided, meandering and straight.* U.S. Government Printing Office, Washington D.C., USA.

Minh Duc, B., Wenka, T., and Rodi, W. (2004). Numerical modeling of bed deformation in laboratory channels. *Journal of Hydraulic Engineering*, 130(9):894–904.

Mollard, J. D. (1973). Air photo interpretation of fluvial features. In *Proceedings of the Canadian Hydrology Symposium, National Research Council*, Ottawa, Ontario, Canada.

Mosselman, E. (1998). Morphological modelling of rivers with erodible banks. *Hydrological Process*, 12:1357–1370.

Mount, J. F. (1970). *California rivers and streams. The conflict between fluvial process and land use.* University of California, California, USA.

Neary, V. S., Wright, S. A., and Bereciartua, P. (2001). Case study: Sediment transport in proposed geomorphic channel for napa river. *Journal of Hydraulic Engineering*, 127(11):901–910.

Odgaard, A. (1981). Transverse slope in alluvial channel bends. *Journal of Hydraulic Division*, 107(12):1677–1694.

Odgaard, J. A. and Bergs, M. (1988). Flow processes in a curved alluvial channel. *Water Resources Research*, 24(1):45–56.

Olesen, K. W. (1987). Bed topography in shallow river bends. *Doctoral Thesis, Delft University of Technology, the Netherlands.*

Olsen, N. and Skoglund, M. (1994). Three-dimensional numerical modeling of water and sediment flow in a sand trap. *Journal of Hydraulic Research*, 32(6):833–844.

Olsen, N. B. O. (1999). Two-dimensional numerical modelling of flushing processes in water reservoirs. *Journal of Hydraulic Research*, 37(1):3–16.

Olsen, N. R. B. (2003). Three dimensional CFD modeling of self-forming meandering channel. *Journal of Hydraulic Engineering*, 129(10):366–372.

Olsen, N. R. B. (2004). *Hydroinformatics, fluvial hydraulics and limnology.* Department of Hydraulic and Environmental Engineering, The Norwegian University of Science and Technology, Trondheim.

Olsen, N. R. B. and Kjellesvig, H. M. (1999). Three-dimensional numerical modelling of bed changes in a sand trap. *Journal of Hydraulic Research*, 37(2):189–198.

Olsen, N. R. B. and Kjellesvig, H. M. (2000). Three-dimensional numerical flow modelling for estimation of maximum local scour depth. *Journal of Hydraulic Research*, 36(4):579–590.

Parker, G., Sawai, K., and Ikeda, S. (1982). Bend theory of river meanders, 2. nonlinear deformation of finite amplitude bends. *Journal of Fluid Mechanics*, 115:303–314.

Patankar, S. V. (1980). *Numerical Heat transfer and fluid flow*. Taylor and Francis Publishers, Rotterdam.

Rodi, W. (1980). *Turbulence models and their application in hydraulics*. A. A. Balkema, Rotterdam.

Schlichting, H. (1979). *Boundary layer Theory*. McGraw-Hill Book Company, New York.

Schumm, S. A. (1977). *The fluvial system*. John Wiley Sons, Inc., New York.

Schumm, S. A., Mosley, M. P., and Weaver, W. E. (1987). *Experimental fluvial geomorphology*. John Wiley Sons, Inc., New York.

Shields, I. A. (1936). Anwendung der Ähnlichkeitsmechanik und der turbulenzforschung auf die geschiebewegung. *Mitteilungen der Preussischen Versuchsanstalt*, 26.

Sun, T., Meakin, P., and Jossang, T. (2001a). A computer model for meandering rivers with multiple bed load sediment sizes 1. theory. *Water Resources Research*, 37(8):2227–2241.

Sun, T., Meakin, P., and Jossang, T. (2001b). A computer model for meandering rivers with multiple bed load sediment sizes 2. computer simulations. *Water Resources Research*, 37(8):2243–2258.

van Rijn, L. (1984a). Sediment transport part i: Bed load transport. *Journal of Hydraulic Engineering*, 110(10):1431–1456.

van Rijn, L. (1984b). Sediment transport part ii: Suspended load transport. *Journal of Hydraulic Engineering*, 110(11):1613–1641.

van Rijn, L. (1984c). Sediment transport part iii: Bed forms and alluvial roughness. *Journal of Hydraulic Engineering*, 110(12):1733–1754.

Wu, W., Rodi, W., and Wenka, T. (2000). 3D numerical modelling of flow and sediment transport in open channels. *Journal of Hydraulic Engineering*, 126(1):4–15.

Wu, W. and Wang, S. (2004). Depth-averaged 2D calculation of flow and sediment transport in curved channels. *Journal of Sediment Research*, 19(4):241–257.

Yalin, M. S. and da Silva, A. M. F. (2001). *Fluvial processes*. IAHR, Delft.

Yen, C. and Lee, K. (1995). Bed topography and sediment sorting in channel bend with unsteady flow. *Journal of Hydraulic Engineering*, 121(8):591–599.

Zeng, J., Constantinescu, G., and Weber, L. (2005). A fully 3d non-hydrostatic model for prediction of flow, sediment transport and bed morphology in open channels. In *Proceedings of the 31st IAHR Congress*, pages 1327–1338, Seoul, South Korea.

Zimpfer, G. L. (1975). *Development of laboratory channels, Unpublished M.S. thesis*. Colorado State University, Fort Collins, Col.

Synopsis

Paper I
3D computation of sediment transport at water intakes
N. Rüther, J.M. Singh, N.R.B. Olsen, E. Atkinson
*Procceedings of the Institution of Civil Engineers,*Vol. 158, WM1

Paper II
Three dimensional modeling of sediment transport in a narrow 90° channel bend
N. Rüther, N.R.B. Olsen
*Journal of Hydraulic Engineering,*Vol. 131, 10

Paper III
Three dimensional modeling of bed deformation and sorting processes in a channel bend with unsteady flow
T. Fischer-Antze, N. Rüther, N.R.B. Olsen, H. Gutknecht
In Review: Journal of Hydraulic Engineering

Paper IV
3D modeling of transient bed deformation in a sine-generated laboratory channel with two different width-to-depth ratios
N. Rüther, N.R.B. Olsen
Proceedings of the third International Conference on Fluvial Hydraulics, River Flow 2006, Lisbon, Portugal

Paper V
Modelling free-forming meander evolution in a laboratory channel using three dimensional computational fluid dynamics
N. Rüther, N.R.B. Olsen
In Review: Geomorphology

Appendix A

Scientific Papers

Paper I

3D computation of sediment transport at water intakes

N. Rüther, J.M. Singh, N.R.B. Olsen, E. Atkinson

ICE, Procceedings of the Institution of Civil Engineers,
Vol. 158, WM1

Proceedings of the Institution of Civil Engineers
Water Management 158
March 2005 Issue WM1
Pages 1–8

Paper 13849
Received 11/05/2004
Accepted 17/11/2004

Keywords:
hydraulics & hydrodynamics/ mathematical modelling/river engineering

N. Ruether
PhD candidate,
The Norwegian University of Science and Technology, Trondheim, Norway

J. M. Singh
Deputy Director, NEA Engineering Services, Kathmandu, Nepal

N. R. B. Olsen
Professor, The Norwegian University of Science and Technology, Trondheim, Norway

E. Atkinson
Independent Consultant, Henley-on-Thames, Oxon, UK

ice

3-D computation of sediment transport at water intakes

N. Ruether, J. M. Singh, N. R. B. Olsen and E. Atkinson

The three-dimensional numerical computational fluid dynamics computer program SSIIM was used to predict the flow field and the sediment transport at the Kapunga water intake in Tanzania. It solved the Reynolds-averaged Navier–Stokes equations in three dimensions to compute the water flow and used the finite-volume method as the discretisation scheme. The model was based on a three-dimensional, non-orthogonal, structured grid with a non-staggered variable placement. The k–ε model was used to predict the turbulence and the SIMPLE method to compute the pressure. The suspended sediment transport was calculated by solving the convection–diffusion equation with the bed boundary condition provided by an empirical formula for the reference concentration. The results from the numerical model were verified using observed performance ratios at the water intake. These ratios were calculated from the sediment concentrations in the river upstream of the intake and passing into the water intake. The computed performance ratios corresponded well with those derived from field measurements. Sensitivity tests showed that the use of a fine grid in combination with a second-order upstream scheme gave the best results. Varying the bed roughness showed that the results were not unduly sensitive to the method used to determine that parameter. The results from the SSIIM model and the field measurements were also compared to the results of an earlier numerical model study in which the commercial computational fluid dynamics program PHOENICS had been used.

NOTATION

∂	partial differential operator
c	sediment concentration
c_a	reference concentration at the bed
d_{50}	sediment size where 50% is smaller
E	entrainment rate
$\boldsymbol{g}$	acceleration due to gravity
j	direction in tensor notation
k	turbulence kinetic energy
k_s	equivalent sand roughness height
PR	performance ratio
$\boldsymbol{u}$	Reynolds-averaged water velocity
$\boldsymbol{u}^*$	shear velocity
$\boldsymbol{V}$	velocity in x-direction
$\boldsymbol{w}$	sediment fall velocity
x	x-direction
y	y-direction
z	z-direction
Γ	turbulent diffusion coefficient
ε	turbulence energy dissipation rate
$\boldsymbol{\nu}$	kinematic viscosity of water
ρ_s	density of sediment
ρ_w	density of water
$\boldsymbol{\tau}_0$	prevailing bed shear stress in N/m^2
$\boldsymbol{\tau}_c$	Shield's shear stress number

1. INTRODUCTION

Appropriate sediment control at water intakes is one of the primary goals of their design. The storage volume of any sedimentation chamber downstream has to last as long as possible and, in the case of a hydro power plant, the turbines must be protected from the incoming sediments. The design of an intake has traditionally been refined by carrying out physical model studies. It has recently become more popular to improve the design process using the results from a three-dimensional (3-D) numerical model study. Applying computational fluid dynamics (CFD) in this field of engineering can improve the final design and accelerate the design process.[1] Demny *et al.*[2] also used CFD to investigate modifications at the trash rack of a water intake. The use of a 3-D model instead of a two-dimensional (2-D), depth-averaged one is strongly recommended as the change in sediment concentration in the vertical direction is the key aspect when designing a water intake and an appropriate sediment excluder. By ignoring the third dimension a model can not be used to test alternative designs for separating water from sediments near the intake. Another advantage of a 3-D model in comparison with a 2-D, depth-averaged one is in the prediction of the secondary currents.

The topic of the present study is the use of a 3-D numerical model to predict the suspended sediment distribution in the flow approaching a water intake. Intake performance can be assessed by a performance ratio PR, defined by equation (1)

$$PR = 1 - \frac{\text{Concentration in intake canal}}{\text{Concentration in the river upstream of the intake}} \quad (1)$$

A performance ratio of unity indicates the maximum possible sediment exclusion, whereas a performance ratio of zero

indicates no concentration reduction between the river and the canal. A performance ratio less than zero indicates that an intake is aggravating sediment concentrations. Within this study, measurements at the Kapunga water intake in Tanzania are compared with the results from two independent 3-D numerical models. First, Atkinson[3] simulated the distribution of the sediment concentration at Kapunga (and an intake in the Philippines) using the commercial 3-D software package PHOENICS. Second, and it forms the focus of this study, the software package called SSIIM[4] was applied to the Kapunga intake. SSIIM had already been tested by modelling sediment flow in a sand trap[5,6] as well as modelling flushing processes in a reservoir.[7]

The aim of the investigation was therefore to test the model on more complex geometries and to give recommendations for the further use of CFD in this field of engineering.

2. THE KAPUNGA WATER INTAKE

The Kapunga water intake supplies the primary canal of the 3800 ha Kapunga Rice Project in southern Tanzania (Fig. 1). The design capacity of the water intake is 4·6 m^3/s. Water is drawn from the Great Ruaha River which typically has a discharge in the wet season ranging from 15 to 50 m^3/s. Flood peaks rise above 200 m^3/s in some years. The riverbed material consists of sand, gravel and cobbles, but the material in transport has been found to consist largely of fine sand and silts. The average grain size distribution observed for the suspended bed material load and the bed material is illustrated in Fig. 2. The d_{50} sizes of the bed material and the suspended bed material load are 1·2 mm and 0·18 mm, respectively.

The head works were designed by Sir William Halcrow and Partners, using the principle of a curved channel sediment excluder and the design was refined using a physical model study. As water flows round a bend in a channel, secondary currents are set up which direct the flow towards the inside of the bend at the bed of the channel, and towards the outside of the bend at the surface. Thus, if an intake is sited on the outside of a bend, the sediment-laden water close to the bed of the channel is excluded. The Kapunga intake is located on the outside of a natural bend which has been stabilised using training works. Further sediment control is provided by a curved sluice channel, as shown in Fig. 1. The outflow from the head works structures is divided between the water intake, the sluice outflow and the flow over the weir. Table 1 shows the discharges for each of these outflows for the five occasions when measurements were taken.

3. DATA

Atkinson[8,9] presents measurements of sediment concentrations at the Kapunga water intake. A detailed set of measurements at the intake was taken to quantify its performance in excluding sediment. The field observations were carried out during the wet season, from February to May in 1991 and in 1992. The geometry of the river bed was taken at the cross-sections shown in Fig. 1. Flow and sediment load were monitored in the river at about 160 m upstream from the weir, in the sluice channel and at the water intake. Sediment concentrations were measured using a pump sampling technique. The measurements were performed at up to seven verticals across the river and up to four heights at each vertical. Both the mean velocity and concentration were obtained by fitting measured values to theoretical profiles and then by integrating. Analysis of these data enabled the sand exclusion performance of the intake to be assessed. The results are listed in Table 2. The performance ratio was found to vary in the range 0·42 – 0·79.

4. THREE-DIMENSIONAL SIMULATION OF SEDIMENT TRANSPORT

4.1. Numerical model PHOENICS

Atkinson[3] presented a numerical model study predicting the sediment exclusion at the intake. The simulations were carried

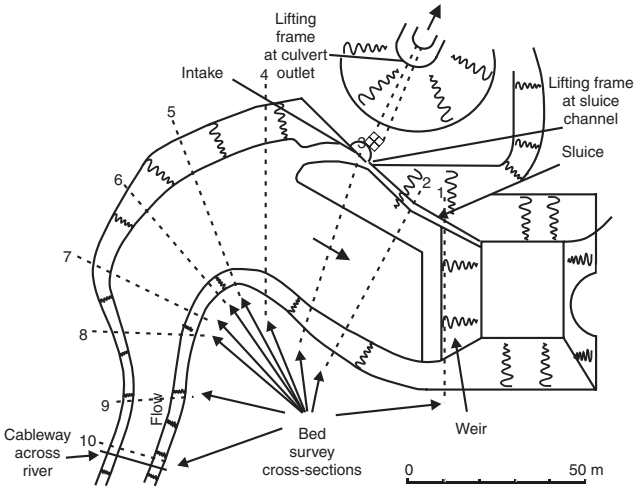

Fig. 1. Plan view of the Kapunga intake; measurement positions of discharge and sediment concentrations are marked by the dotted frame

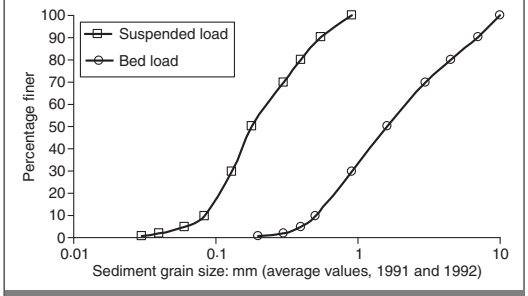

Fig. 2. Grain size distribution

out using the commercial program PHOENICS adapted for the simulation of sediment transport. PHOENICS is a general-purpose CFD package for simulating a wide range of fluid flows. It is based on the Navier–Stokes equation solved on a 3-D grid. To simulate the turbulence Atkinson used the k–ε model. In the case of the Kapunga intake the bed roughness was set to an equivalent roughness height calculated beforehand from an alluvial friction predictor. The sediment transport was simulated by treating each size fraction as a concentration in the flow with settling velocity imposed as a simple downward flux proportional to the local concentration. The boundary condition for the simulation of sediment concentration was assumed to be a function of the bed shear stress following equation (2)

$$E = k\boldsymbol{\tau}^{a} \quad (2)$$

where the entrainment rate is denoted by E, the bed shear stress by $\boldsymbol{\tau}$ and k is a constant. The value of constant a was in the range 1·0–2·5 to give more accurate results.[10] A representative set of conditions was simulated by the model and equation (2) was used to set the entrainment rate.[11] The coefficient k was then determined by calibration: the value of k was set so that the mean concentration predicted by the model was equal to the mean concentration at those conditions predicted by a sediment transport prediction formula. The ratio of the diffusion coefficient to the eddy viscosity, the factor β, was set using the following formula

$$\beta = 1 + 2{\cdot}5\frac{\boldsymbol{w}}{u^*} \quad (3)$$

where $\boldsymbol{w}$ is the sediment fall velocity and u^* is the shear velocity. The calculated performance ratios were compared to the field measurements. The main results are presented in Fig. 6 and listed in Table 3 and will be discussed in detail later in this paper.

	Discharge (m^3/s) in:		
Date	River	Sluice	Intake
08.04.1991	28·40	4·20	0·99
15.05.1991	15·80	6·10	1·22
29.02.1992	40·70	8·00	3·07
16.04.1992	54·70	7·20	2·20
23.04.1992	38·00	4·80	2·96

Table 1. Measured discharges at the Kapunga water intake

4.2. Numerical model SSIIM

The numerical model used in the present study is called SSIIM and is described in detail by Olsen.[12] It solves the Reynolds-averaged Navier–Stokes equations in three dimensions to compute the water flow; the discretisation method employed is the finite-volume method.[4] In CFD there are different numerical methods available to solve the convection diffusion equation on the surfaces of the control volume defined for each computational cell. In the present study, both a first- and a second-order upstream scheme were chosen so that the impact of the calculation method on the results could be tested. A first-order scheme uses linearly interpolated information from only one cell upstream of the cell surface. This procedure converges easily, but can lead to inaccurate results due to the production of false diffusion. Values for the second-order method are calculated using linearly interpolated information from two upstream cells. Although the method involves only the convective fluxes, in theory it should give more accurate results.

For the spatial discretisation, a structured grid with a non-staggered variable placement was used. The k–ε turbulence modelling scheme[13] was used to compute the turbulent viscosity and diffusivity and the SIMPLE method[14] was used to solve for the pressure. The SIMPLE method stands for 'semi-implicit method for pressure-linked equations' and solves the unknown pressure field with an iterative process based on the continuity defect. The suspended sediment transport was calculated by solving the transient convection–diffusion equation (equation (4)) for sediment concentration

$$\frac{\partial c}{\partial t} + \boldsymbol{U}_j\frac{\partial c}{\partial x_j} + \boldsymbol{w}\frac{\partial c}{\partial z} = \frac{\partial}{\partial x_j}\left(\Gamma\frac{\partial c}{\partial x_j}\right) \quad (4)$$

where the Reynolds-averaged water velocity is denoted $\boldsymbol{U}$, the particle fall velocity $\boldsymbol{w}$, the general space dimension x and the vertical dimension z. The diffusion coefficient Γ was set equal to the eddy viscosity taken from the k–ε model. To define the boundary conditions for the suspended sediment concentration, van Rijn's formula[15] (equation (5)) was applied to the cells adjacent to the bed

$$c_a = \frac{0{\cdot}015}{a}\times\frac{d_{50}[(\boldsymbol{\tau}-\boldsymbol{\tau}_c)/\boldsymbol{\tau}_c]^{1{\cdot}5}}{(d_{50}\{[(\rho_S/\rho_W-1)\boldsymbol{g}]/\boldsymbol{\nu}^2\}^{1/3})^{0{\cdot}3}} \quad (5)$$

where a is a reference level set equal to half of the bed form height,[15] d_{50} is the sediment particle diameter, $\boldsymbol{\tau}$ is the shear stress, $\boldsymbol{\tau}_c$ is the critical bed shear stress according to a Shields parameter of 0·047, ρ_S is the density of sediments, ρ_W is the density of water, $\boldsymbol{\nu}$ is the kinematic viscosity of water and $\boldsymbol{g}$ is the gravitational acceleration.

4.3. Configurations and results

The Kapunga intake was modelled with two different grid sizes. The coarse grid is shown in plan on Fig. 3 and consisted of 60 cells in the longitudinal direction and 30 cells in the lateral direction with an average size of 2·5 m by 1·25 m. The fine grid had twice as many cells in both the horizontal directions. In the vertical direction both grids had six equally spaced cells. The 3-D

Discharge Q: m^3/s	Field measurement PR	Coarse grid POW		Coarse grid SOU		Find grid POW		Fine grid SOU	
		PR	±% deviation	PR	±% deviation	PR	±% deviation	PR	±% deviation
15·80	0·48	0·76	37	0·65	26	0·66	27	0·54	11
28·40	0·79	0·87	9	0·83	5	0·82	3	0·77	2
38·00	0·65	0·49	24	0·51	21	0·42	35	0·44	32
40·70	0·57	0·74	23	0·59	3	0·42	26	0·63	9
54·70	0·42	0·53	21	0·54	22	0·38	10	0·50	16
Average	0·58	0·68	23	0·62	15	0·54	20	0·58	14

*All simulations with $d_{50} = 0{\cdot}18$ mm and $k_s = 3 \times d_{90}$.
SOU, second-order upstream method; POW, first-order discretisation method.

Table 2. Performance ratios by field measurements and SSIIM*

simulation of sediment transport with natural geometries can be prohibitively time-consuming. Making some simplifying assumptions can greatly reduce the computation time. In the case of the Kapunga water intake, no bed changes were calculated. This assumption could be made due to the fact that only minor bed changes were observed during the measurement period. Computations for all the five situations listed in Table 1 were carried out to compare the sediment concentrations at the intake with the field measurements. Initially a flat bed with no bed forms was assumed, so according to van Rijn[16] the bed roughness k_s was set to $3 \times d_{90}$ of the bed material. The d_{50} of the transported suspended material was equal to 0·18 mm.[3] The computations were carried out with two different grid sizes and two different discretisation schemes. For the coarse grid with the second-order upstream scheme the computational time was about 30 min on a 3·0 GHz PC depending on the discharge configuration. The computational time was directly proportional to the numbers of grid cells. The difference in computational time between the first- and second-order schemes was very small.

Figure 4 illustrates the velocity vectors at the water surface. The calculations were based on the coarse grid and the second-order upstream scheme for a discharge of $\boldsymbol{Q} = 28{\cdot}4$ m^3/s. According to the figure, the flow is deflected towards the outer part of the bend producing two large recirculation zones. Due to the lack of velocity data, the results of the simulation could not be verified; however, the velocity field produced by the CFD model had been tested previously on an intake,[17] and on an open channel with groynes.[18] In Fig. 5 the sediment concentration close to the bed is given, showing high concentrations in areas of high velocities and lower values in the area of a recirculation zone, where the material tends to settle.

The main results of the computations are illustrated in Fig. 6 and listed in Table 2. In Fig. 6 the performance ratios of the different configurations of SSIIM and those of PHOENICS are plotted against the field measurements. The black line is the line of perfect fit.

Describing firstly the results using the coarse grid of 9000 cells, the calculation of the performance ratios at the Kapunga water intake for five different discharges were calculated using a first-order discretisation method ('POW' in Table 2). The results were in fairly poor agreement with the measurements, except for the river discharge 28·4 m^3/s, where the calculated deviation of 9% was acceptable. In contrast, the calculated results for a discharge of 15·8 m^3/s showed a deviation of up to 37% from the measurement. In order to improve the results, the grid size was doubled in the horizontal direction and a more accurate discretisation was applied. The simulated performance ratios improved with both of these changes but more so with the use of the second-order discretisation scheme. For the first-order scheme with the finer grid the average deviation from the observed ratios was reduced from 23 to 20%. Using the second-

Discharge Q: m^3/s	Field measurement PR	PHOENICS		SSIIM*	
		PR	±% deviation	PR	±% deviation
15·80	0·48	0·73	34	0·54	11
28·40	0·79	0·37	53	0·77	2
38·00	0·65	0·54	17	0·44	32
40·70	0·57	0·50	12	0·63	9
54·70	0·42	0·19	55	0·50	16
Average	0·58	0·47	34	0·58	14

*Fine grid with second-order discretisation scheme, $d_{50} = 0{\cdot}18$ mm and $k_s = 3 \times d_{90}$.

Table 3. Performance ratios by field measurements, PHOENICS and SSIIM

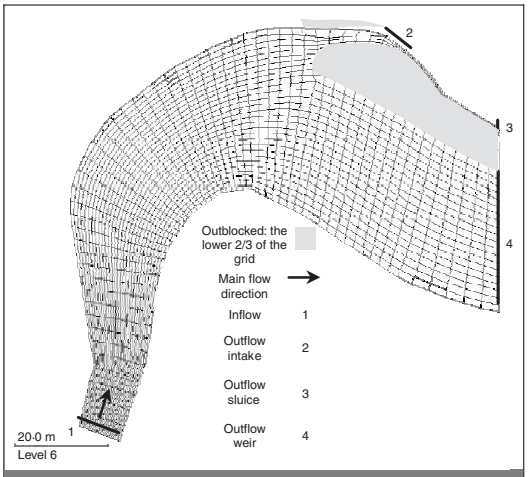

Fig. 3. Numerical grid for the Kapunga water intake

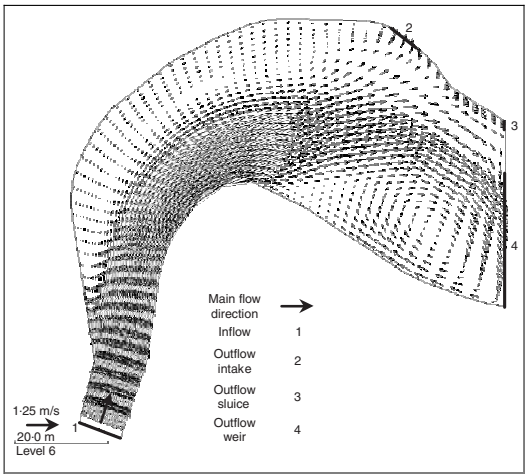

Fig. 4. Velocity vectors at the surface (coarse grid SOU, $Q = 28{\cdot}4\ m^3/s$)

order upstream scheme with the coarse grid caused the deviation to decrease to 15% (Table 2). Further improvement was achieved when the two measures were applied at the same time. The performance ratios then deviated from observation by an average of only 14%. To sum up the results, the values obtained for the best-fitting configuration were compared to the results obtained by Atkinson[3] using PHOENICS. The values are listed in Table 3. It can be seen that, except for the data set with a 38·0 m^3/s river discharge the calculated values by SSIIM fitted the measurements much better. The PHOENICS simulations predicted the performance ratios with an average deviation of 34% whereas SSIIM resulted in an average deviation of 14%.

4.4. Discussion of the results

Use of a fine grid and application of a second-order discretisation scheme should both improve accuracy in a numerical model. The calculation with SSIIM showed that the best results were indeed

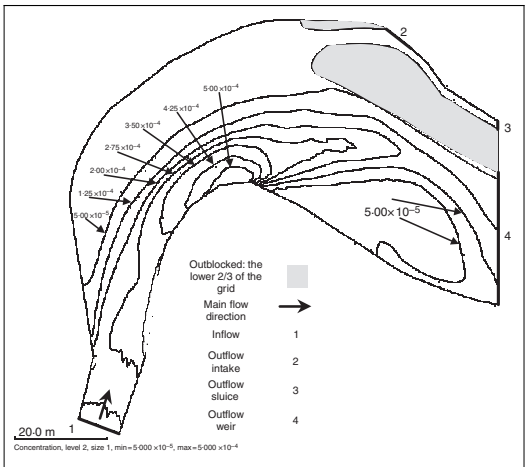

Fig. 5. Sediment concentration close to the bed (coarse grid SOU, $Q = 28{\cdot}4\ m^3/s$)

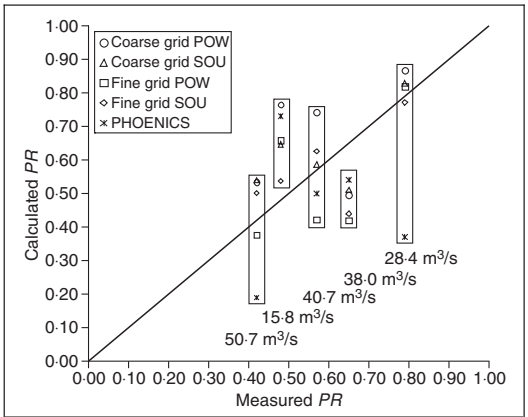

Fig. 6. Performance ratio for the Kapunga water intake

obtained with these improvements. The performance ratios predicted for the different discharges showed agreement with the measurements to within an average deviation of 14%, which is good agreement. It is estimated that the accuracy of the field measurements was about 20%, so the accuracy of the computed results was a good as could be expected.

However the results for $Q = 38{\cdot}0\ m^3/s$ showed a particularly high deviation. No matter which configuration was used, the results deviated by between 21 and 34%. The measurements were taken during 1991 and 1992 where the d_{50} of the transported material showed a range of 0·1 up to 0·3 mm, with an average value of around 0·18 mm. Therefore a sensitivity analysis on the d_{50} value used was carried out. A performance ratio matching the measured value was obtained when a d_{50} of 0·23 mm was chosen instead of the average value of 0·18 mm. It is therefore possible that the large deviation between the measurement and the computations for 38·0 m^3/s was due to uncertainties in the field measurements.

A further sensitivity test on the bed roughness was carried out. The formula for the bed roughness was derived empirically and can vary considerably. Most studies show that the roughness is proportional to the grain diameter. A number of different relationships are presented in the literature. The calculations carried out with SSIIM were based on the bed roughness prediction method given by van Rijn,[16] where the equivalent roughness was set to $3 \times d_{90}$. The parameter test involved changing the roughness value to that given by the formulae of Ackers and White,[19] setting k_s equal to $1{\cdot}25 \times d_{35}$, and of Mahmood,[20] setting k_s equal to $5{\cdot}1 \times d_{85}$. The different roughness algorithms were tested on the coarse grid in combination with the second-order upstream scheme. The results are listed in Table 4 and illustrated in Fig. 7. Here, the performance ratios for the three different bed roughness configurations are plotted for each discharge together with the measured values. In general it can be seen that the results are not unduly sensitive to the uncertainties in the bed roughness value. The average values for the deviation varied from 15 to 19%. Looking at the results in detail in Table 4 one can see that there was an improvement for calculating the 38·0 m^3/s case when using the roughness calculation method of Ackers and White. However, the same approach failed when predicting the

Discharge Q: m^3/s	Field management *PR*	$k_s = 1{\cdot}25 \times d_{35}$*		$k_s = 3 \times d_{90}$*		$k_s = 5{\cdot}1 \times d_{85}$*	
		PR	±% deviation	*PR*	±% deviation	*PR*	±% deviation
15·8	0·48	0·86	44	0·65	26	0·59	19
28·4	0·79	0·88	10	0·83	5	0·80	1
38·0	0·65	0·72	10	0·51	21	0·43	34
40·7	0·57	0·58	2	0·59	3	0·48	16
54·7	0·42	0·59	29	0·54	22	0·49	14
Average	0·58	0·73	19	0·62	15	0·56	17

*Coarse grid with second-order upstream scheme.

Table 4. Performance ratios for different bed roughness

performance ratio for the 28·4 m^3/s river flow. Slight improvements were obtained for 28·4 and 54·7 m^3/s when using the approach by Mahmood, but a general improvement of the results due to the increase or decrease of the bed roughness was not obtained. The average performance ratio showed the best match when using the bed roughness after van Rijn[16] (Table 4).

Some bed forms were observed in the field, affecting the bed roughness. No measurements of the magnitude of the bed forms could be taken. It would be possible to use empirical formulae to compute the bed form height and hence the equivalent bed roughness (for example the formulae given by van Rijn[21]). This would involve considerable uncertainty due to the empirical coefficients employed. The roughness due to the bed forms was therefore not taken into account in the present study. We believe this should be a topic for further studies in CFD modelling of sediment transport in rivers.

5. CONCLUSIONS

The 3-D model presented in this study is able to calculate the distribution of sediment concentration in a river reach at an intake. The calculated performance ratios at the Kapunga water intake showed an accuracy of 15–20% when compared with the measurements. A sensitivity analysis showed that a more accurate discretisation scheme is more important than doubling the number of grid cells. The use of the second-order upstream scheme instead of the first-order method reduced the average deviation by about 8%, whereas the doubling of the number of grid cells improved the result by only about 3%. When using the combination of these two measures, the best results were obtained. The study also showed that the results are not very sensitive to the variation of the bed roughness. Three different approaches were investigated; with regard to the average performance ratio, the method of van Rijn[16] showed the best agreement with the measurements.

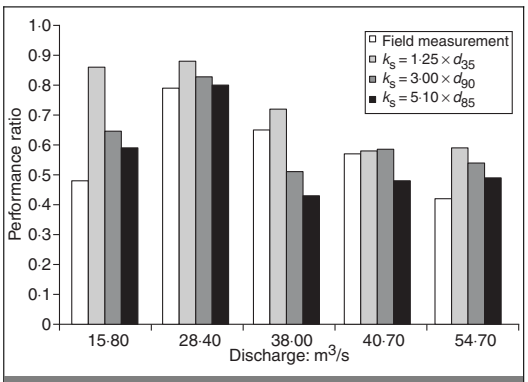

Fig. 7. Calculated performance ratios for different boundary roughness values

6. ACKNOWLEDGEMENTS

The authors would like to acknowledge the funding from the Norwegian Research Council to the first author. The field data were collected by HR Wallingford, UK, in a study funded by the UK Government Department for International Development. The PHOENICS code was used under licence from CHAM Ltd, Wimbledon, UK. In addition the authors acknowledge Manuela Escarameia, Phillip Lawrence and Richard W. P. May at HR Wallingford, UK, for providing data for the present study.

REFERENCES

1. Khan L. A., Wicklein E. A., Rashid M., Ebner L. L. and Richards N. A. Computational fluid dynamics modelling of turbine intake hydraulics at a hydropower plant. *Journal of Hydraulic Research, IAHR*, 2004, **42**, No. 1, 61–69.
2. Demny G., Rettemeier K., Forkel C. and Köngeter J. 3D-numerical investigation for the intake of a river run of power plant. *Proceedings of the 3rd International Conference on Hydroinformatics, Copenhagen, Denmark*, 1998, 1331–1338.
3. Atkinson E. *A Numerical Model for Predicting Sediment Exclusion at Intakes*. Overseas Development Unit, Report OD 130. HR Wallingford, Oxfordshire, UK, 1995.
4. Olsen N. R. B. *Hydroinformatics, Fluvial Hydraulics and Limnology*. Department of Hydraulic and Environmental Engineering, The Norwegian University of Science and Technology, Norway, 2003 (www.bygg.ntnu.no/ ~ nilsol/sib5050/flures5.pdf).
5. Olsen N. R. B. and Skoglund M. Three-dimensional numerical modeling of water and sediment flow in a sand trap. *Journal of Hydraulic Research, IAHR*, 1994, **32**, No. 6, 833–844.
6. Olsen N. R. B. and Kjellesvig H. M. Three-dimensional numerical modelling of bed changes in a sand trap. *Journal of Hydraulic Research, IAHR*, 1999, **37**, No. 2, 189–198.

7. OLSEN N. R. B. Two-dimensional numerical modelling of flushing processes in water reservoirs. *Journal of Hydraulic Research, IAHR*, 1999, **37**, No. 1, 3–16.
8. ATKINSON E. *Measurements at the Kapunga Curved Channel Sediment Excluder, Interim Report*. HR Wallingford, Oxfordshire, UK, 1991, Report OD/TN 60.
9. ATKINSON E. *Measurements at the Kapunga Curved Channel Sediment Excluder, Final Report*. HR Wallingford, Oxfordshire, UK, 1994, Report OD/TN 67.
10. GARCIA M. and PARKER G. Entrainment of bed sediment into suspension. *Journal of Hydraulic Engineering, ASCE*, 1991, **117**, No. 4, 414–435.
11. ATKINSON E., LAWSON J. D. and TOSSWELL P. *Comparison of Physical and Computer Modelling of the Kapunga Intake with Performance of the Prototype*. Overseas Development Unit, ODA, OD/P 121. HR Wallingford, Oxfordshire, UK, 1993.
12. OLSEN N. R. B. *A three dimensional numerical model for simulation of sediment movements in water intakes with multiblock option*, User's manual, 2002 (www.bygg.ntnu.no/ ~ nilsol/ssiimwin/manual3.pdf).
13. RODI W. *Turbulence Models and their Application in Hydraulics*, IAHR, state-of-the-art publication. Balkema, Rotterdam, 1993.
14. PATANKAR S. V. *Numerical Heat Transfer and Fluid Flow*. McGraw-Hill, New York, 1980.
15. VAN RIJN L. C. Sediment Transport Part II: Suspended load transport. *Journal of Hydraulic Engineering, ASCE*, 1984, **110**, No. 11, 1613–1641.
16. VAN RIJN L. C. Sediment Transport Part I: Bed load transport. *Journal of Hydraulic Engineering, ASCE*, 1984, **110**, No. 10, 1431–1456.
17. BOWLES C. B., DAFFERN C. and ASHFORTH-FROST S. An investigation into the flow field at a generalised intake structure using SSIIM: a 3D numerical model, *Proceedings of the ASCE International Water Resources Engineering Conference*, Memphis, TN, 1998, vol. 2, pp. 1114–1119.
18. SEED D. *River Training and Channel Protection—Validation of a 3D Numerical Model*. HR Wallingford, Oxfordshire, UK, 1997, Report SR 480.
19. ACKERS P. and WHITE W. Sediment transport: new approach and analysis. *Journal of Hydraulics Division, ASCE*, 1973, **99**, No. HY, 11, 621–625.
20. MAHMOOD K. *Water Management*. Colorado State University, Fort Collins, CO, 1971, Technical Report No. 11.
21. VAN RIJN L. C. Sediment Transport Part III: Bed forms and alluvial roughness. *Journal of Hydraulic Engineering, ASCE*, 1984, **110**, No. 12, 1733–1754.

Paper II

Three dimensional modeling of sediment transport in a narrow 90° channel bend

N. Rüther, N.R.B. Olsen

*Journal of Hydraulic Engineering,*Vol. 131, 10

Paper II is not included due to copyright.

Paper III

Three dimensional modeling of bed deformation and sorting processes in a channel bend with unsteady flow

T. Fischer-Antze, N. Rüther, N.R.B. Olsen, H. Gutknecht

In Review: Journal of Hydraulic Engineering

THREE-DIMENSIONAL MODELING OF BED DEFORMATION AND SORTING PROCESSES IN A CHANNEL BEND WITH UNSTEADY FLOW

Tim Fischer-Antze[1], Nils Rüther[2], Nils R.B. Olsen[3], M. ASCE, and Dieter Gutknecht[4]

Abstract

A fully three-dimensional non-hydrostatic model was applied to compute the flow and morphodynamic processes in a laboratory flume under unsteady flow conditions. The laboratory experiments provided data for bed deformation and grain sorting processes in a 180° channel bend. The data was used for testing and validating the numerical model by applying three different sediment transport approaches. The original van Rijn formula for uniform sediments was compared with two advanced nonuniform sediment formulas (modified van Rijn and Wu) that considered interaction between individual grain sizes by defining hiding-exposure approaches. The results showed that the default configuration of the model was able to predict bed deformations and grain sorting processes with satisfying magnitude and trend. However, the default approach considerably overestimated the bar evolution. The computed results improved significantly when applying any of the introduced hiding-exposure approaches, representing better the physical processes. For validation, the numerical model was successfully applied on measurements of another laboratory run. This study proves that the three-dimensional numerical model can predict the morphodynamic bed changes and the sorting processes in a channel bend of nonuniform sediments with good agreement.

CE Database Subject Headings:

three-dimensional model, channel bend, sediment transport, channel morphology, particle interactions

---

[1] Research Engineer , Institute for Hydraulic and Water Resources Engineering, Vienna University of Technology, Karlsplatz 13/222, 1040 Vienna, Austria, fischer@hydro.tuwien.ac.at

[2] PhD candidate, Department of Hydraulic and Environmental Engineering, The Norwegian University of Science and Technology, S.P. Andersens vei 5, 7491 Trondheim, Norway, nils.ruther@ntnu.no

[3] Professor, Department of Hydraulic and Environmental Engineering, The Norwegian University of Science and Technology, S.P. Andersens vei 5, 7491 Trondheim, Norway, nils.r.olsen@ntnu.no

[4] Professor, Institute for Hydraulic and Water Resources Engineering, Vienna University of Technology, Karlsplatz 13/222, 1040 Vienna, Austria, gutknecht@hydro.tuwien.ac.at

Introduction

River beds of natural streams can be subject to considerable temporal and spatial changes. Variations in water discharge and water levels cause fluctuations in the sediment transport leading to changes in the morphology of a river. *Knaapen et al. (2001)* distinguishes between planform and bedform dynamics of a river. While the planform describes the shape of a river as seen from the sky, the bedform characterizes the shape of the river bed. The bed can be flat or distorted by a number of more or less rhythmic features. Typical macro bedforms in rivers are bars, they can evolve in straight river reaches as alternate bars or in river bends as point bars. These structures are addressed in this study. The bed sediments grain size distributions develop as a consequence of bed elevation changes. Longitudinal, lateral, and vertical sorting processes in river beds can be observed at the presence of graded sediments. It is often observed in natural rivers that the upper layers of a river bed are composed of coarser sediments that protect the finer sediment layers below, a process denoted as armoring. Morphological changes in rivers, especially when they are caused by river training measures, have a great ecological impact and need to be carefully investigated.

There are many complex physical processes that are responsible for river bed deformations. To a certain degree, natural rivers always exhibit curvature. Therefore a special focus is drawn on processes in river bends in this study. The mechanics of sediment transport in river bends are more complex than in straight channels. The highly nonuniform sediments in a channel bend are subject not only to longitudinal transport but also to transverse transport caused by a spiral motion of the flow induced by secondary currents. Bars build at the inner bank and scours occur at the outer bank. Additionally, the river bed in bends is subject to sorting processes. The secondary currents cause fine material to deposit at the inside of the curves, while erosion takes place at the outer bank, so that the coarser material remains in this region. In combination with bed forms, this effect can cause spatial variation in the roughness of the bed in a bend. There is a direct interaction of flow, sediment transport, and erosion and deposition processes in a bend. The bed changes induced by erosion and deposition affect the flow which in turn influences the distribution of the bed shear stress and thus the bed load component and finally the bed topography. The complex phenomena of flow and morphodynamics in rivers bends have been extensively investigated in literature. Methods to describe or quantify the dynamics are quite diverse. Experimental, numerical and analytical approaches are documented.

Julien & Anthony (2002) investigated sorting mechanisms in a field study in the sharp meander bends of Fall River, Colorado. A model was derived from a three-dimensional moment analysis to account for the effect of particles resting on an embankment inclined at a side slope. The model predicted the longitudinal and

transverse shear stress components and the particle orientation angle that allows an assessment whether a particle moves towards the point bar or the thalweg. Field measurements in two meander bends corroborated the theoretical model: particles finer than d_{50} (1 mm) preferentially moved up the point bar and particles coarser than d_{50} moved towards the thalweg.

In addition to the use of laboratory experiments or field studies, more and more CFD (computational fluid dynamics) models are used to gain insight into the phenomena and processes of complex hydraulics and morphology. Over the last two decades, the computational power has increased tremendously, and CFD models have become progressively more a competitive tool to laboratory experiments. While there is a well-defined state-of-the-art for computing the hydraulics of flows in channels and natural rivers, highly sophisticated computations of sediment transport and associated morphodynamics are still in a state of research. Due to the need of excessive computational resources, especially for multidimensional modeling, the application and development of numerical-morphodynamic models is mainly limited to research institutions. There exists a number of 1D (one-dimensional), 2D (two-dimensional), and 3D (three-dimensional) approaches for the computation of the dynamics of flow and morphology. 1D approaches are well documented but they are inherently limited to 1D flow and sediment transport problems, such as section integrated erosion or deposition processes in a straight river reach. Local bed changes cannot be computed using 1D methods. A widely used alternative to 1D approaches are 2D models, that can predict morphological changes satisfactory when the 3D nature of the processes is of minor importance, such as in many open channel flows, when the width-to-depth ratio is large, so that the vertical velocity component is much smaller than the horizontal components and the pressure distribution is virtually hydrostatic. The advantage of 3D approaches is that many processes in complex river geometries are modeled directly instead of using simplifications. In curved channels, the helical (secondary) flow exists due to the difference between the centrifugal forces acting on the upper and lower layers of the flow. The helical flow plays an important role in the evolution of channel topography. When using a 2D model, it is possible to model morphodynamic processes with a reasonable accuracy in cases with easy geometries including laboratory flume bends. However, an additional number of empirical formulas needs to be introduced with parameters adjusted for the specific situation to account for example for the helical flow effect. These formulas are difficult to apply in a natural river where for example the radius of curvature is not well defined. The strength of a fully 3D model is to predict secondary currents in complex geometries, which are very important when predicting the bed changes in rivers such as flow over groynes and the prediction of the scours in

the vicinity of these. The purpose of this study is to use the present case to test a 3D model that can be used in a general, more complex geometry of a natural river, with formulas only containing general coefficients.

In recent years, several 2D and 3D numerical morphodynamic models have been developed, having the capability to predict bed deformation and in some cases sorting processes for graded sediment mixtures. Multidimensional morphodynamic modeling dates back to the early 1990's. *Spasojevic & Holly (1990)* introduced a 2D unsteady numerical model to compute sediment transport and bed evolution in natural watercourses such as reservoirs, estuaries, and coastal waters accounting for graded sediment transport. The conservation equations were solved using a finite difference method. *Peltier et al. (1991)* established a 2D model applying the k-ε turbulence model. The influence of the bed slope was considered for the computation of the sediment transport capacity. Further development included considerations of nonequilibrium bed-load transport effects (*Jia & Wang (1999)*). *Sloff et al. (2001)* modeled bed composition features in a laboratory flume and a river. Considering side slope effects on the sediment transport rate, spatial variations in roughness, and introducing a bookkeeping system proved to be relevant for the model results. *Minh Duc et al. (2004)* proposed a 2D depth-averaged model using a finite volume method with boundary-fitted grids. The sediment transport module was comprised of semi-empirical models of suspended and non-equilibrium bed load. The secondary flow transport effects were taken into account by adjusting the dimensionless diffusivity coefficient in the depth-averaged k-ε turbulence model. A quasi 3D flow approach was used to simulate the effect of secondary flows due to channel curvature on bed load transport. For the calculation of the bed shear driven resultant bed-load the empirical formulas by *v.Rijn (1984a)* have been used. Among others, the model has been validated by computing the bed changes of the experiments by *Odgaard & Bergs (1988)* and *Yen & Lee (1995)*. The experiments by *Yen & Lee (1995)* were simplified for the numerical model by assuming the sediment to be uniform. As a consequence, the observed sorting processes were not considered by the 2D model. *Wu & Wang (2004)* proposed a 2D depth-averaged model for computing flow and sediment transport in curved channels using the formulas of *Wu et al. (2000b)*. To account for the helical flow effects, a semi-empirical formula was presented to determine the cross-stream distribution of the helical flow intensity in the developed regions of a channel bend. It was used to evaluate the dispersion terms in the depth-averaged 2D momentum equations and suspended load transport equation as well as the bed load transport angle. By adjusting two parameters of the introduced helical flow intensity model, the experiments by *Yen & Lee (1995)* were also used for validation. Here, eight sediment size fractions were used to represent the nonuniform sediment mixture, so that the sediment sorting processes were considered by the model.

A 3D model for the calculation of flow and sediment transport was proposed by *Wu et al. (2000a)*. Suspended load transport was simulated through the general convection-diffusion equation with an empirical settling velocity term. Bed load transport was simulated with a non-equilibrium method and the bed deformation was obtained from an overall mass-balance equation. The empirical formulas by *v.Rijn (1984a)* and *v.Rijn (1984b)* were implemented for the computation of bed and suspended load. The model was not able to account for the effect of transverse bed slope on the bed load transport. The model was tested by calculating the flow and sediment transport of the experiments by *Odgaard & Bergs (1988)*. Due to the fact, that considerable uncertainties prevail concerning the description of parameters of the non equilibrium term, the model was only tested for near-equilibrium steady state situations. *Zeng et al. (2005)* presented a fully 3D model to solve the flow, bed load sediment transport and bed morphology changes in open channel flows. The non-hydrostatic model solves the 3D Reynolds averaged Navier-Stokes equations with integrations up to the wall such that the use of wall functions is avoided. The k-Ω model was used together with a non-equilibrium bed load sediment transport model with additional introduction of down-slope gravitational force effects. The empirical formulas proposed by *v.Rijn (1984a)* for the equilibrium bed load transport rate were used in the study. Among others, the experiments by *Odgaard & Bergs (1988)* were employed to validate the model. Results showed fairly small improvements over simulations using models with wall functions. *Ruether & Olsen (2005)* simulated the velocity distribution and bed level changes over time in a 90° channel bend by a fully 3D numerical model. The authors introduced relationships to determine the particle flow direction on a lateral slope. The results gave an increased accuracy when introducing a particle deviation approach. The same model was applied by *Fischer-Antze et al. (2004)* to simulate morphological bed changes in a reach of the Danube river as a consequence of a flood event in 2002. The numerical model was modified by incorporating the sediment transport formulas by *Wu et al. (2000b)* to account for hiding and exposure effects. Significant measured bed changes in the river reach were successfully modeled by the modified approach.

In the present study, the aforementioned fully 3D non-hydrostatic model was used for the computation of unsteady flow, sediment transport, and morphological changes. The bed module of the model was modified by incorporating the nonuniform sediment transport formulas proposed by Wu et al. (2000b) containing a stochastical approach to account for hiding and exposure processes. *Scheer et al. (2002)* investigated the behavior of 17 uniform and nonuniform sediment transport formulas for graded sediment under equilibrium conditions. The formulas of Wu et al. (2000b) proved to have the largest validity range of all analyzed formulas, so that a rather general applicability was expected. In the benchmark tests, the approach of *Wu et al. (2000b)*

gave the best transport rate predictions and the best predictions for sediment transport composition. In the current study, the original implemented sediment formulas by *v.Rijn (1984a)* were also altered by incorporating a hiding and exposure approach introduced by *Buffington & Montgomery (1997)*, in order to improve the performance of the formulas for nonuniform sediment transport. These two changes to the model were validated on the experiments by Yen et al. (1995). These experiments are challenging for a numerical model as they combine four important processes that are often found in natural river flows: (1) flow in a bend with predominating secondary current, (2) unsteady flow using a triangle shaped hydrograph, (3) experiments with a mobile bed in the vertical direction, and (4) using graded bed sediment material. Three-dimensional unsteady computations of bed deformation and sorting processes in river bends represent a new development in the field of numerical morphodynamic modeling.

Laboratory experiments

The laboratory data used for validating the numerical model introduced in this study were performed by *Yen & Lee (1995)*. The experiments were conducted in a laboratory channel bend having a central angle of 180°, a radius of curvature along central line in bend of r_c = 4 m, and a width of B = 1 m. The base flow was set at Q_0 = 0.02 m³/s, corresponding to a base flow depth of h_0 = 5.44 cm and a shear velocity of the base flow of u_{*0} = 0.031 m/s. The sediments were specified by the initial median diameter of d_{50} = 1.0 mm and the standard deviation of sediment-size gradation of σ_0 = 2.5. All experiments had an initial bed slope of I_0 = 0.002. Bed topography and transverse sediment sorting were investigated. Five experiments were performed, each having the same initial sediment-size gradation but different inflow hydrographs. At various sections of the bend, bed elevations were measured and bed surface sediments were sampled at the peak and the end of the hydrograph in each experiment. The results indicated that for all experiments bars evolved at the inner bank while scours evolved at the outer bank of the channel. As a consequence, lateral sorting processes occurred with the largest intensity in the area around 90°, indicated by diameters larger d_{50} at the outer bank and smaller d_{50} at the inner bank. The maximum deposition height was found between section 75° and 90°, and the maximum scour depth occurred between 165° and 180°. The measurements indicated that the characteristics of the hydrograph had prominent influences on bed topography and transverse sediment sorting. According to *Yen & Lee (1995)*, the cases with a higher ramping rate of the hydrograph had greater deposition heights near the inner bank and larger scour depths near the outer bank. Furthermore, in these cases the sediment was finer near the inner bank and coarser near the outer bank. In this study, bed deformation and sorting processes of two runs were modeled. Run #4 and run #2 were chosen for calibration and validation of the numerical model, respectively. Triangle-shaped

hydrographs showing linearly rising and falling limbs with a base flow of 0.02 m³/s were employed. Run #4 had a duration of 300 min, the peak discharge of Q_P = 0.053 m³/s was reached at t_P = 100 min, while run #2 had a duration of 204 min, the peak discharge of Q_P = 0.0685 m³/s was reached at t_P = 68 min.

Methods

The numerical model calculated the hydrodynamics for a general three-dimensional geometry by solving the Reynolds averaged Navier-Stokes equations with the continuity equation:

$$\frac{\partial U_i}{\partial x_i} = 0 \tag{1}$$

$$\frac{\partial U_i}{\partial t} + U_j \frac{\partial U_i}{\partial x_i} = \frac{1}{\rho} \frac{\partial}{\partial x_i} \left(-P \delta_{ij} - \rho \overline{u_i u_j} \right) \tag{2}$$

where U is the velocity averaged over the time t, x is the spatial geometrical scale, ρ is the water density, P is the pressure, δ is the Kronecker delta and u is the velocity fluctuation in time during the time step δt, when U is subtracted. The left term on the left side of the equation is the transient term. The next term is the convective term. The first term on the right hand side is the pressure term. The second term on the right side of the equation is the Reynolds stress term which is modeled by the k-ε turbulence model employing the eddy viscosity relation:

$$-\overline{u_i u_j} = \nu_t \left(\frac{\partial U_i}{\partial x_j} + \frac{\partial U_j}{\partial x_i} \right) - \frac{2}{3} k \, \delta_{ij} \quad \text{, with} \tag{3}$$

$$\nu_t = \frac{c_\mu \cdot k^2}{\varepsilon} \tag{4}$$

where the turbulent kinetic energy k and its dissipation rate ε determining the eddy viscosity ν_t are obtained from the following equations:

$$\frac{Dk}{Dt} = \frac{\partial k}{\partial t} + U_j \frac{\partial k}{\partial x_j} = \frac{\partial}{\partial x_j} \left[\left(\nu + \frac{\nu_t}{\sigma_k} \right) \frac{\partial k}{\partial x_j} \right] + P_k - \varepsilon \tag{5}$$

$$\frac{D\varepsilon}{Dt} = \frac{\partial \varepsilon}{\partial t} + U_j \frac{\partial \varepsilon}{\partial x_j} = \frac{\partial}{\partial x_j} \left[\left(\nu + \frac{\nu_t}{\sigma_\varepsilon} \right) \frac{\partial \varepsilon}{\partial x_j} \right] + C_{\varepsilon 1} \frac{\varepsilon}{k} P_k - C_{\varepsilon 2} \frac{\varepsilon^2}{k} \tag{6}$$

The production of turbulent kinetic energy P_k is defined as:

$$P_k = \nu_t \frac{\partial U_i}{\partial x_j} \left(\frac{\partial U_j}{\partial x_i} + \frac{\partial U_i}{\partial x_j} \right) \tag{7}$$

A detailed derivation of the formulas for computing the flow field is given by *Olsen (2004)*. The control volume method was used for discretisation, and the convective terms in the Navier-Stokes equations were solved by the second order upwind scheme. A detailed discussion of the scheme is given by *Olsen (1999, (2004)*. An implicit method was used for time integration and the pressure field was computed with the SIMPLE (semi-implicit method for pressure linked equations) method (*Patankar (1980)*). The Rhie and Chow interpolation (*Rhie & Chow (1983)*) was applied to compute the velocities and the fluxes at the cell surfaces. Zero gradient boundary conditions were used for all variables at the outflow boundary. Velocities were specified at the inflow boundary (Dirichlet boundary condition). Wall laws introduced by *Schlichting (1979)* were used for the side walls and the bed. The bed roughness can either be given as a user input or computed by the model as a function of the bed sediment distribution. The latter option was chosen for this study. A non-hydrostatic pressure approach was implemented, and thus the water surface elevation was determined from the computed pressure field:

$$\frac{\partial P}{\partial x_i} = \rho g \frac{\partial z}{\partial x_i} \tag{8}$$

Given the computed pressure field P, from the SIMPLE method, the changes in the water elevation, z, were calculated using Eq. (8). This approach is preferred to the commonly used rigid lid approach as it allows to compute the lateral inclination of the water surface in the channel bend representing the physical processes more accurately.

The bed changes were computed from sediment continuity for the bed cell, as the difference between the inflowing and outflowing sediment fluxes. The defect was converted into a vertical bed elevation by dividing it by the submerged density of the sediments (1320 kg/m³) to find the volume of the deposits for each time step. This was then transformed into bed level changes for the grid. Both the sedimentation and the erosion processes were modeled using the same approach.

The boundary conditions for the sediment transport computations were a user-specified value at the upstream boundary and zero gradients for the water surface, the outlet, and the sides. For the validation test in the present study, zero sediment inflow was given. The boundary conditions at the bed are given by the sediment transport relations for bed load. In the default configuration of the CFD model, fractional sediment transport was computed by the original bed load transport formulas of *v.Rijn (1984a)* applied individually for each fraction.

$$\frac{q_{b,i}}{d_i^{1.5}\cdot\sqrt{\frac{(\rho_s-\rho)\cdot g}{\rho}}} = 0.053\cdot\frac{\left(\frac{\tau-\tau_{c,i}}{\tau_{c,i}}\right)^{2.1}}{d_i^{0.3}\left(\frac{(\rho_s-\rho)\cdot g}{\rho\cdot\nu^2}\right)^{0.1}} \tag{9}$$

where q_{bi} is the transport rate of the *i*th fraction of bed-load per unit width, d_i is the diameter of the ith fraction, $\tau_{c,i}$ is the critical shear stress for d_i which was calculated by an analytical form of the Shields curve, ρ_s and ρ are the densities of sediment and water, respectively, ν is the kinematic viscosity, and g is the gravity acceleration.

Interaction between each individual grain size was not considered. For fractional transport with nonuniform sediments, *Wu et al. (2000b)* introduced an approach where interaction between different size fractions was considered. A correction factor accounted for hiding and exposure mechanisms assumed to be a function of the hiding and exposing probabilities, stochastically related to the size and gradation of the bed material. The probability of particles d_j staying in front of particles d_i was assumed to be the percentage of particles d_j in the bed material, p_{bj}. Therefore, the probabilities of particles d_i hidden and exposed by particles d_j was obtained as:

$$p_{hi} = \sum_{j=1}^{N} p_{bj}\frac{d_j}{d_i+d_j} \tag{10}$$

$$p_{ei} = \sum_{j=1}^{N} p_{bj}\frac{d_i}{d_i+d_j} \tag{11}$$

$$\eta_i = \left(\frac{p_{ei}}{p_{hi}}\right)^m \tag{12}$$

where N is the total number of particle size fractions of nonuniform sediment mixtures, p_{bi} and d_i are the percentage and the diameter of the *i*th fraction, respectively, η_i is the correction factor and m is a constant determined to be –0.6 by default. The exponent in the hiding function is often used as a calibration parameter in a CFD model. In this study, best result were obtained with m = -0.3.

The hiding and exposure factor was then used to modify the criterion for sediment incipient motion for each fraction,

$$\frac{\tau_{ci}}{(\gamma_s-\gamma)d_i} = \theta_c\cdot\eta_i \tag{13}$$

where τ_{ci} is the critical shear stress for particle d_i in nonuniform sediment mixtures, γ_s and γ are the specific weights of sediment and water, respectively and θ_c is a constant set to 0.03. The non-dimensional fractional bed-load transport rate ϕ_{bi} is defined as

$$\phi_{bi} = \frac{q_{bi}}{p_{bi}\sqrt{(\gamma_s - \gamma) g d_i^3}} \tag{14}$$

where q_{bi} is the transport rate of the *i*th fraction of bed-load per unit width. By a regression analysis using least square curve fitting, the following relationship was obtained,

$$\phi_{bi} = 0.0053\left[\left(\frac{n'}{n}\right)^{1.5}\frac{\tau_b}{\tau_{ci}} - 1\right]^{2.2} \tag{15}$$

where *n'* is Manning's coefficient corresponding to grain roughness, here calculated with $n' = d_{50}^{1/6}/20$, *n* is Manning's coefficient for channel bed and τ_b is the bed shear stress.

The third approach tested in this study was a modification of the fractional sediment transport formula of *v.Rijn (1984a)*. In order to take into account that a sediment mixture was used in the flume, a hiding and exposure factor was introduced. The critical shear stress was multiplied with a correction factor ξ_i to yield a corrected shear stress:

$$\tau_{c,i,corrected} = \xi_i \tau_{c,Shields} \tag{16}$$

$$\xi_i = \left(\frac{d_i}{d_{50}}\right)^P \tag{17}$$

According to *Buffington & Montgomery (1997)*, there is no universal exponent *P*. The value has to be determined for the specific flow characteristic. *Kleinhans & v.Rijn (2002)* proposed to use different values of *P* for each individual grain size. In this study the best results were obtained with the exponent *P* set to the constant value of *P =-0.3*.

When fractional transport was computed, sorting mechanisms were considered by the definition of an exchange layer (denoted as active layer) where the sediment continuity equation was solved separately for each fraction. The river was subdivided into three layers, (1) a water layer near the river bed, with a mixture of water and sediments, (2) an upper sediment layer where sediments do not move with the water and an exchange of this layer and the water layer can occur, and (3) a lower sediment layer, denoted inactive layer. In the absence of dunes, the active layer thickness can be thought to scale with a characteristic large size of the bed material

([Kroekenstoel, 2003 #130]). The vertical size of the active layer was usually kept constant, in the order of the largest grain size. The size of the inactive layer is set to a large value. The grain distributions in the two bed layers were obtained by considering sediment continuity for each fraction. If deposition occurred, each fraction f_a in the active layer was computed as:

$$f_a = \frac{f_{a,0}\, z_a + f_d\, z_d}{z_a + z_d} \tag{18}$$

where z_a is the height of the active layer, z_d is the height of the deposition, f_a and f_d denote the fractions in the active layer and of the deposited material, respectively. Because the vertical magnitude of the active layer remained constant, material had to be transferred to the inactive layer.

$$f_i = \frac{f_{i,0}\, z_i + f_a\, z_a}{z_i + z_a} \tag{19}$$

where the index i denotes the inactive layer. Erosion processes were treated in an analogous way. The erosion depth per time step is limited by the thickness of the active layer. Thus, a suitably small time step has to be chosen for morphodynamic computations.

The processes concerning hydraulics, sediment transport, and morphological changes have numerically not been treated separately. The computed bed changes induced by deposition or erosion affected the flow which in turn influenced the distribution of the bed shear stress and thus the bed load component and ultimately the bed topography. In the numerical model, these interactions were considered by changing the bed after each time step. As a consequence, the hydraulics had to be recalculated for each time step.

For validating the introduced CFD model, the geometry of the laboratory experiments of *Yen & Lee (1995)* had to be discretized. A three-dimensional, structured, non-orthogonal, vertically adaptive, and curvilinear grid was set-up. 254 hexahedral cells in the streamwise, 20 cells in the lateral and 5 cells in the vertical direction were used. The grid was only moved in the vertical direction, and not in the horizontal directions. A time step of 20 s was chosen. After each time step, the water surface and the bed surface were updated. For discretization of the sediments, the continuous initial bed sediment sieve curve was decomposed into seven size fractions. The hydraulics were computed in a pre-run for steady initial base flow conditions to provide a developed flow field to the main run.

Results and Discussion

In this section the computed results of the CFD model are compared to measurements of a physical model study, carried out by *Yen & Lee (1995)*. In the study of *Olsen (2003)*, it was shown that morphodynamics were modeled with good agreement in the case of uniform sediments. In the present study, morphological changes were investigated for nonuniform sediments, for this reason the default configuration was compared with two advanced approaches to investigate the sensitivity of nonuniform sediments to different sediment transport approaches. Three approaches for the sediment concentration at the bed were tested in this study: (1) using the default configuration of the CFD model based on the sediment transport formulas of *v.Rijn (1984a)*, (2) applying a modified approach of the *v.Rijn (1984a)* formulas to account for hiding and exposure effects introduced by *Buffington & Montgomery (1997)*, and (3) applying the nonuniform sediment transport formulas of *Wu et al. (2000b)*, also accounting for hiding and exposure effects. In a first step, the computed flow characteristics of the laboratory bend were checked for plausibility. The computed flow field of the base discharge comprised typical secondary flow patterns in the bend region, considered to be the driving force for sorting and bed deformation processes in the bend. A detailed verification of the computed flow field was not possible since measured velocity profiles were not provided. The numerical model's capabilities of simulating the flow field in curved channels was investigated in detail by *Wilson et al. (2003)* indicating that an appropriate formulation of the roughness distribution and a sufficient inlet length were crucial for predicting the presence and the rotational sense of measured secondary currents accurately. As a consequence of the developed flow field in the bend, the water surface was laterally inclined, showing increasing water levels from the inner to the outer bend. Following the theory of frictionless slip streams, the 1D relationship of the lateral water surface gradient is given as:

$$\frac{dh}{dr} = \frac{U^2}{gr} \tag{20}$$

An approximation of the formula yields the lateral difference of the water surface elevation Δh:

$$\Delta h \approx \frac{U^2}{g \cdot r_c} B \tag{21}$$

For the base flow of Q_0 = 0.02 m³/s, relation (21) gives Δh_{eq} = 3.4 mm. The computed water surface of the base flow was analyzed at the cross-section of the apex of the bend. Here, a water level difference of Δh_{CFD} = 3.3 mm was computed. This was an indication that the flow field was computed correctly.

Numerical computations of morphological changes and sorting processes were performed for run #4 (calibration) and run #2 (validation). The parameter sets found for the calibration case were used for the validation case. Firstly, the results of the calibration case are shown in Fig. 1 to Fig. 8, subsequently the validation case is shown in Fig. 9.

Fig. 1 shows computed versus measured bed changes at four cross-sections at the first half of the bend (45°), the bend apex (90°), the second half of the bend (135°), and the end of the bend (180°). Fig. 5 on the left side illustrates the positions of the cross-sections in plan view. The dashed lines in Fig.1 represent the results of the original configuration of the CFD model, computed with the default formulas of *v.Rijn (1984a)*. The general features of the bed changes are well represented by the numerical model. The total erosion and deposition heights are approximately within the correct magnitude. The width of the scour is determined by a sudden inception of a strong downwards gradient at a distance of about 0.2 m from the outer bank. The scour width and scour depth are well represented by the default van Rijn formulas. However, the bar evolution, located at the inner bank, is significantly over predicted. The over prediction is present in all cross-sections.

Additionally to the results of the default approach, the solid lines in Figs. 1 and 2 represent the results of the extended van Rijn and Wu approaches, respectively. Hiding-exposure coefficients of P = -0.3 and m = -0.3 were applied. The results indicate that a significant improvement of the computed bed levels was achieved. While the scour depths were modeled with a similar accuracy compared to the default van Rijn model, the deposition processes at the inner bank were significantly damped. Also, the distinctive region of the scour near the outer bank, was generally well represented by the nonuniform approaches. Furthermore, the plateau-like central region and the shape of the bar evolution was modeled with good agreement. The results indicated, that the consideration of hiding and exposure mechanisms significantly improved the modeled bed deformation results. In Figs. 3 and 4, the variations of the median sediment diameters are shown for the default configuration and the modified van Rijn and Wu approaches, respectively. The default model (dashed lines) generally predicted the variations of the median sediment size in the correct magnitude. However, the fining processes at the inner bank and the coarsening processes at the outer bank were over estimated by the default model. The results of the nonuniform approaches (solid lines) represented the measured data considerably better than the default model. The measured gradient of the sorting process was well represented and the values were computed in the correct range. The modified van Rijn approach performed slightly better than the approach by Wu. The effect of the hiding and exposure approach, characterized by small particles that hide behind coarser particles and are therefore better protected from being transported, was well represented in the results. When comparing

the results with and without consideration of hiding-exposure corrections, the underlying physical processes become evident. One can see that less coarsening occurred for the hiding-exposure approach at the outer bend, because the fine particles were protected and therefore transported to a smaller extent. On the other hand, the inhibited transport of fine material that preferentially deposits at the inner bank leads to a better agreement of the median sediment size at the inner bank region. The reduced deposition heights at the inner bank of the hiding-exposure approaches in comparison with the default approach, as depicted in Fig. 1, can be interpreted by the reduced amount of fine material available from sediment transport and therefore not being available for deposition at the inner bank. As a result, the fining at the inner bank is less pronounced. Obviously, hiding and exposure effects significantly influenced the measured bed deformations and the measured variations of the median sediment diameters.

Figs. 5 and 6 show contour plots of the bed deformations and median sediment sizes in plan view. The contours are displayed in a dimensionless form, the bed deformations Δz were normalized by the initial water depth h_0 = 5.44 cm, and the median sediment sizes d by the initial median sediment size d_0 = 1 mm. The figures show the results of the extended van Rijn and Wu approaches, respectively. The measured contour lines ranged from $\Delta z/h_0$ = -0.75 to 0.75, the rangewas well represented by the numerical models. The typical deposition processes at the inner bank and scour processes at the outer bank were correctly modeled. A deviation from the measured contours was found at the positions of the peak elevation (contour line 0.75) of the point bar. While the peak elevation was measured only slightly upstream the bend apex at cross-section 80°, the computed maximum depositions of the two approaches were situated at the first half of the bend. A secondary point bar was measured at 170°, both models reproduced this morphological structure by the correct elevation height, however, the computed results showed comparably smoother characteristics. This is a phenomenon which is generally observed at morphodynamic models (e.g. [Wu, 2000 #18], [Wu, 2004 #134]). The van Rijn approach performs slightly better here. The largest scour depth represented by contour line –0.75 downstream 180° was calculated with good agreement. Both models reproduced the magnitude and the position of this scour region. However, the scour processes at the upper half of the outer bend were underestimated to some degree by the numerical models. The contours of the measured median sediment sizes indicate a generally constant lateral gradient over the length of the bend. The models were able to reproduce the formation of sediment sorting ranging form d/d_0 = 0.5 to 3.0 with satisfying agreement. Also in this case, the computed contours showed slightly smoother characteristics than the measured contours.

Additionally to the detailed comparisons of measured and computed morphological features, a rather integrative comparison is shown in Fig. 7. This figure depicts the accumulated sediment outflow at the outlet of the laboratory flume over time. The outflowing sediments were collected and weighed at two points in time, at the peak discharge at t_p = 100 min and at the end of the experiment at t_{max} = 300 min. Both the computed sediment outflow using the Wu and the modified van Rijn approach are shown. As can be seen from the sediment hydrographs, the tendency of the measured outflow is represented in a plausible way, characterized by an increase of outflow from t_0 to t_p followed by a decreased outflow from t_p to t_{max}. The van Rijn formula slightly overestimated the measured outflow, while the Wu formula slightly underestimated it. The van Rijn approach performed slightly better.

An appropriate choice of numerical parameters is essential to achieve accurate computed results. The sensitivity of three parameter variations was investigated, the active layer thickness and the number of the cells in the vertical directions were doubled, and the time step was halved. The results showed very similar contour patterns for both, the computed bed changes and the median sediment size distributions for all parameter variations (not displayed). The calculated bed changes in the bend apex (90°) (Fig. 8) were virtually identical for all parameter variations. This also applied to the results of the median sediment size distributions when refining the spatial and temporal resolutions (2 · vertical cells, 1/2 · time step) indicating that the flow and sediment transport processes were sufficiently discretized by the chosen configuration. Stronger deviations were obtained for a variation of the active layer thickness (2 · active layer). Here, the coarsening process was computed less intensive. These findings are in line with [Kroekenstoel, 2003 #130] where the choice of a small active layer thickness produced stronger armoring processes in erosion dominated areas. The results showed, that the active layer thickness is a significant parameter when modeling fractional sediment transport processes. No evidence was given that bed forms were available at the laboratory experiments justifying the chosen active layer thickness in the order of the largest grain size. On the basis of the chosen parameter set (m = -0.3 and default values for all other parameters) using the formulas of *Wu et al. (2000b)*, the numerical model was validated on an independent data set (run #2) comprising an increased peak discharge compared to the calibration case (run #4). As a consequence, larger bed elevation changes were measured in this case. The results show (Fig. 9) that the general features of the bed deformations were reproduced with satisfying agreement. Contour lines 0.0 and 0.5 representing the bar region at the inner bend were computed at similar positions. However, the peak elevation of the bank that was measured by 1.0 very close to the inner bank at 80° could not be modeled. This also applied to the scour region at the outer bend. While the maximum scour at 180° was reproduced correctly

both in magnitude and position, the other erosion regions were generally underestimated by the model, best seen at the local scour peaks at 70° and 150°. The median sediment sizes were modeled with satisfying agreement. While the range of the measured and computed median sediment sizes coincided well, the computational results showed generally smoother characteristics. Coarsening was overestimated slightly in the entire bend region. The concentration of contour lines in the downstream straight reach on the left side in flow direction was well represented by the model.

Summary and Conclusions

A three-dimensional numerical model was used for calculating bed deformation and sorting processes with data from the laboratory experiments by *Yen & Lee (1995)*. Morphological changes were investigated in a 180° bend under unsteady flow conditions using a mobile bed with nonuniform sediments. The model was able to plausibly compute the flow features in the flume. The computed lateral water surface was compared with an analytical approach, the deviations were marginal. The performance of three sediment transport formulas was investigated, the default transport formula in the numerical model introduced by *v.Rijn (1984a)*, and two newly incorporated transport formulas for nonuniform sediments, accounting for the interactions between individual grain sizes by two different hiding and exposure approaches (*Buffington & Montgomery (1997)*; *Wu et al. (2000b)*). The first approach applies a correction factor defined by the ratio of the fractional grain size and the median grain diameter. The second method used a correction factor assuming to be a function of the hidden and exposed probabilities, which are stochastically related to the size and gradation of the bed material. By adjusting the exponent for the hiding-exposure functions the models were tuned to reproduce best the morphological features of one laboratory run. Subsequently the models were validated on another run.

Results showed that the three-dimensional model was able to predict both the magnitude and the general tendencies of the measured bed deformations and sediment size distributions of the laboratory experiments when using the default van Rijn configuration. More detailed analysis, however, revealed deviations from measurements with respect to bed level and sediment size changes indicating a remarkable over-estimation of bar evolution at the inner bank. Computed results improved significantly when the two nonuniform sediment transport approaches were applied. Best results were obtained when the absolute values of the hiding-exposure exponents were reduced for both approaches compared to the default values given for the models. The results of the nonuniform approaches showed less sorting intensity and smaller bar heights, both giving a better fit to the measured data. The computed results of the nonuniform approaches in relation with the default approach represented the physical mechanisms of the hiding-exposure effect well. Both nonuniform approaches predicted

the total sediment transport with satisfying agreement. The superior agreement with respect to the default approach showed that these mechanisms play an important role in nature and that they should be considered when modeling morphological changes with nonuniform sediments (### satz ändern???). Applying the numerical model using the Wu approach to another run for validation purposes showed that the model also here reproduced the significant morphological changes and sediment sorting processes with satisfying agreement.

Future research will be dealing with an application of the *Wu et al. (2000b)* approach for flow in natural rivers: morphodynamic changes at the Austrian part of the Danube river. Also the extended *v.Rijn (1984a)* approach will be used to compute the meandering processes in laboratory channels.

Notations

The following symbols are used in this paper:

r_c = radius of curvature [m]

B = channel width [m]

c = volume sediment concentration [m³/m³]

D = sediment continuity defect [kg/s]

d_0 = initial median sediment diameter

d, d_{50} = grain size of 50 % finer [m] = median sediment diameter

d_{90} = grain size of 90 % finer [m]

d_m = mean sediment diameter [m]

f = sediment fraction [-]

h_0 = water depth of base flow [m]

I_0 = initial energy slope [-]

k = turbulent kinetic energy [m²/s²]

m = exponent for correction factor [-]

N = total number of particle size fractions [-]

n = Manning's coefficient for channel bed [$s/m^{1/3}$]

n' = Manning's coefficient corresponding to grain roughness [s/m$^{1/3}$]

P = pressure [N/m²]

P = exponent for hiding-exposure function [-]

p_{bj} = percentage of the ith fraction of bed material [-]

p_{ei} = total exposed probabilities of particles d_i [-]

p_{hi} = total hidden probabilities of particles d_i [-]

P_k = production of turbulent kinetic energy

Q_0 = discharge of base flow [m³/s]

q_{bi} = transport rate of the ith fraction of bed-load per unit width [m³/(s*m)]

t = time [s]

u_{*0} = shear velocity of base flow [m/s]

u_i = velocity fluctuation [m/s]

U_i = average velocity [m/s]

x_i = spatial geometrical scale [m]

z_a = height of the active layer [m]

z_d = height of the deposition [m]

δ_{ij} = Kronecker delta

ε = dissipation of turbulent kinetic energy [m²/s²]

ϕ_{bi} = non-dimensional fractional bed-load transport rate [-]

η_i = correction factor [-]

ν = kinematic viscosity [m²/s]

ν_t = eddy viscosity [m²/s]

θ_c = non-dimensional critical shear stress [-]

ρ = density of water [kg/m³]

ρ_s = density of sediments [kg/m³]

σ_0 = initial standard deviation of sediment size gradation [m]

τ_b = bed shear stress

τ_c, τ_{ci} = critical shear stress for d_m, d_i

ω = dissipation per turbulent kinetic energy [1/s]

Acknowledgements

The first writer was funded by the Institute for Hydraulic and Water Resources Engineering, Vienna University of Technology and the second writer was funded by the Norwegian Research Council, BeMatA Program.

References

Buffington, J. M. and Montgomery, D. R., 1997, A systematic analysis of eight decades of incipient motion studies, with special reference to gravel-bedded rivers, Water Resources Research, 33 (8), pp. 1993-2029.

Fischer-Antze, T., Gutknecht, D. and Olsen, N. R. B., 2004, Morphological changes of the Danube River east of Vienna over the last nine years *in* XXII. Conference of the Danubian Countries, Brno, Czech Republic.

Jia, Y. and Wang, S., 1999, Numerical model for channel flow and morphological change studies, J. Hydraulic Engineering, 125 (9), pp. 924-933.

Julien, P. Y. and Anthony, D. J., 2002, Bed load motion and grain sorting in a meandering channel, J. Hydraulic Research, 40 (2), pp. 125-132.

Kleinhans, M. G. and v.Rijn, L. C., 2002, Stochastic prediction of sediment transport in gravel Sand-gravel bed rivers, J. Hydraulic Engineering, 128 (4), pp. 412-425.

Knaapen, M. A. F., Hulscher, S. J. M. F., De Vriend, H. J. and Van Harten, A., 2001, Height and wavelength of alternate bars in rivers: modelling vs. laboratory experiments, J. Hydraulic Research, 39 (2), pp. 417-426.

Minh Duc, B., Wenka, T. and Rodi, W., 2004, Numerical modeling of bed deformation in laboratory channels, J. Hydraulic Engineering, 130 (9), pp. 894-904.

Odgaard, A. and Bergs, M., 1988, Flow processes in a curved alluvial channel, Water Res. Research, 24 (1), pp. 45-56.

Olsen, N. R. B., 1999, Computational fluid dynamics in hydraulic and sedimentation engineering.

Olsen, N. R. B., 2003, Three-dimensional CFD modeling of self-forming meandering channel, J. Hydraulic Engineering, 129 (5), pp. 366-372.

Olsen, N. R. B., 2004, Hydroinformatics, fluvial hydraulics and limnology, Department of Hydraulic and Environmental Engineering, The Norwegian University of Science and Technology, www.ntnu.no/~nilsol/cfd, Trondheim.

Patankar, S., 1980, Numerical Heat Transfer and Fluid Flow, T. Francis.

Peltier, E., Duplex, J., Latteux, B., Pechon, P. and Chausson, P., 1991, Finite element model for bed-load transport and morphological evolution, Pages 227-233 *in* Computer modelling in ocean engineering 91, Arcilla et al.

Rhie, C. and Chow, W., 1983, Numerical study of the turbulent flow past an airfoil with trailing edge separation, AIAA Journal, 21 (11).

Ruether, N. and Olsen, N. R. B., 2005, Three dimensional modeling of sediment transport in a narrow 90° channel bend, J. Hydraulic Engineering. in press.

Scheer, P. v. d., Blom, A. and Ribberink, J. S., 2002, Transport Formulas for Graded Sediment - Behaviour ot transport formulas and verification with data, University of Twente, 2002R-002, Enschede.

Schlichting, H., 1979, Boundary layer theory, McGraw-Hill Book Company, New York.

Sloff, C. J., Jagers, H. R. A., Kitamura, Y. and Kitamura, P., 2001, 2D morphodynamic modelling with graded sediment *in* 2nd IAHR Symp. on River, Coastal and Esturaine Morphodynamics, Obihiro, Japan.

Spasojevic, M. and Holly, F. M., 1990, 2-D bed evolution in natural watercourses. New simulation approach, Journal of Waterway, Port, Coastal and Ocean Engineering, 116 (4), pp. 425-443.

v.Rijn, L. C., 1984a, Sediment Transport, Part I: Bed Load Transport, J. Hydraulic Engineering, 110 (11), pp. 1431-1457.

v.Rijn, L. C., 1984b, Sediment Transport, Part II: Suspended Load Transport, J. Hydraulic Engineering, 110 (11), pp. 1613-1641.

Wilson, C. A. M. E., Boxall, J. B., Guymer, I. and Olsen, N. R. B., 2003, Validation of a three-dimensional numerical code in the simulation of pseudo-natural meandering flows, J. Hydraulic Engineering, 129 (10), pp. 758-768.

Wu, W., Rodi, W. and Wenka, T., 2000a, 3d numerical modelling of flow and sediment transport in open channels, J. Hydraulic Engineering, 126 (1), pp. 4-15.

Wu, W. and Wang, S., 2004, Depth-averaged 2-D calculation of flow and sediment transport in curved channels, J. Sediment Research, 19 (4), pp. 241-257.

Wu, W., Wang, S. and Jia, Y., 2000b, Nonuniform sediment transport in alluvial rivers, J. Hydraulic Research, 38 (6), pp. 427-434.

Yen, C. and Lee, K., 1995, Bed topography and sediment sorting in channel bend with unsteady flow, J. Hydraulic Engineering, 121 (8), pp. 591-599.

Zeng, J., Constantinescu, G. and Weber, L., 2005, A fully 3D non-hydrostatic model for prediction of flow, sediment transport and bed morphology in open channels *in* IAHR conference 2005, Seoul, Korea.

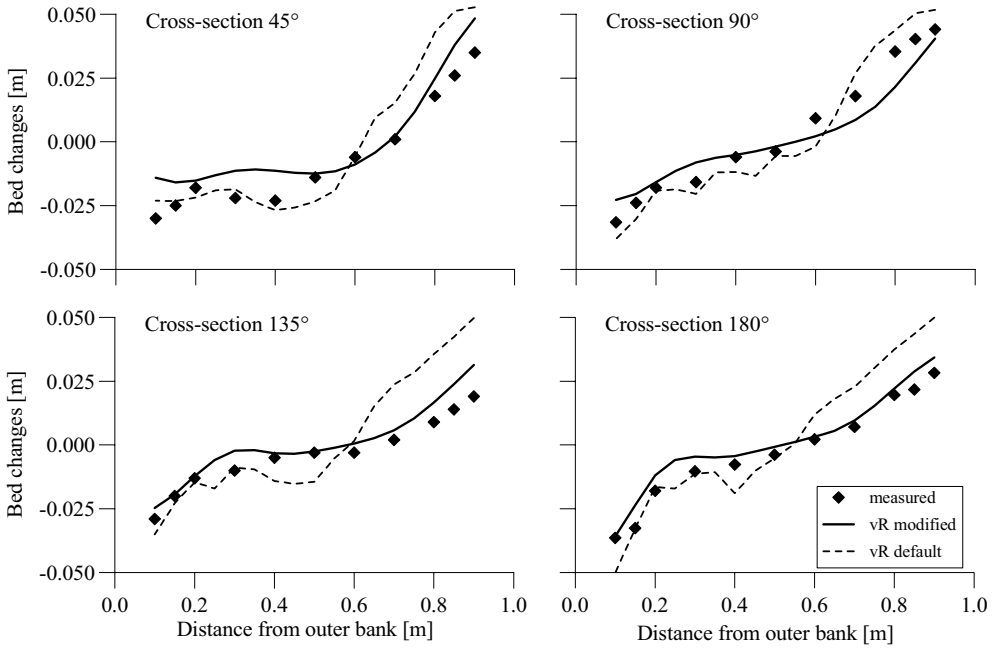

Fig. 1: Bed changes at four cross-sections using the default and the modified van Rijn formulas

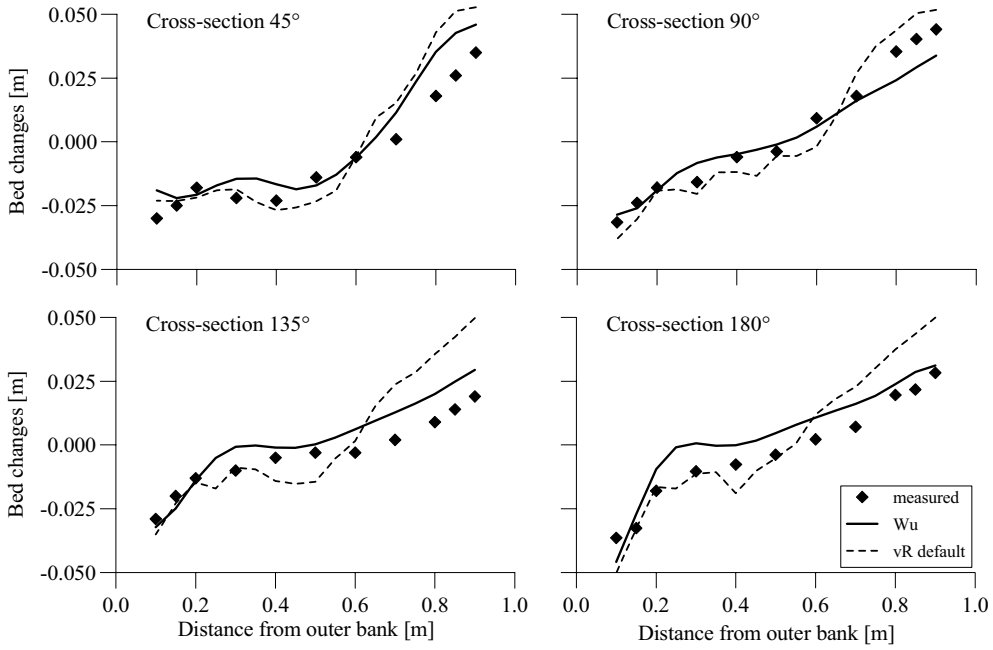

Fig. 2: Bed changes at four cross-sections using the default van Rijn and Wu formulas

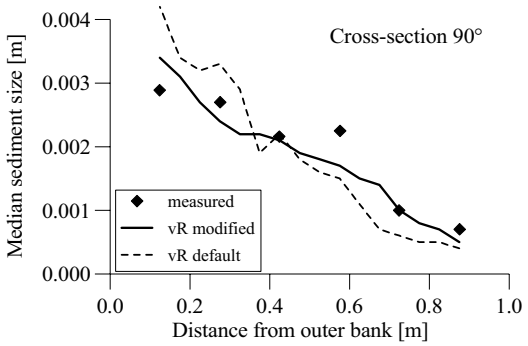

Fig. 3: Median sediment sizes at the bend apex using the default and the modified van Rijn formulas

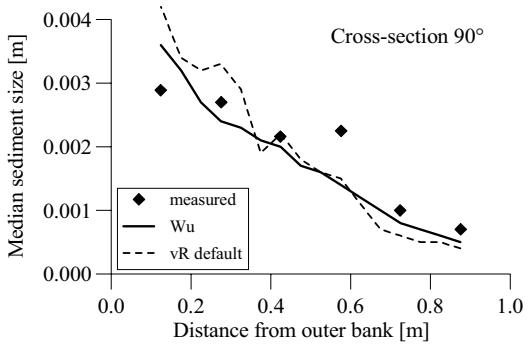

Fig. 4: Median sediment sizes at the bend apex using the default van Rijn and Wu formulas

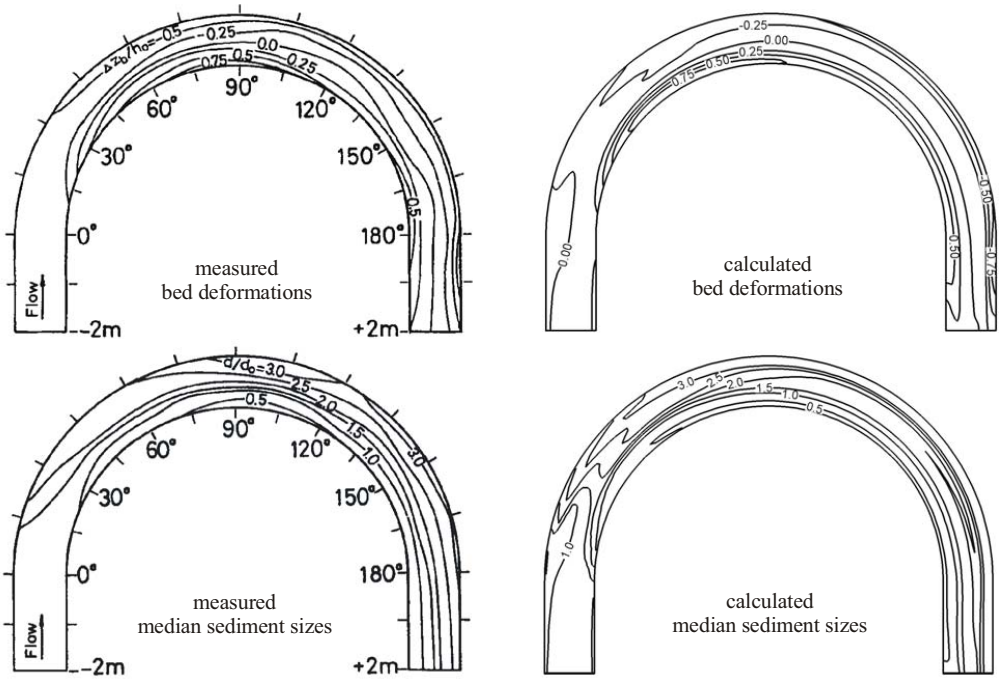

Fig. 5: Plan view of bed deformations and median sediment sizes using the modified van Rijn formulas

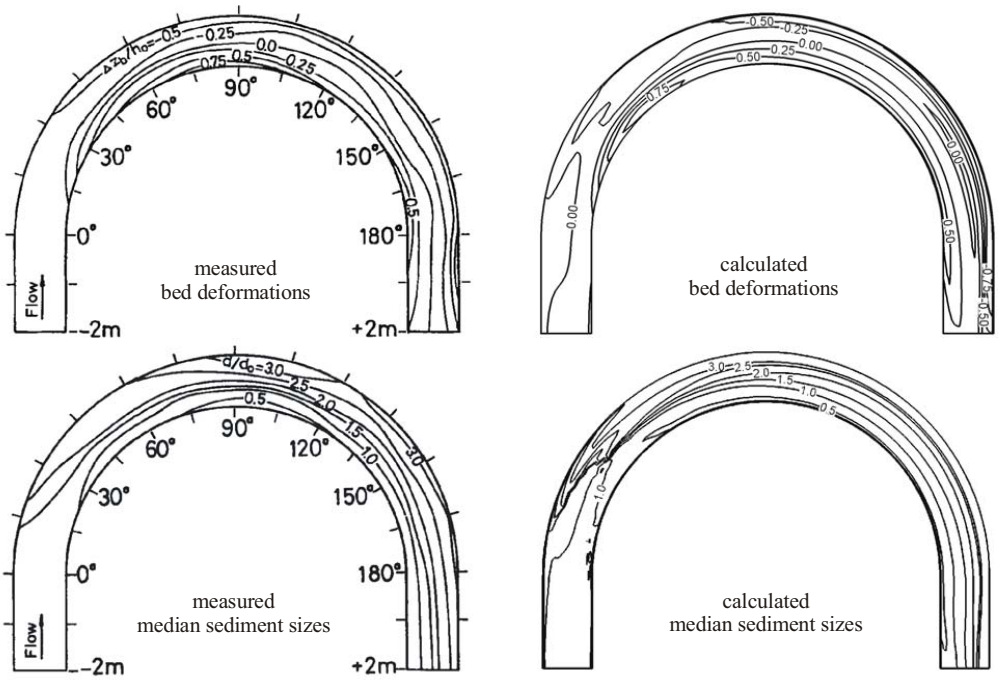

Fig. 6: Plan view of bed deformations and median sediment sizes using the Wu formulas

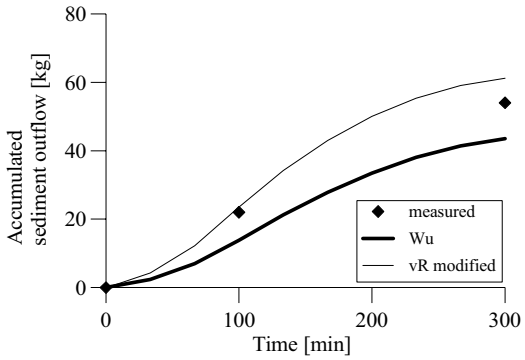

Fig. 7: Accumulated sediment outflow using the Wu and modified van Rijn formulas

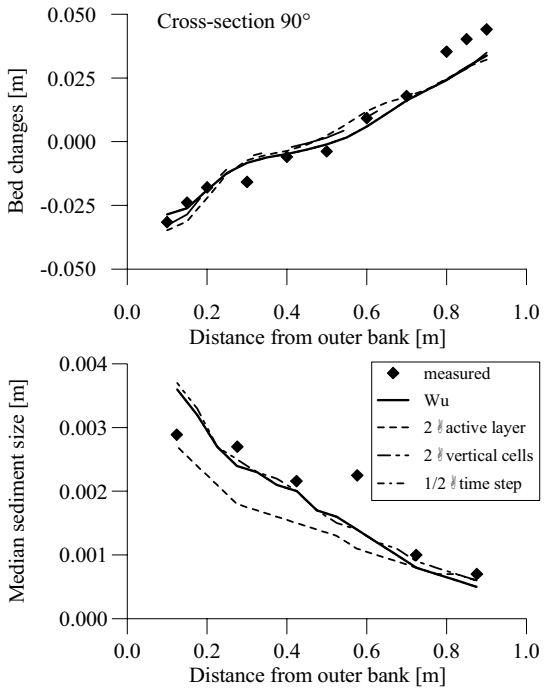

Fig. 8: Sensitivity analysis at the bend apex using the Wu formulas

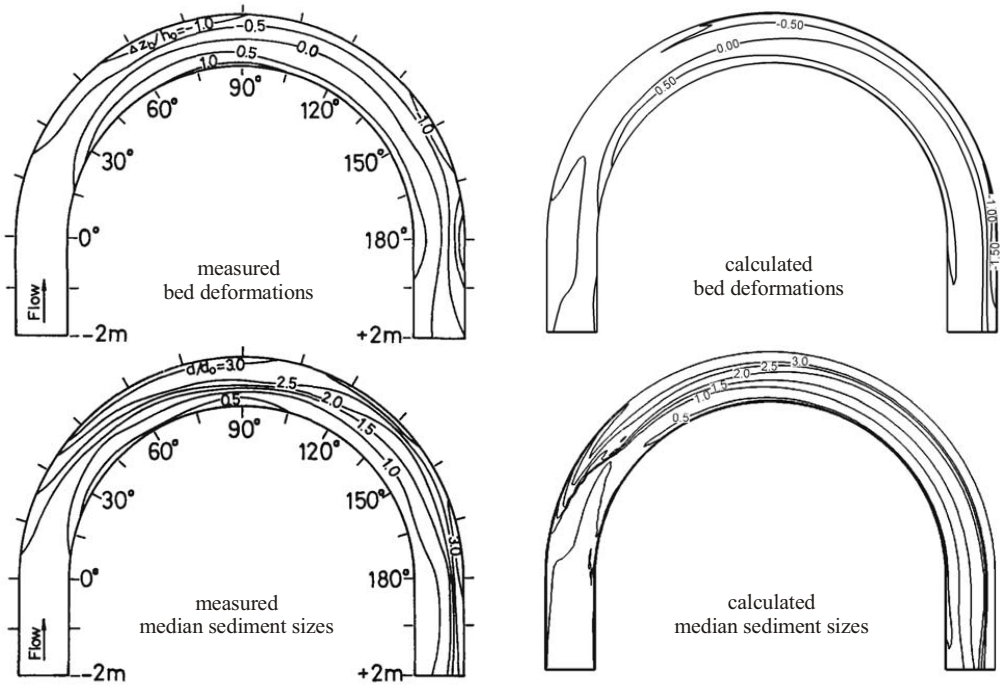

Fig. 9: Validation: plan view of bed deformations and median sediment sizes using the Wu formulas

Paper IV

3D modeling of transient bed deformation in a sine-generated laboratory channel with two different width-to-depth ratios

N. Rüther, N.R.B. Olsen

Proceedings of the third International Conference on Fluvial Hydraulics, River Flow 2006, Lisbon, Portugal

3D modeling of transient bed deformation in a sine-generated laboratory channel with two different width to depth ratios.

N. Rüther & N.R.B. Olsen
Department of Hydraulic and Environmental Engineering, Norwegian University of Science and Technology in Trondheim, Norway

ABSTRACT: A three dimensional numerical model is presented to calculate the sediment transport rate and the corresponding transient bed changes in sine-generated meandering laboratory channels. Transient flow pattern as well as bed movements in simple bended laboratory channels have been successfully modeled with 2D and 3D numerical models before. However, when it comes to the successive formation of meander bends, the spatial propagation of the helical flow and its effect on the bed deformation is not fully understood yet. It is strongly depending on the deflection angle Θ of the meander bend and the width to depth ratio of the channel. In addition to this geometric characteristic, bed forms were prevailing in the experiments. The present study showed how a three dimensional numerical model is able to calculate the flow field and the sediment transport in a sine-generated laboratory channel with two consecutive meander bends and occurring bed forms.

1 INTRODUCTION

Water flow and sediment transport in meandering river is of high interest in the field of river engineering. The major local erosion in river bends under steady or unsteady flow conditions is causing huge problems to the riverine structures. Prediction of the time-dependent bed changes and the lateral bed load transport with the corresponding lateral migration with the help of computer programs is becoming more and more popular. The major problem herein is the fact that the flow field in river bends is highly three-dimensional. The flow is dominated by transverse secondary currents. The sediments are eroded by the accelerated flow at the outer part of the bend and transported by the secondary currents to the inner part. Here they tend to deposit due to the reduced velocity and shear stress, forming a so called point bar. This effect is highly depending on the geometry of the channel, e.g. deflection angle of the bends or number of consecutive bends, and also on the width to depth ratio of the channel. With the increasing computer power over the last 15 years, it is now possible to carry out fully 3D computations for such cases. Demuren & Rodi (1986) used a three dimensional model where the turbulence was predicted by the k-ε model, to calculate the flow and the transport of a neutral tracer in a meandering channel. Recently, Wilson et al (2003) computed the fully developed three dimensional velocity distributions in a meandering channel over a fixed natural bed and showed good agreement with measurements. Ruether & Olsen (2005) computed the bed changes over time in a sharply bended 90˚ channel with special respect to steep transversal slopes. Wu et al (2000) computed the flow in a 180˚ bend including suspended and bed load transport. Zeng et al (2005) computed the bed changes in a 180° bend, too. All of the results showed good agreement with measured data. Bed forms did not occur in any of the previous studies.

The present study focused on the simulation of the bed changes in a laboratory channel with sine-generated consequent bends, deflection angle $\Theta = 70$˚, and prevailing bed roughness caused of bed forms, like dunes and ripples.

2 SEDIMENT TRANSPORT IN MEANDERING CHANNELS; EXPERIMENTAL DATA

The laboratory data used in the present study were taken from da Silva & Tarek (2006b). Movable bed experiments were carried out in a sine generated channel. The 0.8 m wide flume was filled with sand of the size of D_{50} = 0.65 mm of about 0.2 m and steady, uniform flow was established. The sediments were relatively well sorted with a ratio of D_{60} to D_{10} of 1.89. The measured data for two experimental runs were then compared to the numerical simulation. The two different experiments were denoted Run 1 und Run 5 where the bed changes were meas-

ured after 60 min and 170 min for Run 1 and 5, respectively.

Table 1. Hydraulic conditions of the experiments

	Exp-1	Exp-5		Exp1	Exp-5
Q [m^3/s]	0.011	0.0076	**u* [m/s]**	0.04	0.042
B [m]	0.8	0.8	**B/h_{av} [-]**	10.67	18.18
h_{av} [m]	0.075	0.044	**Re* [-]**	53	54
S [-]	1/450	1/250	**Re [-]**	13750	9475
u_{av} [m/s]	0.18	0.22	**T [min]**	60	170

As it can be seen from table 1, the most significant difference of the two experiments is the width to depth ration of 10.67 and 18.18, respectively. For both experiments, the hydraulic conditions are listed in table 1. Figure 1 shows the experimental setup. The flow is top to bottom. (In the following Figures the flow is from left to right.)

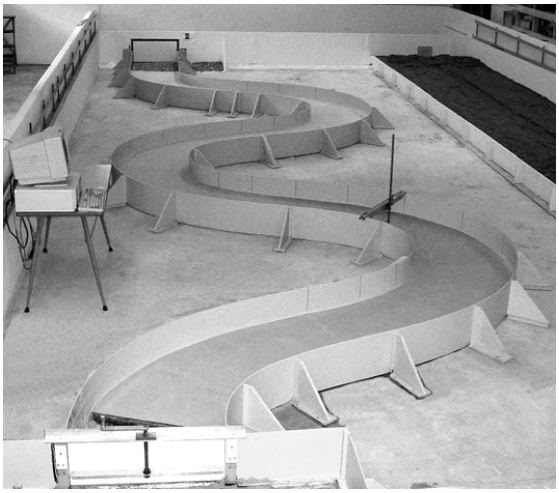

Figure 1. Experimental set up. (da Silva & Tarek, 2006b)

According to the different hydraulic setups, two different bed patterns were observed. The bed deformation in Run 1, depicted in Figure 3 can be described in the following way: The locations of the deepest erosion were determined to be in the two cross over parts of the flume. Point bars developed at the inner side of each of the apex, growing with the increasing downstream coordinate. The magnitude of the bed changes over time was in the range of -0.12 m and +0.4 m. In addition one can see that the location of the maximum erosion and deposition in each of the bends were not located in the same cross section.

The bed deformation in Run 5 is depicted in Figure 5. The areas of maximum erosion are located at the outside end of each of the bends with a maximum bed change of -0.12 m. Similar to Run 1, the characteristic point bars developed and grow with the downstream, increasing coordinate. Where as the scour in the most downstream cross section was with -0.08 m less deep than the scours further upstream. In opposite to Run 1, the location of the maximum erosion and deposition were found to be in the same cross section, just slightly downstream of the apex.

Figure 2 shows the location of the cross section being compared. Cross section 11 and 15 are located right after the first bend and cross section 26 and 30 right after the second bend.

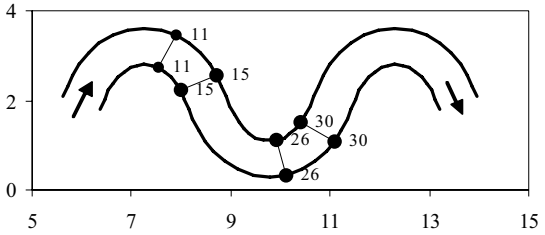

Figure 2. Location of the compared cross section.

3 NUMERICAL SIMULATION OF TRANSIENT BED DEFORMATION

3.1 *Numerical model*

The flow field for the three-dimensional geometry is determined by solving the continuity equation and the Reynolds averaged Navier-Stokes equations:

$$\frac{\partial U_i}{\partial x_i} = 0 \tag{1}$$

$$\frac{\partial U_i}{\partial t} + U_j \frac{\partial U_i}{\partial x_i} = \frac{1}{\rho}\frac{\partial}{\partial x_i}\left(-P\delta_{ij} - \rho\overline{u_i u_j}\right) \tag{2}$$

U is the velocity averaged over the time t, x is the spatial geometrical scale, ρ is the water density, P is the pressure, δ is the Kronecker delta and u is the velocity fluctuation over time during one time step Δt. The control volume method was used as discretization method (Olsen 2004). The Reynolds stress term was modeled by the k-ε turbulence model. The model computed the turbulent stresses $\overline{u_i u_j}$, using the eddy viscosity relation:

$$-\overline{u_i u_j} = \nu_t\left(\frac{\partial U_i}{\partial x_j} + \frac{\partial U_j}{\partial x_i}\right) - \frac{2}{3}k\,\delta_{ij} \text{ with } \nu_t = \frac{c_\mu \cdot k^2}{\varepsilon}, \tag{3}$$

where the turbulent kinetic energy k and its dissipation rate ε determining the eddy viscosity ν_t were obtained from the following equations:

$$\frac{Dk}{Dt} = \frac{\partial k}{\partial t} + U_j\frac{\partial k}{\partial x_j} = \frac{\partial}{\partial x_j}\left[\left(\nu + \frac{\nu_t}{\sigma_k}\right)\frac{\partial k}{\partial x_j}\right] + P_k - \varepsilon \tag{4}$$

$$\frac{D\varepsilon}{Dt} = \frac{\partial \varepsilon}{\partial t} + U_j\frac{\partial \varepsilon}{\partial x_j} = \frac{\partial}{\partial x_j}\left[\left(\nu + \frac{\nu_t}{\sigma_\varepsilon}\right)\frac{\partial \varepsilon}{\partial x_j}\right] + C_{\varepsilon 1}\frac{\varepsilon}{k}P_k - C_{\varepsilon 2}\frac{\varepsilon^2}{k} \tag{5}$$

The production of turbulent kinetic energy P_k was defined as:

$$P_k = \nu_t \frac{\partial U_i}{\partial x_j}\left(\frac{\partial U_j}{\partial x_i}+\frac{\partial U_i}{\partial x_j}\right) \quad (6)$$

An implicit method was used for transient terms and the pressure field was computed with the *SIMPLE* method (Patankar, 1980). The Rhie and Chow interpolation (Rhie and Chow, 1983) was applied to compute the velocities and the fluxes at the cell surfaces. Zero gradient boundary conditions were used for all variables at the outflow boundary. The upstream velocities were defined by a Dirichlet boundary condition. Wall law functions for rough boundary introduced by Schlichting (1979) were used for the side walls and the bed. Initially the bed roughness was computed by the model as a function of the bed sediment distribution. However in case where fine bed material prevailed and bed roughness is mostly affected by dunes and ripples, this approach was not giving appropriate results. Instead, reasonable results were obtained by using the following approach. First the bed form height was calculated with an equation developed by v. Rijn (1984c). The value was depending mainly on the water depth y, the characteristic sediment grain d_{50} and the prevailing shear stress τ.

$$\frac{\Delta}{y} = 0.11\cdot\left(\frac{d_{50}}{y}\right)^{0.3}\cdot\left(1-e^{-0.5\left(\frac{\tau-\tau_{c,i}}{\tau_{c,i}}\right)}\right)\cdot\left(25-\left(\frac{\tau-\tau_{c,i}}{\tau_{c,i}}\right)\right), \quad (7)$$

where Δ is the bed form height and $\tau_{c,i}$ the critical shear stress for each fraction. Then the bed form height is converted into bed roughness k_s with the following equation.

$$k_s = 3.0\cdot d_{90} + 1.1\cdot\Delta\cdot\left(1.0-e^{\left(\frac{-25\cdot\Delta}{7.3\cdot y}\right)}\right) \quad (8)$$

A non-hydrostatic pressure approach was implemented, so the water surface elevation was determined from the computed pressure field, resulting in an authentic computation of lateral slope of the water surface in the bends.

Similar to the upstream boundary condition of the velocities, the boundary conditions for the inflowing sediment transport was specified with a Dirichlet boundary condition and zero gradients for the water surface, the outlet, and the sides. In the present study no sediment inflow was used. The boundary conditions at the bed are given by the sediment transport relations for bed load. In the default configuration of the model, fractional sediment transport was computed by the bed load transport formulas of v.Rijn (1984a) applied individually for each fraction.

$$\frac{q_{b,i}}{d_i^{1.5}\cdot\sqrt{\frac{(\rho_S-\rho_W)\cdot g}{\rho_S}}} = \zeta\cdot\frac{\left(\frac{\tau-\tau_{c,i}}{\tau_{c,i}}\right)^{1.5}}{d_i^{2}\left(\frac{\rho_S/(\rho_W-1)\cdot g}{\nu^2}\right)^{0.1}}, \quad (9)$$

where $\zeta = 0.053$ is used as the default value in the original equation.

The computational domain was subdivided into three layers, a water layer near the river bed, with a mixture of water and sediments, an upper sediment layer were the bed load is calculated, denoted active layer and a lower sediment layer, denoted inactive layer. When fractional transport was computed, sorting mechanisms were considered to happen in the active layer. The height of the active layer was kept constant, equally to the size of the largest grain in the sediment mixture. The height of the inactive layer is set to a large value in order to supply the active layer with the sufficient amount of sediments. The grain size distributions in the two bed layers were obtained by considering sediment continuity for each fraction.

Finally the bed changes were computed from sediment continuity in the bed cell, as the difference between the inflowing and out flowing sediment fluxes. The defect was converted into a vertical bed elevation by dividing it by the submerged density of the sediments, 1320 kg/m³, to find the volume of the deposits for each time step. This volume was then transformed into bed level changes for the grid. Both the sedimentation and the erosion processes were modeled using the same approach.

For the simulation of the laboratory experiments described in chapter 2, the geometry needed to be discretized. A three-dimensional, structured, non-orthogonal, vertically adaptive and curvilinear grid with a non-staggered variable placement was generated. 173 hexahedral cells in the stream wise, 16 cells in the lateral and 5 cells in the vertical direction were used. A time step of 5 seconds was chosen. After each time step, the water and the bed surface were updated.

For discretization of the initial sediment distribution the continuous bed sediment sieve curve was decomposed into five size fractions. Starting with the smaller fraction, the sediment mixture contains of 10 % with a size of 0.3 mm. 20 % of 0.45 mm, 20 % of 0.58 mm, 20 % of 0.7, 20 % of 0.82 and 10 % of 1mm.

3.2 *Results and discussion*

3.2.1 *Simulation results of Run 1*

Since the hydraulic performance of the present model was tested intensively in meandering channels (Wilson et al., 2003), the present study was

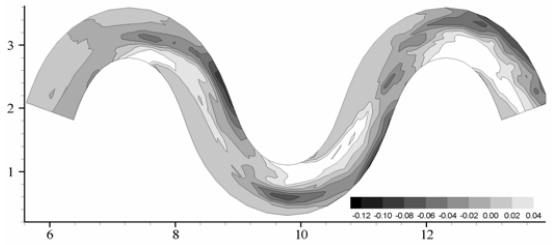

Figure 3. Measured bed changes in Run 1

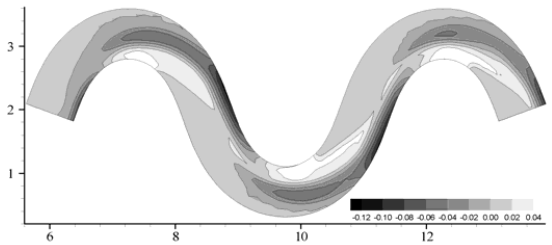

Figure 4. Calculated bed changes in Run 1

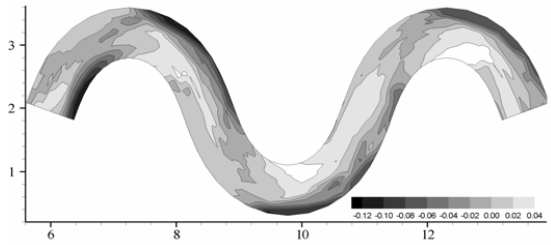

Figure 5. Measured bed changes in Run 5

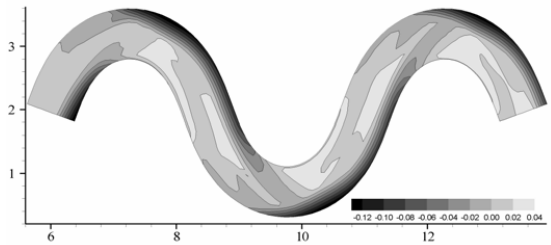

Figure 6. Calculated bed changes in Run 5

focusing on the performance of predicting bed deformation only.

Two different laboratory setups were simulated. The hydraulic conditions of each experiment are described in chapter 2. The results are presented herein. Comparing the plan view of Run 1, depicted in Figure 3 for the experiments and in Figure 4 for the simulation, one can see the overall agreement with the measured data. The first two bends are characterized by a typical point bar at the apex, accompanied by a small scour in the center of the channel. The maximum scour was located further downstream, almost at the cross over, on the outside of the channel. Looking at simulated bed changes in the first two bends, one can see that the bed deformation was predicted well. The location of the maximum scours and bar positions matched. However there was some disagreement in the pattern of the last bend. In the experiment, the scour was located far more at the outside of the bend as in the previous two bends. This characteristic was not found in the results of the numerical run. So far there is no physical explanation for this longitudinal asymmetric bed development (da Silva, 2006a).

The bed pattern seen in the plan view can also be shown in a longitudinal view. Figure 7 and Figure 10 show the left and the right side, respectively. One can see that the position of the maxima match well, but the absolute magnitude of the scours is slightly overestimated.

The Figures 8, 9, 11 & 12 show the comparison of the data to the numerical results in the cross sections. Four cross sections are depicted. The locations of the cross section are shown in Figure 2. These cross sections were chosen since they were located where the maximum erosion was found in the experiments. One can see that especially in cross section 15 & 30 the calculated bed changes matched the measurements very well. In the Figures 8 & 9, one can see that the simulated scour locations were shifted towards the left channel side.

3.2.2 *Simulation results of Run 5*

The plan views of the bed changes from the experimental and from the numerical model are depicted in the figures 5 and 6, respectively. As well as for the results in Run 1 one can see that the overall pattern matched. The magnitude of the bed changes also matched. However, the scouring in the longitudinal direction was over estimated. The scour spread too far downstream.

Figure 13 shows that the scour in the last bend is not as deep as the previous two bends. This characteristic is not reproduced by the numerical results. Otherwise one can see that the positions of the maxima are calculated to be at the same locations as in the physical model. From Figures 14, 15, 17 & 18 it is observed that the computed bed elevations at cross section 26 match particularly well with the measured data. Figure 14 & 17 show that the deposition pattern is slightly overestimated, but still being in reasonably good agreement with the measured data.

For Run 5, in the sediment transport capacity formula, the default value of $\zeta = 0.053$ was changed to $\zeta = 0.009$. This means that the sediment transport capacity had to be reduced to get reasonable results.

4 CONCLUSION AND RECOMMENDATIONS

The transient bed changes of a meandering laboratory channel with two different width to depth ratios have been successfully modeled. The calculated

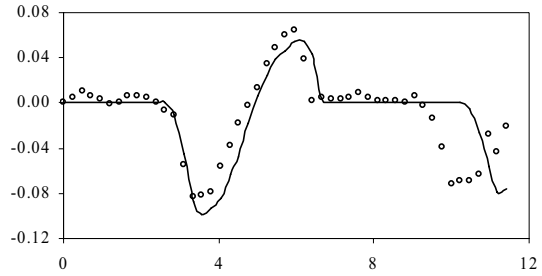

Figure 7. Run 1; Longitudinal view, left channel side

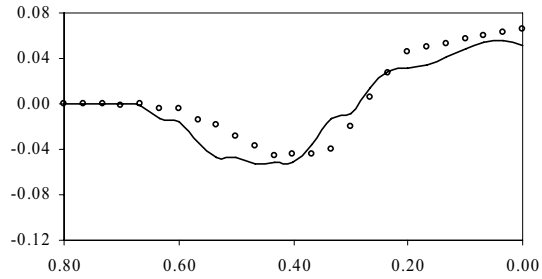

Figure 8. Run 1; Crossectional view, #11

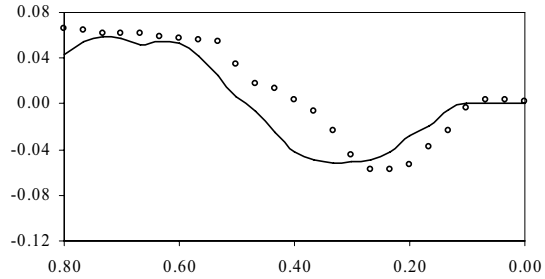

Figure 9. Run 1; Crossectional view, #26

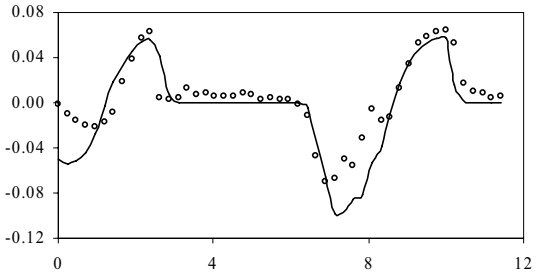

Figure 10. Run 1; Longitudinal view, right channel side

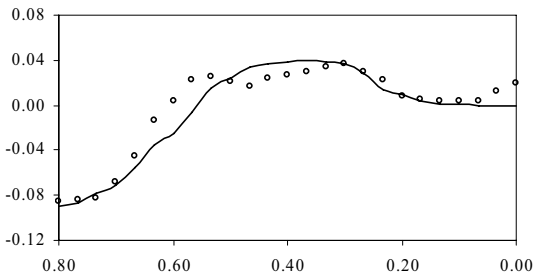

Figure 11. Run 1; Crossectional view, #15

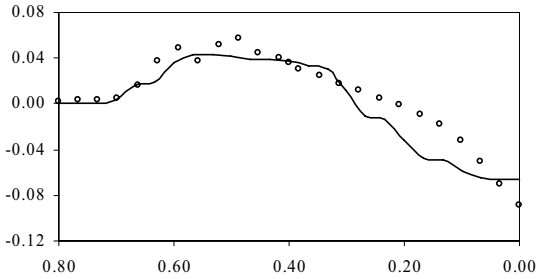

Figure 12. Run 1; Crossectional view, #30

bed changes are in good agreement with the measurements for both cases. The numerical model was enhanced with a roughness approach taking into account the presence of bed forms. The results were very sensitive to the formulas for bed form height and bed roughness. The roughness approach seemed to be strongly connected to the development stage of a bed form and therefore to the sediment transport capacity. In the opinion of the authors there is more research needed for the universal implementation of a roughness approach taking bed form roughness into account. Furthermore, a wider range of the width to depth ratio should be tested in order to validate the present results. It seems that the width to depth ratio has a larger influence on the bed pattern in meandering channels as it is believed in literature today. To make any reliable conclusion, the model should be tested on data from experiments with different deflection angles Θ, too.

ACKNOWLEDGEMENT

The authors would like to thank Dr. A.M. da Silva who was so kind to distribute the data used in this study and giving fruitful advices for a successful modeling of the data. In addition, the first author likes to thank the Norwegian Research Council for their support through the BeMatA Program.

REFERENCE

Demuren , A.O., Rodi, W. 1986. Calculation of flow and pollutant dispersion in meandering channels, *Journal of Fluid mechanics*, 172, 63-92.

Olsen, N. R. B 2004 *Hydroinformatics, fluvial hydraulics and limnology*, Department of Hydraulic and Environmental Engineering, The Norwegian University of Science and Technology, http://folk.ntnu.no/nilsol/tvm4155/flures5.pdf.

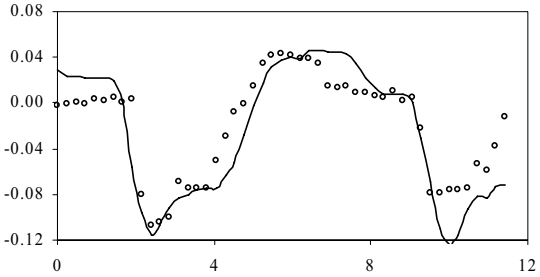

Figure 13. Run 5; Longitudinal view, left channel side

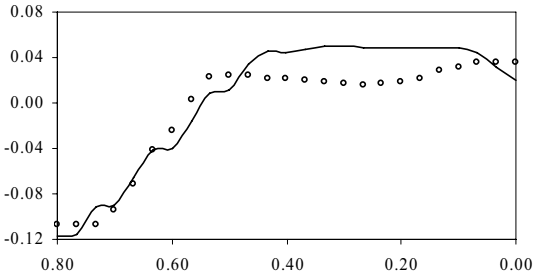

Figure 14. Run 5; Crossectional view, #11

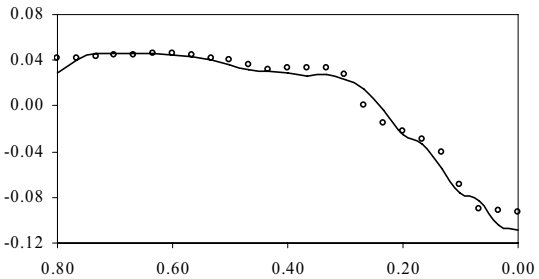

Figure 15. Run 5; Crossectional view, #26

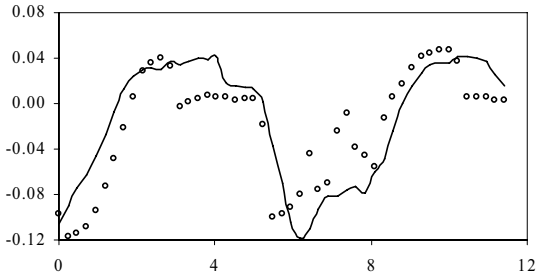

Figure 16: Run 5; Longitudinal view, right channel side

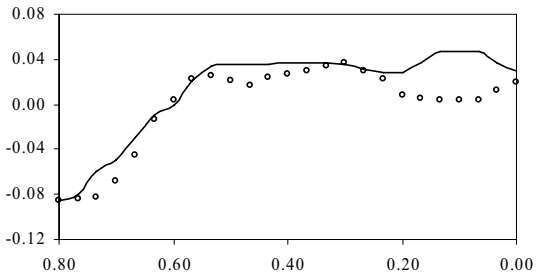

Figure 17. Run 5; Crossectional view, #15

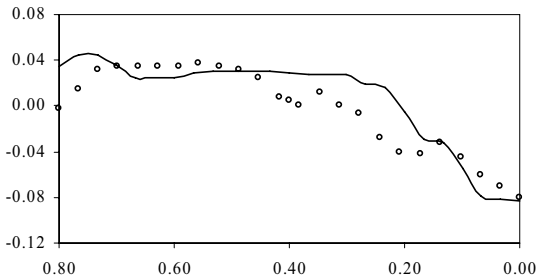

Figure 18. Run 5; Crossectional view, #30

Patankar, S., 1980, *Numerical Heat Transfer and Fluid Flow*. Taylor and Francis Publishers

Rhie, C. and Chow, W., 1983, Numerical study of the turbulent flow past an airfoil with trailing edge separation, *AIAA* Journal, 21 (11).

Rijn, L. C. van, 1984a, Sediment Transport, Part I: Bed Load Transport, *J. Hydraulic Engineering*, 110 (11), pp. 1431-1457.

Rijn, L. C. van, 1984b, Sediment Transport, Part II: Suspended Load Transport, *J. Hydraulic Engineering*, 110 (11), pp. 1613-1641.

Rijn, L. C. van, 1984c, Sediment Transport, Part III: Bed forms and alluvial roughness, *J. Hydraulic Engineering*, 110 (12), pp. 1733-1754.

Ruether, N. and Olsen, N. R. B., 2005, Three dimensional modeling of sediment transport in a narrow 90° channel bend, *J. Hydraulic Engineering*, 131 (10), pp. 917-920.

Schlichting, H., 1979, *Boundary layer theory*, McGraw-Hill Book Company, New York.

Silva, A.M.F. da, 2006a. Personal communication.

Silva, A.M.F. da, El-Tahawy, T. 2006b. Location of hills and deeps in meandering streams: an experimental study. *Proc. 3rd Int. Conference on Fluvial Hydraulics, River Flow 2006*, A.A. Balkema, Netherlands.

Wilson C.A.M.E., Boxall, J.B., Gymer, I., Olsen, N.R.B. 2003, Validation of a three-dimensional numerical code in the simulation of a pseudo-netrual meandering stream, *J. Hydraulic Engineering,* 129 (10), pp. 758-768.

Wu, W., Rodi, W. and Wenka, T., 2000. 3d numerical modelling of flow and sediment transport in open channels, Journal of Hydraulic Engineering, 126 (1), pp. 4-15.

Zeng, J., Constantinescu, G. and Weber, L. 2005. A fully 3D non-hydrostatic model for prediction of flow, sediment transport and bed morphology in open channels, *Proc., 31st IAHR Congress,* Seoul, Korea.

Paper V

Modelling free-forming meander evolution in a laboratory channel using three dimensional computational fluid dynamics

N. Rüther, N.R.B. Olsen

Submitted in May 2006: Geomorphology, in review

Modelling free-forming meander evolution in a laboratory channel using three dimensional computational fluid dynamics

N.Rüther (corresponding author) and N.R.B.Olsen

Department of Hydraulic and Environmental Engineering

Norwegian University of Science and Technology

S.P. Andersensvei 5, 7941 Trondheim, Norway

Telefon: +47 7359 4756, Telefax: +47 7359 1298, e|mail: nils.ruther@ntnu.no

ABSTRACT

The present paper investigated the use of computational fluid dynamics (CFD) in predicting the formation, development and migration of free-forming meander bends. The three dimensional (3D) CFD model computes water flow and sediment transport in alluvial channels and predict vertical and horizontal bed changes. Different algorithms and parameters were tested to provide an insight into the application range of CFD when modelling free-forming meander formation. The computational domain was discretized by an unstructured grid. A control volume method was used for the discretization of the Navier-Stokes equations for the flow calculation and of the convection-diffusion equation for the sediment transport calculation. Turbulence was modelled by the k-epsilon turbulence model. The simulation was started from an initially straight grid, with neither sediment feed nor any perturbation at the inflow boundary. The model computed the river bed evolution over a real time period of three days. Results were compared with laboratory experiments and showed that the CFD model can predict many of the characteristics of the alluvial meander formation and migration. However, there are some limitations and uncertainties that have to be clarified in future investigations.

Key words: Computational Fluid Dynamics, modelling, sediment transport, meander, alluvial channel, bank retreat, erosion, fluvial geomorphology

1 Introduction

Modelling of sediment transport in river and channel bends has been a topic of research over several decays. Initially, researchers found universal relations for sediment transport on generally sloped river beds. The goal was to correlate the bed load transport rate in the transversal direction to that in the longitudinal one. The results were the first generation sediment transport models predicting transport rates in bended flow with the related bed deformation (Engelund, 1974, Odgaard, 1981, Parker, 1984 and Struiksma et al, 1985). Later on the researchers became more interested in predicting formation and migration of meander bends. So-called process-based models wherein a rate of bank erosion proportional to the near bank velocity was assumed were suggested by several researchers (Ikeda et al., 1981, Parker and Andrews, 1986, Lancaster and Bras, 2002, Edwards and Smith, 2002). Those models were considerable effective when predicting long-term behaviour and a large scale meandering river system. Shortcomings were reported when predicting detail migration rates over a shorter time period. In addition to this type of models, some researchers suggested the use of physically based model. Herein, sediment transport and bank erosion rates are calculated to assess the advance or retreat of a channel bank line (Osman and Thorne, 1988). With the time and increasing computer power, two dimensional (2D) hydrodynamic models were coupled with sediment transport models to predict lateral and vertical erosion rates of alluvial channels. Mosselman (1998), Duan et al (2001) and Darby et al (2002) presented a 2D hydrodynamic model on a structured grid, including algorithms for basal bank erosion to predict migration of meander evolution. To incorporate the effects of the three dimensional (3D) flow in a channel bend, the 2D hydrodynamic approach was enhanced with empirical formulae. Mosselman (1998) came to the conclusion that these formulae were the main reasons for the shortcomings in his simulations. In the study of Olsen (2003) a fully 3D model

was presented and verified on the same data set Duan et al (2001) used. The results from the simulation showed good agreement when predicting the meander migration from an initially straight channel with an upstream perturbation in terms of a single bend. Going one step further, Rüther and Olsen (2003 & 2005) showed first results on the simulation of meander evolution when using no initial perturbation. Their work focused on the formation of alternate bars and the initiation of meandering starting from a completely straight channel. In addition, migration and rotation of meander bends could be modelled as well as characteristic meander bend topography. These results were obtained by using sediment feed to the entrance of the flume. Modelling such a complex flow situation was relatively straight forward since the sediment coming from upstream prevented the channel from significant vertical erosion. Consequently, the vertical water surface location could be assumed to be constant. The goal of the present study is to model the plan form evolution of an initially straight alluvial channel with neither an initial perturbation nor sediment feed from upstream, and verify the CFD program on the data recorded by Friedkin (1945). The challenge herein was to implement a free surface algorithm which allows the water level to move down vertically according to the erosion and other bed changes in the channel.

2 Base data

The base data was delivered by an investigation of Friedkin (1945). Friedkin did basic research on the behaviour of a trapezoidal laboratory channel. He documented the vertical and lateral movement of the channel during an experimental run of 72 hours. A 40.0 m long tilting flume with a 12.0 m wide effective section was filled up with sand of about 0.6 m depth and an initially straight, trapezoidal shaped channel, with an average width of 0.6 m, a depth of 0.088 m and a slope of 0.009 was excavated. It was then exposed to a constant discharge Q = 8.5 l/s with a

water depth of 0.05 m. The sand material was fairly homogenous with a grain size distribution of d50 and d90 with 0.2 mm and 0.26 mm, respectively. The Figures 1 & 2 show the plan form before and after the experiment. The result showed a meandering channel with a maximum meander amplitude and wavelength of about 3.0 m and 12 m respectively. The meandering evolution started downstream at the first third of the channel length. In addition, Figure 2 shows that the bend size grow with increasing longitudinal distance. This is due to the fact that the there was no sediment feed from upstream. Also, the valley area had deepened during the experiment due to the fact that the flow had washed out sediments. Furthermore, one can see in Figure 2 that during the experiment the meandering main channel had changed its course several times.

Placement of Figure 1 & Figure 2

3 Modelling free-forming meander evolution

3.1 Numerical Methods

3.1.1 Flow and turbulence simulation

The numerical model used in the present study was developed by Olsen (2004). The flow field for the three-dimensional geometry was determined by solving the continuity equation and the Reynolds averaged Navier-Stokes equations:

$$\frac{\partial U_i}{\partial x_i} = 0 \qquad \text{with } i=1,2,3 \quad (1)$$

$$\frac{\partial U_i}{\partial t} + U_j \frac{\partial U_i}{\partial x_i} = \frac{1}{\rho} \frac{\partial}{\partial x_i} \left(-P\delta_{ij} - \rho \overline{u_i u_j} \right) \quad (2)$$

U is the velocity averaged over the time t, x is the spatial geometrical scale, ρ is the water density, P is the pressure, δ is the Kronecker delta and u is the velocity fluctuation over time during one time step Δt. The control volume method was used as discretisation method (Olsen 2004) and the convective terms in the Navier-Stokes equations were solved by the second order upwind scheme. The Reynolds stress term was modelled by the k-ε turbulence model (Rodi 1980). This two-equation turbulence model computed the turbulent stresses $\overline{u_i u_j}$, using the eddy viscosity relation:

$$-\overline{u_i u_j} = \nu_t \left(\frac{\partial U_i}{\partial x_j} + \frac{\partial U_j}{\partial x_i} \right) - \frac{2}{3} k \, \delta_{ij} \text{ with } \nu_t = \frac{c_\mu \cdot k^2}{\varepsilon}, \quad (3)$$

where the turbulent kinetic energy k and its dissipation rate ε determining the eddy viscosity ν_t were obtained from the following equations:

$$\frac{Dk}{Dt} = \frac{\partial k}{\partial t} + U_j \frac{\partial k}{\partial x_j} = \frac{\partial}{\partial x_j} \left[\left(\nu + \frac{\nu_t}{\sigma_k} \right) \frac{\partial k}{\partial x_j} \right] + P_k - \varepsilon \quad (4)$$

$$\frac{D\varepsilon}{Dt} = \frac{\partial \varepsilon}{\partial t} + U_j \frac{\partial \varepsilon}{\partial x_j} = \frac{\partial}{\partial x_j} \left[\left(\nu + \frac{\nu_t}{\sigma_\varepsilon} \right) \frac{\partial \varepsilon}{\partial x_j} \right] + C_{\varepsilon 1} \frac{\varepsilon}{k} P_k - C_{\varepsilon 2} \frac{\varepsilon^2}{k} \quad (5)$$

The production of turbulent kinetic energy P_k was defined as:

$$P_k = \nu_t \frac{\partial U_i}{\partial x_j} \left(\frac{\partial U_j}{\partial x_i} + \frac{\partial U_i}{\partial x_j} \right) \quad (6)$$

An implicit method was used to solve transient terms and the pressure field was computed with the *SIMPLE* method (Patankar, 1980). The Rhie and Chow interpolation (Rhie and Chow, 1983) was applied to compute the velocities and the fluxes at the cell surfaces. Zero gradient boundary conditions were used for all variables at the outflow boundary. The upstream velocities were defined by a Dirichlet boundary condition. Wall law functions for rough boundary, eq. (7), introduced by Schlichting (1979) were used for the side walls and the bed.

$$\frac{U}{u*} = \frac{1}{\kappa} \cdot \ln\left(\frac{30y}{k_s}\right), \quad (7)$$

where $u*$ is the shear velocity, κ a constant of 0.4, y the water depth and k_s the equivalent sand roughness. In cases where fine bed material prevailed, k_s is mostly dominated by form roughness of dunes and ripples. Therefore the boundary roughness k_s was herein determined by the following approach. First the bed form height was calculated with an equation developed by v. Rijn (1984c). The value was depending mainly on the water depth y, the characteristic sediment grain d_{50} and the bed shear stress τ.

$$\frac{\Delta}{y} = 0.11 \cdot \left(\frac{d_{50}}{y}\right)^{0.3} \cdot \left(1 - e^{-0.5 \cdot \left(\frac{\tau - \tau_{c,i}}{\tau_{c,i}}\right)}\right) \cdot \left(25 - \left(\frac{\tau - \tau_{c,i}}{\tau_{c,i}}\right)\right), \quad (8)$$

where $\tau_{c,i}$ is the critical shear stress for each fraction, Δ the bed form height and d_{50} the characteristic grains size. Then the bed form height was converted into bed roughness k_s with the following equation.

$$k_s = 3.0 \cdot d_{90} + 1.1 \cdot \Delta \cdot \left(1.0 - e^{\left(\frac{-25 \cdot \Delta}{7.3 \cdot y}\right)}\right) \quad (9)$$

A non-hydrostatic pressure approach was implemented, so the water surface elevation was determined from the computed pressure field. This resulted in an authentic computation of lateral slope of the water surface in the bends. The free surface was computed by first solving the differential Equation (10).

$$\frac{\partial z}{dx} = \frac{1}{\rho g} \cdot \frac{\partial p}{\partial x} \quad (10)$$

In the numerical solution, the difference in vertical elevation of the surface cell was based on the pressure gradient ∂p . A formula was developed for the water surface elevation in one cell as a

function of the water surface elevation changes in the neighbour cells. This equation was solved iteratively. Similar to the upstream boundary condition of the velocities, the boundary conditions for the inflowing sediment transport was specified with a Dirichlet boundary condition and zero gradients for the water surface, the outlet, and the sides.

3.1.2 Sediment transport simulations

Consider the computational domain is discretized in *n*-number of cells in the vertical direction. Illustrated in Figure 3, the white area is named real computational domain and is where the water and sediment transport takes place. The light and dark grey shaded area is named virtual active and inactive sediment layer, respectively and they are located below the river bed. The sediment transport was calculated in the real computational domain. The convection-diffusion equation,

$$\frac{\partial c}{\partial t} + U_j \frac{\partial c}{\partial x_j} + w \frac{\partial c}{\partial x} = \frac{\partial}{\partial x_j}\left(\Gamma \frac{\partial c}{\partial x_j} \right), \quad (11)$$

was solved for the determination of the suspended load concentration in the water. An empirical formula for the suspended load transport capacity was used as a boundary condition for the differential equation. The formula was developed by v.Rijn (1984b) :

$$c_{bed,susp.load,i} = 0.015 \frac{d_i}{a} \frac{\left(\frac{\tau - \tau_{c,i}}{\tau_{c,i}} \right)^{1.5}}{\left(d_i \left(\frac{\rho_S / (\rho_W - 1) \cdot g}{\nu^2} \right)^{1/3} \right)^{0.3}} \quad (12)$$

It was applied to the cells closest to the bed. Additionally, the bed load was calculated in these cells. The bed load formula by v.Rijn (1984a) was used:

$$\frac{q_{b,i}}{d_i^{1.5}\cdot\sqrt{\frac{(\rho_S-\rho_W)\cdot g}{\rho_S}}}=\eta\cdot\frac{\left(\frac{\tau-\tau_{c,i}}{\tau_{c,i}}\right)^{1.5}}{\left(d_i\left(\frac{\rho_S/(\rho_W-1)\cdot g}{\nu^2}\right)^{1/3}\right)^{0.3}}, \qquad (13)$$

where $\eta = 0.053$ is used as the default value in the original equation. If using multiple grain sizes, eq. (13) is solved for each fraction. The amount of bed load is then converted to a concentration by using eq.(14).

$$c_{bed,bedload,i}=\frac{q_{b,i}}{a\cdot U_{bed}}, \qquad (14)$$

where a is equal to the height of the bed cell.

Earlier investigations have shown that a sediment particle located on a sloped bed has a different criterion for incipient motion than a particle on a horizontal bed. The gravitational force affects the stability on a sloping bed. To take this in to account, the present study used a relation by Brookes (1963), reducing the critical shear stress for particles on sloped beds. The reduction is expressed with a factor *R* defined as

$$R=-\frac{(\sin\alpha\sin\beta)}{\tan\Phi}+\sqrt{\left(\frac{(\sin\alpha\sin\beta)}{\tan\Phi}\right)^2-\cos^2\alpha\left[1-\left(\frac{\tan\alpha}{\tan\Phi}\right)^2\right]} \qquad (15)$$

The factor *R* is a function of β, the angle between the streamline and the direction of the bed shear stress, of α, the transversal slope of the channel bed and a slope parameter Φ being similar to the angle of repose. The critical shear stress coefficient for a particle of the size *i* is then written

$$\tau^*_{c,i}=R\cdot\tau^*_{c,i,0} \qquad (16)$$

The virtual computational domain, in Figure 3, is illustrated as the light and dark grey shaded area, located below the real computational domain. It consists of two layers, an upper one which

is called active and a lower one, called inactive. The two layers are responsible for the continuity of the sediment calculation in the computational domain. The active layer supplies the real computational domain with sediments in case of erosion and takes away sediments in case of deposition. The thickness of the layer is determined by the amount of sediment being taken during one time step. In addition, when fractional transport was computed, sorting mechanisms took place in the active layer. The height of the inactive layer was set to a large value in order to supply the active layer with the sufficient amount of sediments. The grain size distributions in the two bed layers were obtained by considering sediment continuity for each fraction.

Finally, the bed changes were computed from sediment continuity in the bed cell, as the difference between the inflowing and out flowing sediment fluxes. The defect was converted into a vertical bed elevation by dividing it by the submerged density of the sediments, 1320 kg/m^3, to find the volume of the deposits for each time step. This volume was then transformed into bed level changes for the grid. Both the sedimentation and the erosion processes were modelled using the same approach.

3.1.3 Mesh and mesh adjustment

The CFD program used a three dimensional unstructured grid with a mixture of tetrahedral and hexahedral cells to model the geometry. To allow changes in the bed morphology mainly in the lateral direction, the CFD program included an algorithm for wetting and drying (Olsen, 2003). This algorithm generated new cells in areas where erosion took place and let cells disappear where sediment deposited. Consequently the grid changed in shape and size over time as the geometry of the meandering channel was formed. Initially, the computational domain was allocated to a two dimensional grid which determined the area where lateral changes could

happen. Once a two dimensional cell was activated, or wetted, it was discretized with a certain amount of cells in the vertical direction. This number was depending on the depth in the computational domain. The criterion for the formation or disappearance of a cell was correlated to a certain minimum water depth ζ_1 at the four corners of each cell. A second value, ζ_2 was the responsible criterion for the formation of just one cell over the depth. Meaning, in areas with $\zeta_1 \leq y \leq \zeta_2$ only one cell was used and if $y \leq \zeta_1$ or $\zeta_1 \geq y$ cells will dry up or be wetted, respectively.

3.2 Simulation Results

3.2.1 Plan form evolution

Figure 4 shows the simulated plan form evolution of the experiment of Friedkin.
From an initially straight channel, a meandering channel developed and three consecutive following meander bends were formed. After the first third of the channel length, the meander bends start to grow. Increasing continuously in size, the last meander bend has amplitude of about 4 m.
The presented figure was the result of the simulation when applying eq. (16) to the cells close to bank line of the main channel. Sediment particles on side slopes then had a lower critical shear stress resulting in higher erosion rates. The formula could be applied due to the fact that there was no cohesion of the bed material in the banks. Consequently, the sediment particle moved independent from each other, and no bank failures or similar phenomena were modelled.
The importance of the use of such relation in the modelling of free forming meander evolution is demonstrated with Figure 5. Here, the plan form evolution of the simulation is illustrated without

using eq. (16). The channel is more or less straight showing some random alternation with locally eroded channel banks. This is due to the fact that there less side erosion.

Placement of Figure 4 & 5

When using empirical formulae in combination with CFD, one must be aware of the sensitivity of coefficients. In this study, the parameter ζ was expected to have the most influence on the results. Different values between 0.002 and 0.02 m were tested. With values higher than ζ=0.01 m, the channel got unreasonable narrow. Simulation results with lower values showed only minor changes to the base configuration. It is assumed that the parameter is connected to the average depth of the main channel. Therefore, this parameter is specific for the present case, and it is not considered to be universal.

In Figure 6 one can see the evolution of the plan form of the free-forming meandering channel over time. Figure 6a is taken at 833 minutes of the total running time. The channel has not started to move laterally. The figure shows a scour with a corresponding deposition pattern moving in longitudinal direction through the channel. The time distance between each of the following pictures, 6 b), c), d) & e) is 833 minutes. The alternation of deeps and shoals in Figure 6 b) is followed by the initialisation of the meandering plan form in Figure 6c). In the consequent figures, the channel amplitude as well as the wavelength increases over time. Comparing Figure 6 d) & e) to the others in Figure 6, one can see that the lateral movement tended to converged. The evolution in the last two time steps was considerably slower than the movement in the previous time steps.

Placement of Figure 6

Figure 7 shows the development of the computational domain. The grid illustrated in grey shows the evolution at a real time of 55.56 hours. The black displayed grid is at the end of the

simulation. During the time the grid shifted, 16.67 hrs, the same point at the centreline of the grid was moving about 3 m downstream. Consequently the speed of the longitudinal channel movement was about 0.18 m/hr.

Placement of Figure 7

3.2.2 Effects of the three dimensional flow pattern

The water flow and the sediment movement in a channel bend are mainly influenced by a spiral motion of the water body called the secondary current. This process is initialized by the centrifugal forces accelerating water particles at the water surface towards the outer part of the bend. This causes a pressure difference between the inner and the outer streamline of the bended flow, forcing a near bed current pointing towards the inner part of the bend. The superposition of this secondary current with the main flow direction produces the well known spiral motion occurring on river bends. Being influenced by this spiral motion the transported sediment particles are moving slightly more towards the inner part of the bend where they deposit due to lower main flow velocities, forming a point bar. This process destabilizes the balance of the sediment distribution in a cross section, causing erosion at the outer part of the bend. The transversal bed slope increases with increasing scour depth and point bar height. To predict this helical flow without using empirical formulas, one has to use a three dimensional CFD model. By discretising the domain over the depth, it is possible to calculate the velocity and its direction in each of the cells in the vertical direction.

Placement of Figure 8

Figure 8 shows the velocity vectors and the channel bed and at the water surface, respectively. The deviation between the vectors in the two directions is a measure for the strength of the helical

flow of the water body. The resulting bed evolution can be seen in the Figure 9. The calculated water depth in one of the downstream bends was illustrated. One can see the steep lateral gradient on the outside of the bend as well the bar development on the inside. At the location where the helical flow had its maximum, one can observe the location of the maximum scour.

Placement of Figure 9

Figure 10 a) & b) show the cross-section at the cross over and at the apex of the bend. In addition, the velocity distribution over the width is illustrated. The bed levels and the velocities in the cross section at the cross over appear to be symmetrical. The highest velocity with 0.28 m/sec, was in the centre of the cross-section where the maximum depth is located. Towards the sides the velocities decrease with decreasing water depth. The water surface is nearly horizontal. Bed levels and velocity distribution in the cross-section at the apex are unsymmetrical, shifted towards the outside of the bend. The bed pattern observed in Figure 9 was also reflected. One can observe the steep lateral gradient at the outside of the bend and the bar development at the inside. The location of the maximum depth was shifted towards the outside due to the helical flow. Consequently the lateral water surface was tilted which can also be seen in the Figure 10 b. The maximum velocity was with a value of 0.22 m/sec slightly smaller than the velocity in the section at the cross over.

Placement of Figure 10 a) & b)

4 Discussion

The result of a numerical model simulation of a free forming meander formation was presented in paragraph 3.2. In this paragraph the result is evaluated and compared to the physical model test (Friedkin 1945). The result is depicted in Figure 11. The center line of the meandering alluvial

channel is extracted and illustrated with a solid line and compared against the centerline of the channel developed in the physical model test, marked with a dashed line.

Placement of Figure 11

Looking first at the upstream part of the channel, the initiation of alternation and meandering started roughly at the same location: at the longitudinal coordinate of 11 m. However, the wave length in the consequent meander bends, between x = 12 and 21 m, was strongly underestimated by the numerical model, leading to the development of an additional bend. The meander evolution in the most downstream end of the channel was better predicted. The computed wave length of the channel deviates here only 15 % from the physical model results.

A meander formation from an initial straight channel without any sediment feed from upstream, the meander size will increase in the downstream direction. Figure 5 shows that the growing amplitude at each location of the plan view matches very well to the measured values. This is also an improvement compared with results from previous studies.

5 Conclusion

A CFD model has been used to simulate a self forming meander pattern over time. From an initially straight alluvial channel with neither an initial perturbation nor sediment feed, the model computes the initiation and the migration of the meander bends. Hence, the program predicts the process of erosion and sedimentation as well as the lateral movement of the channel. The results matched the measurements of a physical model study concerning the meander amplitude and downstream growth of the meander bends. The maximum meander wavelength was underestimated by around 15 %. In addition, the helical flow and the characteristic river bed development in a meander bend could be identified in the numerical simulation. The results

showed that for the present case, modeling of free forming meander formation using CFD is functioning well. However, the investigations showed that the model has to be tested to other cases, too, in order to obtain a universal predictor for meander formation in alluvial channels. Especially when applying the model to natural cases where the bank material is influenced by cohesion and vegetation, more complex bank erosion algorithms may need to be developed.

Notation

c = volume sediment concentration [m^3/m^3]

d, d_{50} = grain size of 50 % finer [m] = median sediment diameter

d_{90} = grain size of 90 % finer [m]

i = index for the three space directions [-]

i = index for the sediment fraction [-]

k = turbulent kinetic energy [m^2/s^2]

ks = equivalent sandroughness [m]

P = pressure [N/m^2]

P_k = production of turbulent kinetic energy

Q = water discharge [m^3/s]

q_{bi} = transport rate of the ith fraction of bed-load per unit width [$m^3/(s*m)$]

t = time [s]

u^* = shear velocity [m/s]

u = velocity fluctuation [m/s]

U = average velocity [m/s]

x_i = spatial geometrical scale [m]

y = water depth [m]

1

α = angle of the transversal slope

β = angle between the streamline and the direction of the bed shear stress

δ_{ij} = Kronecker delta

Δ = bed form height [m]

ε = dissipation of turbulent kinetic energy [m²/s²]

Φ = angle of repose of the sediment particle

Γ = diffusion coefficient [m²/s]

η = coefficient in the bed load capacity formula

ν_t = eddy viscosity [m²/s]

κ = constant equal to 0.4

ρ = density of water [kg/m³]

ρ_s = density of sediments [kg/m³]

τ = bed shear stress [N/m^2]

τ_c, τ_{ci} = critical shear stress for d_m, d_i

τ^*_c = non-dimensional critical shear stress [-]

ζ = coefficient for wetting & drying of the computational domain

2

3

Acknowledgement

The first author would like to thank the Norwegian Research Council for their support through the BeMatA research program

References

Brooks, H.N. (1963). Discussion of "Boundary shear stress in curved trapezoidal channels." By Ippen, A.T. and Drinker, P.A. Journal of Hydraulic Division, ASCE, Vol.89, No.3, 327-333.

Duan, J., Wang, S.S.Y., Jia, Y., 2001. The applications of the enhanced CCHE2D model to study the alluvial channel migration process. Journal of Hydraulic Research, Vol.39, No.5, pp. 1-12.

Darby S.E., Alabyan, A.M., Van de Viel, M.J., 2002. Numerical simulation of bank erosion and channel migration in meandering rivers. Water Resources Research, Vol.38 (9): 1163

Edwards B.F., Smith, H.D., 2002. River meandering dynamics. Physical Review E, Vol. 65, 046303-1 – 046303-12.

Engelund, F., 1974. Flow and topography in channel bends. Journal of Hydraulic Division, Vol.100, No. HY11, pp. 1631-1648.

Friedkin, J.K., 1945. A laboratory study of the meandering of alluvial rivers. US Army Corps of Engineers Waterways Experiment Stations, Vicksburg, Mississipi, USA.

Ikeda, S., Parker, G., Sawai, k., 1981 Bend theory of river meanders, 1. Linear development. Journal of Fluid Mechanics, Vol. 112, pp. 363-377.

Lancaster S.T., Bras R.L., A simple model of river meandering and its comparison to natural rivers. Hydrological Processes, Vol. 16, pp. 1-26.

Mosselmann, E. 1998. Morphological modelling of rivers with erodible banks. Hydrological Processes, Vol. 12, pp. 1357-1370.

Odgaard, A.J., 1981. Transverse bed slope in alluvial channel bends. Journal of Hydraulic Division, Vol.107, No. HY12, pp. 1677-1694.

Olsen, N.R.B., 2003. Three dimensional CFD modelling of free-forming meander channel. Journal of Hydraulic Engineering, Vol. 129, No 5, pp. 366-372.

Olsen, N.R.B., 2004. Hydroinformatics, fluvial hydraulics and limnology. Department of Hydraulic and Environmental Engineering, The Norwegian University of Science and Technology, Norway. (http://folk.ntnu.no/~nilsol/tvm4155/flures5.pdf)

OssmanM.A., Thorne, C.R., 1988. River bank stability analysis, I: Theory, Journal of Hydraulic engineering, Vol. 114(2), pp. 134-150

Parker, G., 1984. Lateral bedload transport on side slopes . Journal of Hydraulic Engineering, Vol. 110, No 5, pp. 366-372.

Parker g., Andrews, E.D. (1986). On the time developement of meander bends. Journal of Fluid Mechanics, Vol.162, pp.139-156

Patankar, S.V., 1980. Numerical Heat transfer and fluid flow. Taylor and Francis Publishers.

Rhie, C. and Chow, W., 1983, Numerical study of the turbulent flow past an airfoil with trailing edge separation, AIAA Journal, 21 (11)

van Rijn, L.C., 1984a. Sediment Transport Part I: Bed load transport. Journal of Hydraulic Engineering, Vol.110, No. 10, pp. 1431-1456

van Rijn, L.C., 1984b. Sediment Transport Part II: Suspended load transport. Journal of Hydraulic Engineering, Vol.110, No. 11, pp. 1613-1641

Rijn, L. C. van, 1984c. Sediment Transport, Part III: Bed forms and alluvial roughness, Journal Hydraulic Engineering, Vol.110 No.12, pp. 1733-1754.

Rodi, W., 1980. Turbulence models and their application in hydraulics. IAHR state-of-the-art publication, Monograph Series, 3rd Edition, A.A. Balkema, Rotterdam, the Netherlands.

Rüther, N., Olsen, N.R.B. 2003. CFD modelling of alluvial channel instabilities. Proc. 3rd IAHR Symposium on River, Costal and Estuarine Morphodynamics 2003, Barcelona, Spain

Rüther, N., Olsen, N.R.B. 2005. Advances in 3D modelling of free-forming meander formation from initially straight alluvial channels. 31st. IAHR Congress, Seoul, Korea.

1 Schlichting, H., 1979, Boundary layer theory, McGraw-Hill Book Company, New York.

2 Struiksma, N., Olesen, K.W., Flokstra, C., De Vriend, H.J. (1985). Bed deformation in curved

3 alluvial channels. Journal of Hydraulic Research, Vol.23, No.1, pp. 57-79

4

Figures

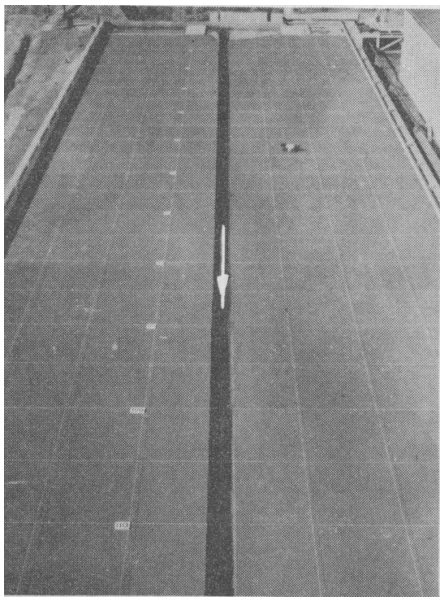

Figure 1: Initial experimental setup. Friedkin (1945)

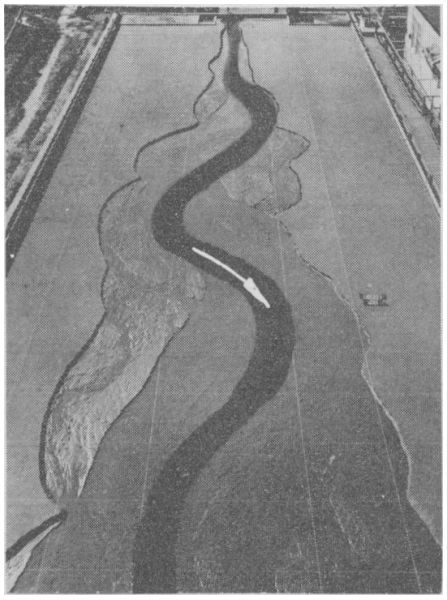

Figure 2: Plan form evolution in the experiment. Friedkin (1945)

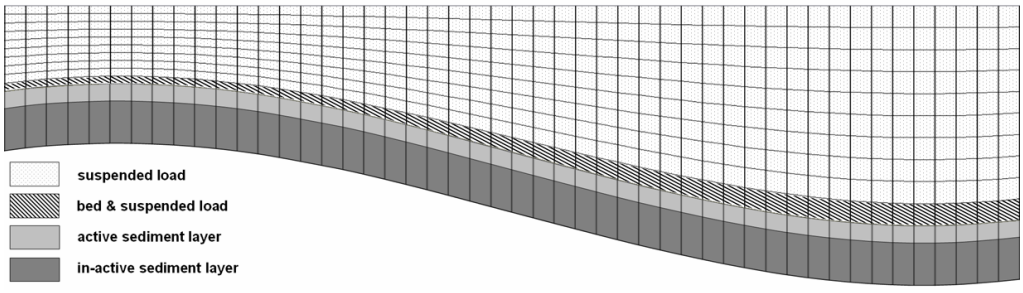

Figure 3: Longitudinal cut through the computational domain

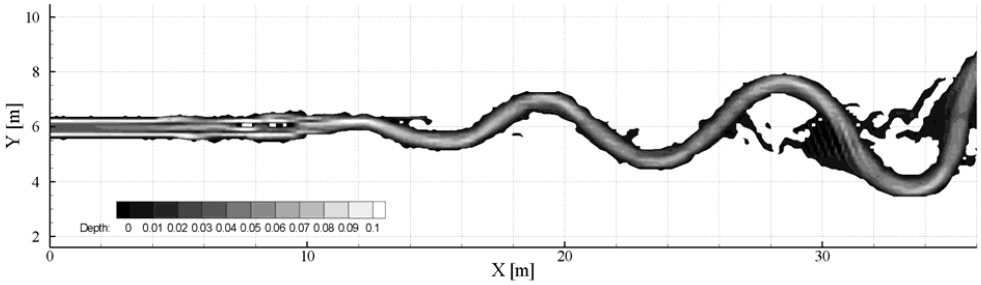

Figure 4: Calculated water depth with the use of eq. (16) for cells close to the border of the channel; measures in [m]

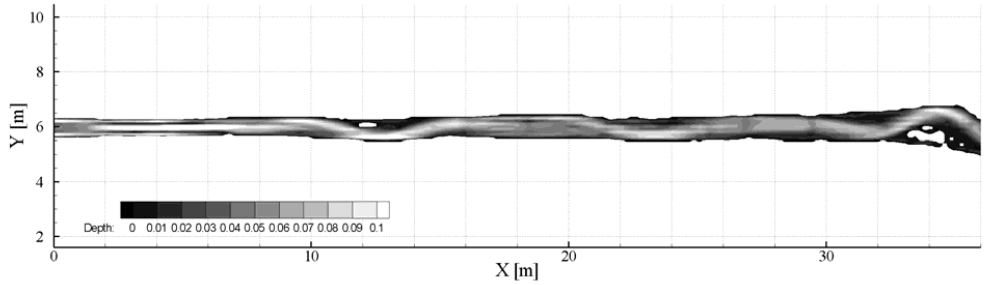

Figure 5: Calculated water depth, w/o using eq. (16); measures in [m]

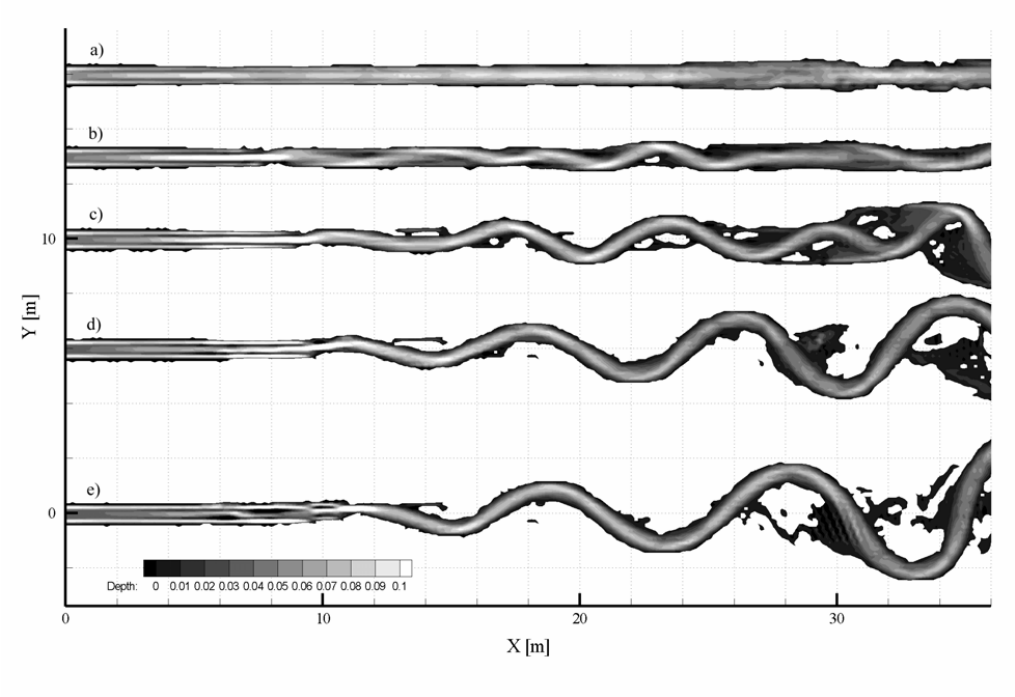

Figure 6: Evolution over time. Flow direction is from left to right. Time distance between each of the figures is ≈ 14hrs.

1

2

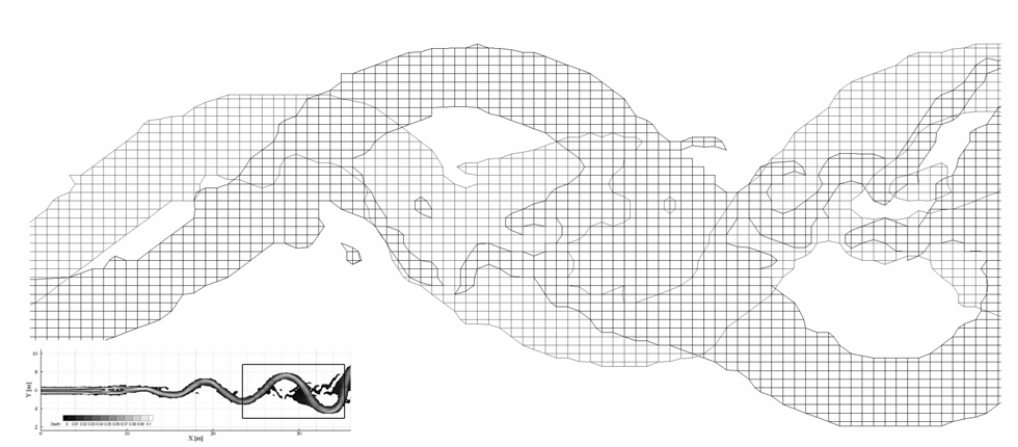

3

4 Figure 7: Formation of the grid at time t = 55.5 hrs (light grey) and at time t=72 hrs (dark grey)

5

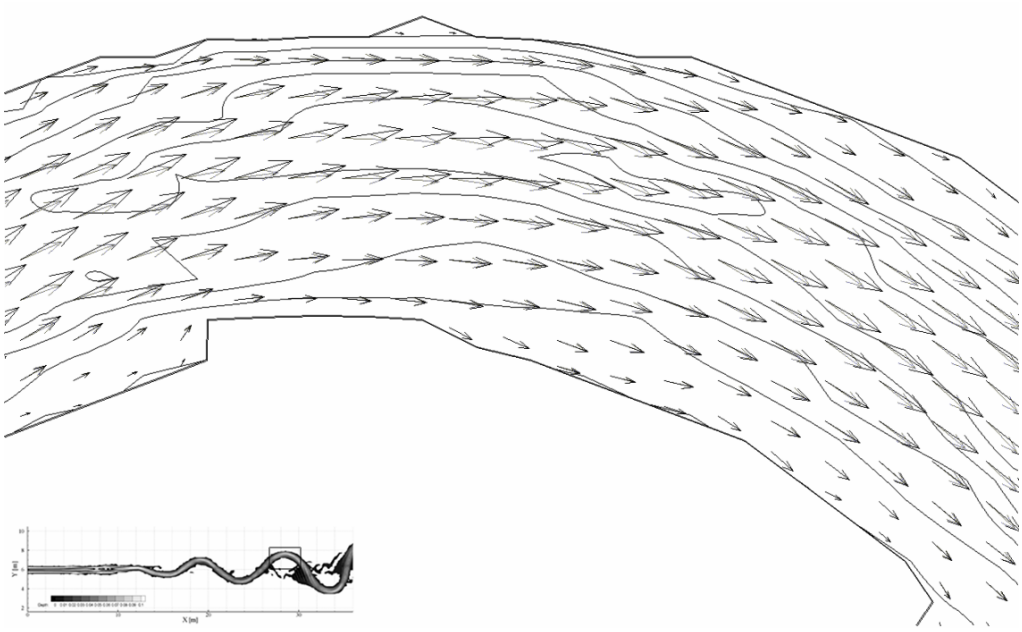

Figure 8: Velocity vectors at the channel bed (grey) and at the water surface (black). Flow direction is from left to right.

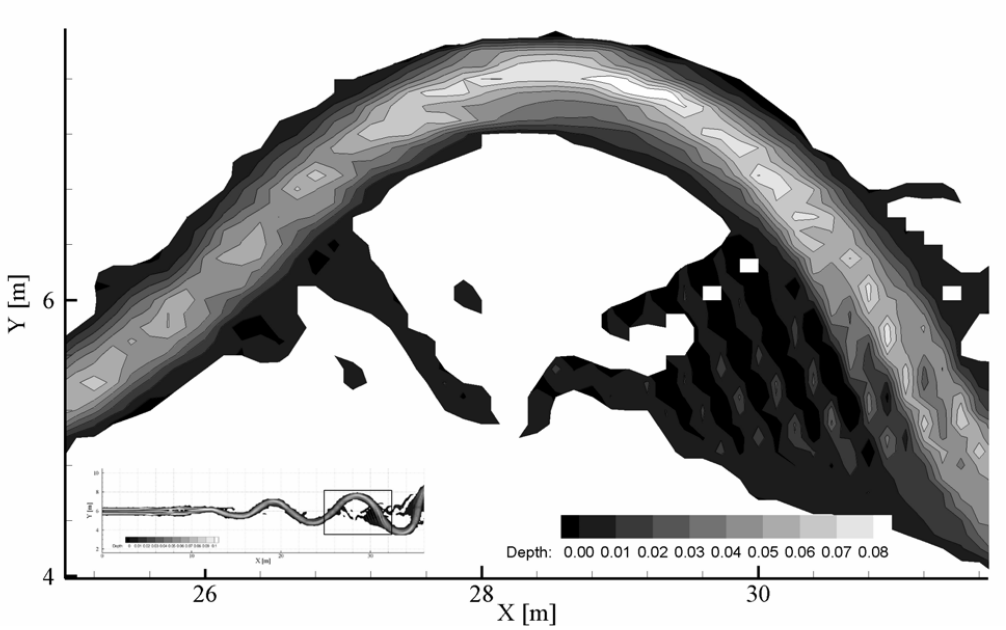

Figure 9: Water depth in a meander bend; measures in [m]. Flow direction is from left to right

1

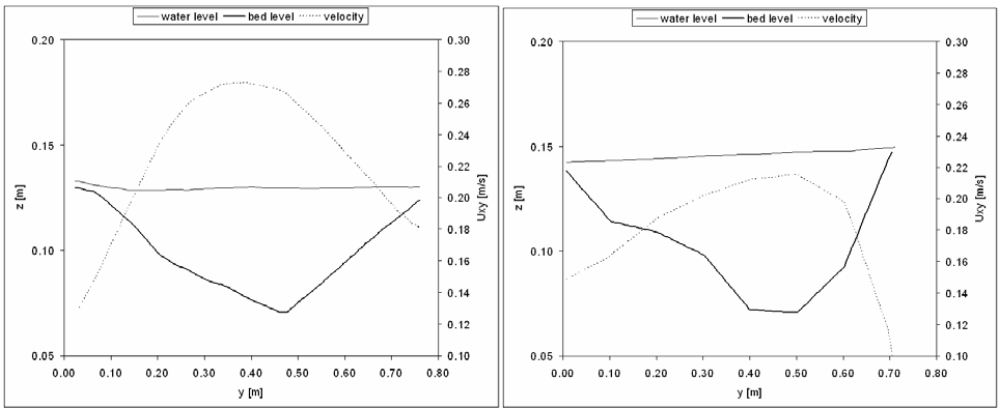

2

3

4 Figure 10: a) cross section at x=25.5m and b) at 28.0m

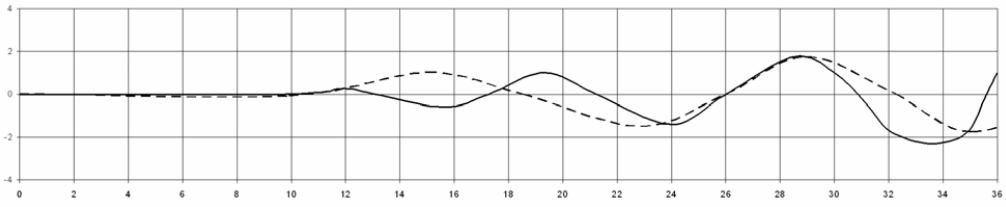

Figure 11: Centreline of the channel in the experiment (dashed), and in the simulation (solid). Measures are in [m]

About the author

I was born on 19^{th} December 1972 in Bonn. I went to primary school from 1979 to 1983, and to grammar school from 1983 to 1988. After receiving my final degree from high school (Abitur) in May 1993, I started studying civil engineering at the Technical University in Karlsruhe in October 1993.

My first contact with sediment transport was in Nantes, France. During my stay at the *École Centrale de Nantes*, where I studied for two semesters, I was able to work at the *Service Maritime et Navigation*. As a student researcher I was involved in the *Plan Loire Grandeur Nature*. The study was about the reintegration of old river branches in the main river system, as an enhancement of the biodiversity and as potential flood retention areas. This initiated my interest for further studies in sediment transport and river hydraulics. Later on, during my studies at the Technical University of Karlsruhe, I had the opportunity to work on a project studying the incipient motion of coarser sized material in steep mountain rivers in Pakistan. During field work in Pakistan I measured bed load movement in steep torrents and subsequently I calibrated the field bed load sampler at the Theodor-Rehbock Laboratories at University of Karlsruhe. The experience in the field, the subsequent theoretical considerations and the encouragement of my then-supervisor, convinced me to emphasize my studies on hydraulic and sedimentation engineering.

After finishing my studies with the degree of *Diplom Ingenieur* in May 2001, I started working at the Institute of Water Resources Management, Hydraulic and Rural Engineering at the University of Karlsruhe as a research associate under the supervision of Professor Andreas Dittrich.

I was working in the framework of an EU project about riparian forest management, modeling the flow through riparian forest, idealized by rigid and flexible sticks in a laboratory channel. During that period I gained profound knowlegde of CFD and especially the use of the CFD code *SSIIM*.

In October 2002, I started this PhD study at the Norwegian University of Science and Technology in Trondheim under the supervision of Professor Nils Reidar B. Olsen.

Nils Rüther

Trondheim, November 2006